EXPERIMENTAL ANALYSIS OF PARTICULATE MOVEMENT IN A LARGE EDDY SIMULATION CHAMBER

by

ANGELINA MARIANNA PADILLA

B.S., University of California, Davis, 2006

A THESIS

submitted in partial fulfillment of the requirements for the degree

MASTER OF SCIENCE

Department of Mechanical and Nuclear Engineering
College of Engineering

KANSAS STATE UNIVERSITY
Manhattan, Kansas

2008

Approved By:

Major Professor
M.H. Hosni

Abstract

Millions of people travel by commercial aircraft each year. The close proximity of passengers aboard an airplane leads to one of the primary reasons that air quality in an aircraft cabin is of interest. In recent years there have been multiple reported instances of people contracting illnesses after being aboard an aircraft for an extended period of time. In order to better understand air quality in an aircraft cabin, an experimental study of particulate transport in a half cabin model of a Boeing 767 was performed. In the study, both 3μm and 10μm particles were tested separately by injecting them into the cabin through a vertical tube, 609.6 mm (24 in) above the floor, at a single location on the centerline of the half cabin test section. Resulting particulate concentrations were measured at five locations along the centerline of the half cabin test section. It was found that for the 3μm particles, the normalized concentration was about one for all of the locations except directly above the injection site. Therefore, the concentrations were approximately the same as the well-mixed concentration, where the well-mixed concentration is the concentration in the test cabin if the test cabin is uniformly mixed. For the same test conditions, the normalized concentrations for the 10μm particles were well below one, around 0.1. Several more concentration measurements using the 10μm particles were taken at the same five locations, both on and off the centerline, and for different particle injection and cabin pressure conditions. The concentration results using a diffuser cone to inject the 10μm particles into the test cabin and a neutral cabin pressure were higher than the results found using the straight injection tube, but they were not very repeatable. After pressurizing the cabin to slightly above ambient pressure and using the diffuser cone, the resulting average normalized particle concentrations along the centerline were found to be between 0.4 and 1.5 and repeatable within the estimated measurement uncertainty. Therefore, it appears that the 3μm particles follow the airflow in the test cabin well, but it is not clear if the 10μm particles do as well.

Table of Contents

List of Figures

List of Tables

Acknowledgements

First and foremost I would like to thank Dr. Hosni, Dr. Beck and Dr. Jones. Their guidance was invaluable. I would also like to thank Steve O'Halloran for showing me the ropes and Paul Lebbin for leaving everything in order. A thank you also goes to Eric Waters for coming to my aid when things were not working. Chao-Hsin Lin and Ray Horstman from Boeing Inc. also deserve a thank you for their support and understanding. Finally, I would like to thank my parents along with the rest of my family and friends for encouraging me to excel, even if it was a couple thousand miles away from home.

CHAPTER 1 - Introduction

Travel by aircraft has steadily increased over the past several years. According to the Federal Aviation Administration, over 750 million people traveled by aircraft in 2007 (FAA 2008b). With more people traveling by airplane each year, air quality aboard an aircraft has become of greater interest. There are several different reasons why air quality is of interest. Two major reasons are basic comfort aboard an aircraft and the possibility of contracting an illness. Both passengers and the flight crew are interested in air quality that is comfortable and safe, especially due to the high density of people aboard a commercial aircraft. The possibility of contracting an illness is of greater concern than basic comfort. This concern has been amplified by the media. A quick search on a news website will result in several stories, in the past few years alone, about illness and its possible transmission on an aircraft.

In response to these concerns Boeing funded a research project titled "Large Eddy Simulation Validation Lab Test – Particle Diffusion." This is the fourth phase of the project investigated by the Kansas State University research team. The objective of this phase of the project was to collect monodispersed particle concentration measurements inside a half cabin test section that has the same dimensions as Boeing's computational fluid dynamics model of a Boeing 767. The data collected in this two-year research project was to supplement data collected in the first three phases. The data collected in the first and second phases were velocity measurements inside the test cabin. The third phase investigated gas dispersion in the test cabin by taking carbon dioxide measurements. The data from the first three phases can be found in (Lebbin 2006).

As for the fourth phase which is documented here, the main objective was divided into two parts. The first part was to acquire, install, and validate the particle injection and particle measurement equipment. The validation of the equipment was challenging and it is described in detail in Chapter 7. The second part was to inject monodispersed particles pointwise into the test cabin as uniformly as possible while measuring the particle concentrations at various locations inside the test cabin, test cabin inlet duct, and test cabin outlet duct.

The data collected in this phase will be used to help validate the large eddy simulation model used by Boeing to model air flow in a Boeing 767 mockup. This information could help

predict particle dispersion in an actual Boeing 767 aircraft. Ultimately, the large eddy simulation technique may be used to determine how many people would likely be exposed to an accidental or intentional release of contaminants on an aircraft.

CHAPTER 2 - Literature Review

2.1 Aircraft Cabin Air Quality

There are a limited number of regulations and several standards pertaining to aircraft cabin air quality and thermal comfort. The few regulations that exist in the United States are set forth by the Federal Aviation Administration (FAA) in Title fourteen of the Code of Federal Regulations. These regulations are for cabin pressure, cabin ozone concentration and cabin ventilation; they are mostly aircraft design requirements, not operation requirements. The FAA regulations primarily address heath requirements, and only cover a few of the factors that are used to determine air quality and thermal comfort. The principle factors in aircraft cabin thermal comfort and air quality are temperature, relative humidity, pressurization, ventilation, and air contaminants. A couple of the standards that cover these factors are the ASTM D7034-05 (standard guide for deriving acceptable levels of airborne chemical contaminants in aircraft cabins), and the proposed ASHRAE STD 161, which will be a comprehensive set of standards for aircraft air quality.

2.1.1 Temperature

FAA regulations state that the aircraft must be designed so that cabin temperature cannot differ by more than 3°C (5 °F) between different zones, and after a failure situation the cabin temperature cannot be above 60°C (140°F) for any period of time and 38°C (100°F) for more than 90 minutes (FAA 2008a). Although temperature may seem to be the most important parameter in defining thermal comfort, it is also probably the most difficult for which to establish a regulation that would be widely acceptable. There are two primary reasons for this: there is a difference of activity between the passengers and the flight attendants and each individual has a different preferred temperature. According to the 2003 ASHRAE Applications Handbook, the environmental control system is designed to maintain the cabin at 24°C (75 °F) with a full passenger load on a hot day and a 20% filled cabin on a cold day. It also states that on a commercial aircraft (over 19 passengers) the temperature in each passenger zone is individually controlled by the crew, within a temperature range of 18-29°C (65-85 °F). This temperature

range is supported by several studies in which the reported average temperature was within this range (Brundrett 2001); (Space et al. 2000); (O'Donnell et al. 1991). Consequently, even though passengers and the flight crew may notice the temperature more than other thermal comfort factors, the temperature meets health standards and is within the recommended temperature range of 22-28°C (70-83 °F) for office work in a low humidity environment (ASHRAE Standard 55 2004).

2.1.2 Relative Humidity

The relative humidity in an aircraft tends to be low. Several studies showed that the average relative humidity was 20% and below (Nagda and Hodgson 2001); (Space et al. 2000); (O'Donnell et al. 1991); (ASHRAE 2003). These levels of relative humidity are analogous to those found in the north during winter (Space et al. 2000). The primary reason for these low levels is that the air at flying altitudes has very little moisture, less than 25% of the amount found at sea level, and when the air is heated to cabin temperatures the relative humidity decreases (ASHRAE 2003). Therefore, the air delivered to the cabin by the aircraft's environmental control system has a relative humidity of less than 5% (Leder and Newman 2005); (Nagda and Hodgson 2001). Furthermore, airline industries prefer a relative humidity below 25% to prevent condensation which leads to corrosion, bacteria and fungal growth (Space et al. 2000). Consequently, the amount of moisture on an aircraft depends on the number of passengers, since they are the major contributors (O'Donnell et al. 1991); (ASHRAE 2003). The relative humidity of the air can be higher if the ventilation system uses recirculation. However, the relative humidity will still be low because in order to maintain cabin pressure ten or more air exchanges per hour are required (Nagda and Hodgson 2001) and typically only 50% of the air gets recirculated (Hunt et al. 1995); (Thibeault 2002).

Exposure to low relative humidity levels over an extended period of time can result in physical symptoms such as dryness of the skin, eyes, nose and mouth (ASHRAE 2003). These subjective symptoms have been reported by both passengers and crew after flying in several studies, especially for flights over three hours (Hunt et al. 1995);(Brundrett 2001). Increased fluid intake is recommended instead of increasing the humidity (Thibeault 2002). According to the 2003 ASHRAE Applications Handbook, no serious adverse health effects have been documented as a result of low humidity on an aircraft and the Air Transport Medicine

Association finds a relative humidity of 12-21% in an aircraft cabin to be acceptable (Brundrett 2001). Moreover, studies on human perception of the air quality in the aircraft cabin showed that an increase in temperature or humidity level led to the air being perceived as stale or stuffy; although these effects were small over the low humidity range found in the aircraft cabin (Nagda and Hodgson 2001).

2.1.3 Pressure

The FAA regulation regarding cabin pressure, last updated in 1996, states that a commercial aircraft must be designed to operate at a maximum cabin pressure altitude of 2440 m (8,000 feet) under normal conditions. Therefore, the cabin must be pressurized to the equivalent pressure at 2440 m (8,000 feet) and even after a failure the cabin pressure altitude cannot exceed 4572 m (15,000 feet) (FAA 2008a). This is a safety requirement based on the quantities of oxygen found in the air at this level of pressurization (Thibeault 2002). At an altitude of 2440 m (8,000 feet) the air contains 82% of the amount of oxygen found at sea level (Space et al. 2000). The results of a study of 84 passengers showed that the average oxygen saturation level for the passengers was 97% at ground level and reduced to an average of 93% at cruising altitude (Humphreys and Deyermond 2005). An oxygen saturation level of 90% is still considered acceptable for healthy individuals; although it is near the threshold (Thibeault 2002).

The cabin pressure is determined by two design factors: the maximum cruising height and the design pressure difference across the cabin walls. As the aircraft ascends and descends, the pressure change in the cabin is monitored so that it changes at a slower rate than the pressure outside of the cabin. After the aircraft reaches the maximum cruising speed, it cannot ascend without causing the pressure change inside the cabin to be the same as the pressure change outside the cabin (Brundrett 2001). It is recommended that the maximum rate of change during ascent and descent is 91.4 m/min (300 fpm) and 152 m/min (500 fpm), respectively (ASHRAE 2003). Different aircraft models have different wall pressure differentials ranging from 0.48 atm (7.5psi) for the Boeing 777 to 0.6atm (8.9psi) for the Boeing 747. This results in a different cabin pressure altitude at the same flight altitude depending on which plane is being used. In one study by Brundrett 2001, the cabin pressure altitude was measured in 204 flights over 20 months by 28 carriers and it was found that the cabin pressure altitude ranged from sea level to 8915ft (2720m). The mean cabin pressure altitude for domestic flights within the US was 6216ft

(1894m) and the mean for international flights was 5812ft (1772m) (Brundrett 2001). Therefore, the maximum cabin pressure altitude, and consequently the corresponding cabin pressure for the studies, did not meet FAA standards, but the averages did.

2.1.4 Ventilation

The purpose of ventilation on an aircraft is to provide fresh air to the crew and passengers and to remove contaminants and odors from the cabin. The current ventilation standard, updated in 1996, states that under normal operating conditions at least 0.25 kg (0.55 pounds) of fresh air per minute must be provided to each passenger (about 283 lpm (10 cfm) at 2440 m (8,000 feet))(FAA 2008a). This was reduced from 570 lpm (20 cfm) in the late 1980's (Harding 1994). It was found that recirculated air can provide the same level of comfort as fresh air as long as it is well mixed and there are no pockets of stagnant air (Thibeault 2002). As of 1996, nearly half of the aircrafts had ventilation systems that supplied a combination of fresh and recirculated air to the cabin (Smith 1996). Generally, in a modern commercial aircraft half of the air supplied to the passengers is fresh air and the other half is filtered, recirculated air (Hunt et al. 1995); (Thibeault 2002). Therefore, the ventilation system is designed to provide 283 lpm (10 cfm) of fresh air and 283 lpm (10 cfm) of filtered, recirculated air to each passenger. Regardless of whether the ventilation system uses recirculated air or not, the equivalent of the total volume of air on the aircraft will have been supplied to the cabin after 2-3 minutes (ASHRAE 2003).

The same amount of air is provided along the length of the aircraft with the possible exception of the cockpit. This results in a different airflow per person between the economy and business or first class zones since there are more people in a row in the economy class than there are in the higher classes. Therefore, if an aircraft only had an economy class, and it was filled to capacity, the amount of fresh air per person would only be 184 lpm (6.5 cfm) for a standard body aircraft and 226 lpm (8 cfm) for a wide-body aircraft (ASHRAE 2003). In one study, published in 1991, of 45 flights on aircrafts with a seating capacity of 101, the outdoor air supply did not meet manufacturer standards of 10 cfm per person on over half the flights and did not meet the comfort value of 7.1 lpm (15 cfm) per person, calculated from the ASHRAE62-1989 ventilation standard, on over two-thirds of the flights (O'Donnell et al. 1991). It should be noted that the comfort standard used in this study was for transportation vehicles in general and not specifically for aircraft vehicles. The cockpit may have higher air exchange rates than the rest of the aircraft,

because the air volume is smaller and the large window area and the numerous electrical instruments increase the temperature in the cockpit (Lindgren 2003).

2.1.5 Air contaminants

There are several different types of air contaminants that can be found on an aircraft and they come from a variety of different sources. The different types of air contaminants can be divided into three categories: physical, chemical and biological (Thibeault 2002). The sources of contaminants on an aircraft are the outside air, the aircraft itself and the passengers or the flight crew. The FAA only regulates three air contaminants, which are ozone (O_3), carbon monoxide (CO) and carbon dioxide (CO_2). Generally, aircrafts are equipped with filters, which cannot be bypassed, to remove physical and biological contaminants from the recirculated air. Ideally aircrafts are equipped with high-efficiency particulate air (HEPA) filters with a minimum efficiency of 94-99.97% and a most penetration particle size of 0.1-0.2 μm (ASHRAE 2003). Consequently, with the use of a HEPA filter, solid contaminants in the submicron and micron range get removed from the air supply. However, aircrafts are not required to use HEPA filters in the ventilation system.

2.1.5.1 Physical Air Contaminants

Physical contaminants are particulate matter such as pollen, dust, hair, fibers, tobacco and microorganisms. Particulates in the air can come from the interaction of humans with objects, such as a person brushing off a surface or chemical reactions. Particles that are less than 10 μm can be potential health hazards. Particles of this size can be inhaled and they can penetrate deep into the lungs (Thibeault 2002). According to the Environmental Protection Agency (EPA), exposure to inhalable particulates can cause health problems such as asthma, chronic bronchitis, reduced lung function, irregular heartbeat, heart attack and can lead to death for people who have heart or lung disease (EPA 2007). The EPA provides regulations on particle sizes 10 μm and smaller in the National Ambient Air Quality Standards (NAAQS). Current standards, updated 2006, state that the maximum 24-hour average exposure level for particles 10 μm and smaller (PM-10) is 150 $\mu g/m^3$. For particles 2.5 μm and smaller (PM-2.5), the annual average exposure level is 15.0 $\mu g/m^3$ and the 24-hour average is 35 $\mu g/m^3$. The previous maximum, annual average exposure concentration regulation for PM-10 was revoked due to insufficient evidence of a correlation between exposure levels and health problems (EPA 2008).

Several studies have conducted particle measurements in an aircraft with varying results. In one study by O'Donnell et al. 1991 of 45 flights lasting 30-60 minutes, the total number of particulates greater than 0.8 μm was measured in the cabin. Measurements were taken at two locations in the economy section of the cabin: in front of the first row on the right side, when facing forward, and in front of the last row on the left side. The mean concentration measured was 105 $\mu g/m^3$ and the maximum concentration was 200 $\mu g/m^3$ (O'Donnell et al. 1991). The actual sizes of the particles was not reported, but the maximum concentration would not meet EPA regulations if all the particulates measured were 10 μm or smaller. In another study of five flights, of which four out of the five had over 11 hours of non-stop flight time, the average particle concentration for respirable particles was 7.6 $\mu g/m^3$, with maximum concentrations ranging from 74 $\mu g/m^3$ to 1980 $\mu g/m^3$ (Lee et al. 1999). Other studies show similar results, where the average concentration meets EPA regulations but the maximum concentrations do not (Hunt et al. 1995);(Lindgren 2003).

2.1.5.2 Chemical Air Contaminants

All of the air contaminant regulations are for chemical contaminants. The most current regulation regarding the ozone concentration inside the aircraft cabin was revised in 1998. The regulation states that the ozone concentration in the cabin should not exceed the sea level equivalent of 0.25 parts per million (ppm) by volume (at a temperature of 25°C and a pressure of 760 mmHg) at any time and the time weighted average concentration should not exceed 0.1ppm over any three hour interval (FAA 2008a). These values are higher than the current ambient air EPA standard, which states that the 8-hour maximum should not exceed 0.075 ppm (EPA 2008). The current standard is effective as of 2008; the previous 1997 EPA standard for ozone was 0.08 ppm, which is still lower than the FAA regulation.

Ozone is toxic and it can cause inflammation of the respiratory tract and will irritate the lungs at low concentrations (Brundrett 2001). The primary source of ozone is the fresh air supply. Ozone concentrations in the atmosphere vary depending on the season, altitude, latitude and weather conditions. Ozone concentrations increase at higher flight altitudes and at 11887 m (39,000 ft), ozone plumes can be encountered with sea level equivalent concentrations as high as 0.62 ppm. Consequently, any aircraft that will encounter ozone concentrations higher than FAA regulations is generally required to use a catalytic ozone converter. The catalytic ozone converter breaks the ozone down into oxygen, at a minimum efficiency of 60% which occurs

near the time it needs to be replaced (ASHRAE 2003). Studies have shown ozone concentrations to be well below comfort standards and sometimes they are undetectable (Lee et al. 1999; O'Donnell et al. 1991); (Hunt et al. 1995).

The other two chemical contaminants regulated by the FAA are CO and CO_2. The regulation for CO states that concentrations cannot exceed 1 part in 20,000 and CO_2 concentrations cannot exceed the sea level equivalent of 0.5 percent by volume (FAA 2008a). Possible sources of CO in an aircraft cabin are cigarette smoke and vapors from the engine transported into the cabin via the fresh air supply (Thibeault 2002). In the 1990's smoking was banned on all flights within the U.S. and since then many airlines have banned smoking on all their flights. Consequently, smoking is not a probable source for CO (Smith 1996). All studies reviewed found that measured CO concentrations were low, below 1ppm, throughout the flight (Lee et al. 1999); (Hunt et al. 1995). The primary source of CO_2, on the other hand, is human breathing (Thibeault 2002); (ASHRAE 2003). Most studies compared CO_2 concentrations to a 1000 ppm limit, calculated from the ASHRAE 62 ventilation standards, along with the FAA regulation of 5000 ppm. The stricter 1000 ppm limit takes a comfortable odor level into consideration along with health requirements. Studies showed that the maximum CO_2 concentration during cruising ranged from 1500 ppm to 3000 ppm and the minimum concentrations measured ranged from 300 ppm to 600 ppm (Hunt et al. 1995); (Lee et al. 1999); (Thibeault 2002); (Lindgren 2003); (O'Donnell et al. 1991). Therefore, the maximum concentrations, which usually occurred at the beginning and end of the flights, met FAA regulations and the average concentration met both FAA regulations and ASHRAE comfort standards. The reason for the higher CO_2 concentrations at the beginning and end of the flights is the lower level of fresh air supplied at non-cruising conditions and higher levels of activity by passengers and crew (Lee et al. 1999).

Other chemical air contaminants that are a concern are volatile organic compounds (VOC's) and semi-volatile organic compounds (SVOC's), which are compounds that evaporate easily. Potential sources of VOC's are off-gassing from food and beverages, cleaning products, perfumes, paints, the fresh air supply and people. The primary source of SVOC's of concern is insecticides, since many international flights are required to spray insecticide before entering a foreign country to reduce the probability of transmitting disease via insects; particularly, mosquitoes. The World Health Organization (WHO) stated that the insecticides used on aircrafts

would not cause health problems as long as WHO regulations were followed (Thibeault 2002). All reviewed studies showed that VOC and SVOC concentrations were well below levels that cause health concerns and sometimes they were undetectable (ASHRAE 2003); (Nagda and Rector 2003); (Thibeault 2002); (O'Donnell et al. 1991).

2.1.5.3 Biological Contaminants

Some of the potential biological contaminants that can become airborne are bacteria, fungal spores, animal dander and viruses (ASHRAE 2003). The primary source of biological contaminants on an aircraft is people. There are two ways that respiratory infections like the common cold, influenza, tuberculosis, smallpox and severe acute respiratory syndrome (SARS) can be transmitted: droplet spread and airborne route. Infections get transmitted via droplet spread when someone coughs, sneezes or talks. The droplets from the infected individual contain organisms and the droplets settle out of the air relatively quickly and land on surfaces. People who come in contact with the droplets can become infected. For airborne route, the relatively small droplets remain suspended in the air and they can be transported away from the infected individual infecting people further away (Leder and Newman 2005). On an aircraft both modes of transmission are a concern, since passengers are seated close to one another. Factors, identified by the Center for Disease Control in Atlanta, that determine if someone will become infected on an aircraft are: proximity and exposure time to the infected individual, and the ineffectiveness of the infected individual to transmit the disease (Lindgren 2003). Other factors to be taken into consideration are the location of the individual on the aircraft and the ventilation rate (Ko et al. 2004).

As mentioned above, HEPA filters capable of removing submicron and micron particles at a minimum efficiency of 97% are recommended on the recirculated air supply (ASHRAE 2003). Bacteria generally have diameters greater than 1 μm so they will be removed with the use of a HEPA filter (Thibeault 2002). Furthermore, bacteria do not survive in low humidity environments like the aircraft cabin (Leder and Newman 2005). Contrarily, viruses thrive in low humidity environments and have diameters 0.003-0.05 μm (ASHRAE 2003). However, they usually clump together or attach to dust particles which will make them larger in diameter (Leder and Newman 2005). Therefore, although viruses thrive in low humidity environments they will also be removed from the air supply with the use of a HEPA filter. A study compared the number of people who developed cold symptoms after flying on aircrafts with recirculated air to

the number of people who developed cold symptoms after flying on aircrafts with 100% fresh air. Through surveys, it was found that there was not a noteworthy difference between the number of passengers who became ill after flights with recirculated air compared to the number of passengers who became ill after flights with 100% fresh air (Zitter et al. 2002).

Many studies have been conducted on infection transmission on an aircraft since the major outbreak of influenza on an aircraft in Alaska in 1979. In that case, a plane full of passengers had a 3-hour ground delay, during which the ventilation system was turned off, and one of the passengers was sick and infected 72% of the other passengers and 40% of the crew. Now adequate ventilation must be supplied for ground delays greater than 30 minutes (Leder and Newman 2005). It was found in one study that doubling the ventilation rate reduced the risk of infection by particles by one half (Ko et al. 2004). Other studies have found that microbial aerosol concentrations were equal or lower than the concentrations found in the common home (Hunt et al. 1995). It is known that SARS was transmitted by air travel and the WHO indicates that the primary people at risk are those seated within two rows of the infected passenger, although other studies indicate that three rows in front of the infected individual due to coughing is a better estimate (Leder and Newman 2005). Finally, another study found the average bacteria count on an aircraft to be 50 CFU/m^3 and the average fungi count to be 45 CFU/m^3, well below the Hong Kong Interim Indoor Air Quality Guidelines of 1000 CFU/m^3 (Lee et al. 1999).

2.2 Related Aircraft Chamber Studies

2.2.1 Velocity Measurement Studies

There have been a few studies that have measured velocity magnitudes in chambers modeled after aircraft cabins, both experimentally and numerically. In a recent study by Bosbach et al., a full scale model of a section of an A380 aircraft cabin was used for testing (Bosbach et al. 2006). The model was 1350 mm in height, 2000 mm wide, and 3430 mm in length. It modeled the upper right-hand corner of an aircraft cabin, including the overhead luggage compartments which were curved with a radius of 490 mm. The airflow entered the chamber through three slits, 1010 mm long and 10 mm high, just beneath the luggage compartments and exited at floor level on the same wall as the airflow inlet. The airflow entered at a combined rate of 2400 lpm (85 cfm), which corresponds to a velocity of 0.66 m/s (2.2 ft/s). Velocity measurements were taken experimentally using Particle Image Velocimetry (PIV).

Measurements of the entire cross section of the chamber were taken and each velocity vector represented an area 70mm x 70mm. A single measurement of the velocity field in the chamber showed eddies approximately 200mm x 200mm in size with relatively small velocity magnitudes at the center of the chamber and between the inlet and outlet ports. Along the edge of the chamber (with the exception of between the inlet and outlet ports) the velocity was higher in magnitude and the flow followed the chamber wall from the inlet to the outlet. The average velocity measurements did not show eddies in the center of the chamber, just one small eddy near the outlet and one large eddy encompassing most of the flow in the chamber. The maximum velocities occurred along the outer edge of the chamber and the minimum occurred in the center. The numerical results matched the experimental results.

A similar study was conducted by (Lebbin 2006). In the study measurements were taken in a full scale half cabin model; the dimensions were similar to a section of a Boeing 767, except all walls were flat. The chamber had a height of 2134 mm (84 in), a width of 2134 mm (84 in), and a length of 2134 mm (84 in). There was a single inlet into the chamber 2134 mm (84 in) long and 51 mm (2 in) high. The airflow entered the inlet uniformly, beneath the overhead compartment along the axis of symmetry, with a velocity of 0.61 m/s (2.0 ft/s), which corresponds to a flow rate of 4163 lpm (147cfm). The flow exited the chamber at the floor level on the wall opposite the inlet. The overhead luggage compartment above the inlet was 373 mm (14.7 in) wide and the overhead compartment above the outlet was 800 mm (31.5 in) wide, both compartments were 427 mm (16.8 in) in height. Velocity measurements were also taken in this study, except they were only taken at five locations in the chamber along the centerline, which was a plane of symmetry. The centers of two measurement locations were 685.8 mm (27 in) away from the inlet; one was at a height of 609.6 mm (24 in) and the other was at a height of 1219 mm (48 in). The center of the third location was 1067 mm (42 in) away from the inlet at a height of 9144 mm (36 in). The centers of the final two locations were 1448 mm (57 in) away from the inlet; one was at a height of 609.6 mm (24 in) and the other was at a height of 1219 mm (48 in). Several instruments were used to measure the velocity including a draught probe, a hot wire anemometer, a sonic anemometer and a PIV system. The measurement window for the PIV measurements was 360 mm x 360 mm at each location and a much higher resolution than the (Bosbach et al. 2006) study was used.

A third study by Sun et al. 2005 with results presented in Zhang et al. 2005, also describes velocity measurements taken in a mock-up of a Boeing 767. The mock-up included seats and manikins with electrical heaters around their waist for passengers. It contained five rows of seven seats (A-G) with manikins in each seat and aisles between seats B and C and between E and F. The mock-up had overall dimensions of 4700 mm (185 in) wide, 4300 mm (170 in) deep, and 2100 mm (83 in) deep. In this study, the effects of cabin occupancy and temperature on the velocity in the cabin were investigated using volumetric particle streak velocimetry (VPSV). This was done by injecting helium filled bubbles at the center row of the mockup. Then simultaneous pictures were taken of the cabin. The air flow rate into the cabin was 37.74 lpm per 559 mm (80 cfm per 22 in) of cabin length (Sun et al. 2005). It was found that the overall flow structure was similar to those found in (Lebbin 2006)and (Bosbach et al. 2006). Furthermore, velocities were found in the range of 0 to 0.3 m/s with an average being around 0.2 m/s. As far as the effect of passenger occupancy, an increase in occupancy resulted in a decrease in velocity variation in the cabin. Moreover, a wall colder than interior cabin temperature could increase the velocity at the window seat by about double from 0.228 m/s to 0.538 m/s (Zhang et al. 2005).

Although the setup in the (Lebbin 2006) study was slightly different from the setup in the (Bosbach et al. 2006) study, the average PIV velocity flow field looks similar in both studies. The minimum velocities in both studies were in the center and the velocities increased away from the center. The velocity magnitudes in the (Lebbin 2006) study were less than half of the magnitude of the velocities found in the (Bosbach et al. 2006) study, but the (Lebbin 2006) study did not measure the velocities near the walls. A large eddy simulation (LES) conducted by (Lin et al. 2005), with the same model configuration as the (Lebbin 2006) study, yielded the same velocity flow field results as both the (Bosbach et al. 2006) and (Lebbin 2006) studies. The Lin et al. 2005b study had the same velocity magnitudes occurring near the walls and inlet as the Bosbach et al. 2006 study and had the same velocity magnitudes as the Lebbin 2006 study at each of the five measured locations. Velocities measured in the (Zhang et al. 2005) study were also similar in magnitude to the (Lebbin 2006) and had the same overall flow structure as those found in all the studies.

2.2.2 Studies on Velocity, Ventilation and Influencing Factors

A couple of studies investigated the effect of temperature differences in an aircraft cabin. A numerical study by Singh et al. investigated the effects of heat loads on air distribution in an aircraft cabin using a Re-Normalization Group (RNG) κ-ε model (Singh et al. 2002). The cabin section used in this study had the airflow inlet in the ceiling of the cabin and the flow was in the opposite direction, counterclockwise instead of clockwise, of the flow fields found in the studies described above. Nevertheless, the same primary velocity flow field characteristics found in the studies described above were found in this study. The largest velocities were along the walls with very low velocities in the center of the cabin. The addition of heat loads in the cabin increased the area along the edge of the cabin where the maximum velocities occurred and decreased the velocities in the center of the cabin. A smoke visualization test in a section of an aircraft cabin was also performed in the Singh et al. study. The smoke visualization results were similar to the numerical results. A notable feature clearly seen in the smoke visualizations was that without the heat loads there was a small recirculation zone near the inlet and with the addition of heat loads the recirculation zone near the inlet increased in magnitude.

Another experimental study by Wang et al. 2008 investigated the ventilation effectiveness in a mockup of a Boeing 767-300. To model breathing, CO_2 into the mockup near each of the thirty-five manikin's mouth at a flow rate of 0.31 lpm (0.0106 cfm). The concentration measurements were taken approximately two feet away from each manikin's nose to avoid interference with the injection. Measurements were only taken in the second, third and fourth rows to minimize the potential for boundary effects from the ends of the mockup to interfere with the measurements. It was found that the momentum from the air supply jet was the main driving force for movement in the cabin and that there was a recirculation zones in each of the aisles. The mean age of the air[1] differed slightly between the rows; the mean age was four minutes for row two, and it was five to six minutes for rows three and four. Furthermore, when the supply air was increased from 736 m^3/hr (432.7 cfm) to 1262 m^3/hr (741.8 cfm), the mean age of the air decreased by about one minute. In general, the mean age of the air decreased linearly with the air supply rate. The ventilation effectiveness factor (VEF) was also calculated by taking the inverse of the CO_2 measurements that had been normalized by the exit concentration. It was found that the VEF for all seats was greater than one, which means the

[1] Mean age of the air is the average length of time that the air is in the cabin.

CO_2 concentration measured was lower than it would be if the cabin was well mixed. The VEF was highest at seats B, D and F, which correspond to the lowest CO_2 concentrations at these seats (Wang et al. 2008). These results seem to agree with the findings of the other studies mentioned above.

2.2.3 Gas Transport Studies

Other studies have investigated gas transport in an aircraft cabin. A study by Horstman investigated the transport of CO_2 in a half cabin model of an aircraft numerically (Horstman 1988). It was found that the concentrations of CO_2 emitted into the air, modeling breathing, had dispersed covering the cross-section of the cabin after three minutes had elapsed. The maximum CO_2 concentrations remained near the source. Similar results were found for a single puff of smoke. In a study by Lebbin, experimental measurements of CO_2 were measured inside a model aircraft cabin (Lebbin 2006). The concentration for several source and measuring location combinations were measured. In general, it was found that if the sampling location was very near, a few inches or several centimeters, to the source then the dimensionless concentration ranged from three to four. As the measuring location moved away from the source, the dimensionless concentration decreased until it reached one about 609.6 mm (24 in) away from the source. If the measuring location was 609.6 mm (24 in) above the source the dimensionless concentration was about two, while if the measuring location was 609.6 mm (24 in) below the source, the dimensionless concentration was about three. If the source was about 914.4 mm (36 in) diagonally above the measuring location than the dimensionless concentration was 1.5 and increased to about 2.0 a few inches or several centimeters closer to the source. Conversely, if the source was about 914.4 mm (36 in) diagonally below the measuring location, then the dimensionless concentration was 2.0 and it increased to about 2.5 a few inches or several centimeters closer to the source.

A similar study was performed by Wang 2006 using the same mockup of a Boeing 767 as the one used in the Sun 2005 and the Zhang 2005 studies. In this study electrical heaters were placed around the manikin's necks and carbon dioxide (CO_2) was injected into the cabin in the breathing area at a rate of 4.5 lpm (0.16 cfm) for five minutes. Three different injection locations were investigated: the front left seat (4A), the back right seat (2G) and the center seat (3D). When the tracer gas was injected in the center seat the overall normalized concentrations

were higher in the cabin than when the tracer gas was injected at either of the window seats. For seats in the same row as the injected tracer gas the normalized concentration was above one, indicating that the exposure rate would be higher than if the cabin was uniformly mixed. For all other seats the concentration was less than one, with the total normalized exposure concentrations ranging from 0.45 to 0.75 in the nearest two rows and 0.2 in the furthest row (5). Furthermore, these results show that it takes 20 to 30 sec for the maximum concentration to be reached for each row away from the source. So, for the row directly behind the source it takes 20 sec after release and in the row behind that one it takes 50 sec to reach the maximum concentration. Moreover, for this study it was found that if the source was located in the center of the cabin the concentration did not distribute symmetrically across the row. More tracer gas went to the right (rows E-G) than the left (rows A-C). Finally, it was found that by increasing the supply air flow rate by 20% could reduce the concentrations in the cabin by 20 to 50 % (Wang et al. 2006).

It is difficult to compare the Wang 2006 study to the Lebbin 2006 study because both the CO_2 injection method and the measurement locations were quite different. Nevertheless, they both indicated that the farther away from the source the lower the concentration, and that the location of the source makes a difference in the relative concentrations measured in the cabin.

2.2.4 Particle Transport Studies

A few studies have investigated particle flow in ventilated spaces. The studies investigating particle flow in an aircraft cabin are computational. One study by Lin et al. 2005a modeled a single release of particles from a person into an aircraft cabin by performing a Reynolds-averaged Navier-Stokes simulation. Only two rows of a B767-300 aircraft were used in the simulation, and the source was in the center of the back row. The initial particle release into the cabin from the source was 100 particles during 0.01s and it was assumed that the particles were small enough that they would not settle out of the air. It was found that after one second there was a concentration of greater than 1 particle/m^3, one percent or more of the original concentration, around all six seats in the center of the cabin. A similar numerical study was conducted of four rows of a two aisle cabin that had seven seats across (Chen et al. 1998). It was assumed that the source emitted $5x10^5$ particles per second for 0.2 s, which corresponds to 1 $x10^5$ particles, and that the particles were 1 μm in diameter. It was found that after one second, a

concentration of one percent of the original concentration or more had reached the back, but not the front of the seat in the row in front of the source. After three seconds the concentration was at least one percent of the source in the seat in the row in front of the source. After one minute, the concentration around three of the four rows was at least one percent of the source.

A study by Gao and Niu 2007 investigated whether introducing personalized ventilation systems would reduce the pollutant concentration at the breathing zone. A CFD model of five rows of a Boeing 767-300 was used. Two air supply schemes were investigated. The first scheme had the air supplied to the cabin through two inlets in the ceiling at a rate of 600 lpm (21.2 cfm) per person and the other had air supplied at a rate of 450 lpm (15.9 cfm) through the overhead inlets, while the rest of the air supply 150 lpm (5.3 cfm) was supplied through a ventilation seat to the breathing zone. An inhalation flow rate of 8.4 lpm (0.30 cfm) was used for each passenger. The velocity range in the cabin was 0.1-0.4 m/s. One micron particles were released into the cabin close to the position of a person's nose. When ten particles were tracked, it was found that the particles could travel two rows in front of or behind the injection location before the particles settled out or were exhausted from the cabin. In a simulation of a sneeze, particle concentrations were higher than 1% of the initial concentration two to three rows in front of the injection site 5.5 seconds later (Gao and Niu 2007). Qualitatively, the results seem to agree within a few seconds; however, a direct comparison could not be made since the results of the three studies were not on the same scale.

In the Gao and Niu. 2007 study 9600 particles were tracked and it was found that after a sneeze, 0.31% of the particles were deposited on the person who sneezed, 34.04% were deposited on other passengers, 28.13% on the ceiling, 9.51% on the walls, 8.10% on the floor, 0.15% in the inlet and 19.76% were exhausted from the cabin. Therefore, 80% of the particles were deposited inside the cabin. Finally, with the use of personalized ventilation it was found that the 50-60% of the air inhaled was from the personalized ventilation. Therefore, the exposure to the particles in the air reduces by a little over 50% (Gao and Niu 2007). These results seem to imply that large particle losses in the cabin may not be unreasonable and that the use of personalized ventilation may decrease the number of inhaled particle by the passengers.

2.3 Particle Generation and Measurement

2.3.1 Particle Generation

There are several factors to take into consideration for particle generation including the particle material, size, shape and concentration. Particles can be either liquid or solid, monodispersed or polydispersed and they can be generated and aerosolized in a variety of different ways. Particles can be generated and aerosolized through controlled condensation, a vibrating orifice aerosol generator (VOAG), a spinning top aerosol generator (STAG), a nebulizer or atomizer, and by dry powder dispersion.

Monodispersed particles can be generated by using a VOAG or STAG, through controlled condensation, re-crystalization and nebulization. The STAG was the only technique for decades that could generate relatively large quantities, around a couple thousand particles per second, of monodispersed aerosol particles 1-50 μm in diameter. Particles are generated by injecting a liquid from a syringe on a rotating disk. As the disk rotates ligaments of the liquid get drawn off the disk by centrifugal force, which form into particles. The size of the particle is determined by the liquid used and the speed at which the disk is revolving (Gussman 1981). However, solutions can be used to generate particles smaller than 15 μm and suspensions can be used to generate solid particles (Mitchell and Stone 1982). There have been many improvements to the original design. In the early 1980's modifications such as a drying column for smaller particle generation and improved needle control were made (Gussman 1981), (Mitchell and Stone 1982).

The VOAG can also generate both solid and liquid monodispersed particles. A solute which is either a liquid (i.e. DOP oil) or a solid (i.e. sodium chloride or sugar) is combined with a solvent (i.e. propanol) to make a solution that will be injected through a vibrating orifice. The concentration of the solution determines the size of the particles; the frequency of the orifice and the air flow rate through the device determine the concentration of the particles. The particles pass through a drying column, often with a radioactive source to remove the electrostatic charge of the particles, to allow the solvent to evaporate. Particles sizes 0.5-50 μm can be generated using this device (Baron and Willeke 2001).

Using controlled condensation, both liquid and solid particles can be generated. In this technique, an aqueous solution containing the nuclei (i.e. sodium chloride) is atomized and dried

in a drying column. Then the nuclei are bubbled along with a carrier gas through a substance with a low volatility (oil or wax). The nuclei and vaporized substance go through a reheater, to ensure that the substance is vaporized, and then to a condensing column where the monodispersed particles are formed. The particles will be either liquid or solid depending on whether the substance used is liquid or solid at room temperature. The particle diameter is determined by the ratio of the vapor concentration to the number of nuclei (TSI 2002). Particle sizes generated using this technique range from 0.03 to 2 μm, with concentrations 10^{13} particles/m^3 (Baron and Willeke 2001).

Monodispersed solid particles can be generated using a suspension of commercial particles, made out of polystyrene or polyvinyltoluene, in a nebulizer or atomizer. There are two types of nebulizers: air-blast and ultrasonic. In an air-blast nebulizer, compressed air flows into a chamber that has the suspension or solution in it. The suspension or solution gets drawn up through a tube and the compressed air atomizes it. After the solvent evaporates, only the solid or liquid particles remain. In an ultrasonic nebulizer, a piezoelectric crystal vibrates in an alternating electric field causing a mist to form above the surface of a liquid, thus atomizing it. The liquid particles generated using a nebulizer are polydispersed; the mean particle diameters are 1-10 μm with a standard deviation of 1.4-2.5 μm. The solid particles generated are 0.01-100 μm. Agglomerates and small particles of surfactant usually found in the suspension/solution are potential problems with using this technique (Baron and Willeke 2001).

Solid, polydispersed particles can be generated using dry powder dispersion. This includes a variety of different techniques that deliver powder at a constant rate and aerosolize it. One of these techniques is the Wright Dust Feed in which a compressed powder is scraped and dispersed using an air source. Other techniques use conveyors, gears or a rotating plate in conjunction with an air source or suction to disperse the powder. Concentrations and particle size vary greatly (Baron and Willeke 2001).

2.3.2 Particle Measurement

Particle measuring instruments for particle sizes greater than 1 μm can be grouped into inertial analyzers and optical counters. Inertial analyzers include impactors, cyclones, inertial spectrometers, and real-time aerodynamic particle sizers (APS). Inertial analyzers accelerate the particles through the instrument to separate the particles into different size ranges. The number

of size ranges depends on the device. In a cascade impactor up to eight impactors are placed in series to yield eight different size ranges. With the exception of the APS, these particles are collected on a substrate. The particles are then measured using a microscope to determine size and weighed to determine concentration (Cox and Miro 1997). Both optical and scanning and transition microscopes are used to measure particles greater than 1 μm (Baron and Willeke 2001). No time history data is available for the measurements, since only a single set of measurements is collected after each use of the instrument (Cox and Miro 1997). Furthermore, long sampling periods are frequently required to collect enough mass to measure (Nagda and Rector 2001).

APS instruments are different from other inertial analyzers. The particles are not collected; instead, after they are accelerated they cross two laser beams. The length of time it takes to cross both beams varies depending on the particle size. The number of particles crossing the beams during a specified time interval determines the concentration. Continuous sampling is possible with the APS, along with a time history. Both liquid and solid particles can be measured; however, liquid particles tend to seem smaller than they really are since they become elongated after they are accelerated. For 15 μm particles, they can appear to be 20% smaller. This percentage decreases with particle size until it is insignificant for 2 μm particles. Another issue with the APS is that coincidence loss can occur, when two particles cross the beams at the same time and are counted as a single particle, for concentrations higher than 1000 particles/cm^3 (Cox and Miro 1997). Finally, the sampling efficiency of the APS will effect the concentration measurements and could lead to an underestimation of the concentration by 60% or more (Chen et al. 1998).

Optical counters include optical particle counters (OPC) and laser particle counters (LPC). Optical counters measure the amount of light refracted by a particle on a photosensitive detector in order to determine the particle size. In OPCs each particle crosses a single beam of white light, while in LPCs the particle crosses a beam of laser light. Each particle is counted, so a concentration can be determined for each size range. Coincidence can be an issue, so OPCs and LPCs work best with spherical particles that have a known refractive index (Cox and Miro 1997). Optical counters usually have to be calibrated using the type of particle to be measured in order to give accurate results (Cox and Miro 1997); (Baron and Willeke 2001).

CHAPTER 3 - Experimental Setup

This section describes the facilities and the instrumentation used for this project. It also outlines the manner in which the instruments were setup. Furthermore, it describes the different kind of measurements that were taken along with the parameters that were controlled.

3.1 Environmental Chamber

The test cabin and all of the instrumentation were housed in the Room Air Laboratory environmental chamber. The environmental chamber had dimensions of 7300 mm long, 4900 mm wide and 2700 mm tall (287 in long, 193 in wide and 106 in tall). It was well insulated on all six sides. One hundred percent fresh air was supplied directly to the environmental chamber after it was conditioned. The air conditioning system consisted of a 10 ton chiller unit that was connected to an air handling unit (AHU) equipped with a blower and an eight kilowatt heater.

3.2 Boeing Aircraft Test Cabin

The test cabin was a half-cabin model, with dimensions similar to those of a Boeing 767. A photograph of the cabin is shown in Figure 3-1. The half-cabin model was designed and constructed to match the computational fluid dynamics (CFD) model used by Boeing for their large eddy simulations (LES). Full dimensions of the test cabin are shown in Figure 3-2. The floor and one wall (back wall with the access door) were made out of plywood, while the rest of the walls were made of Plexiglas.

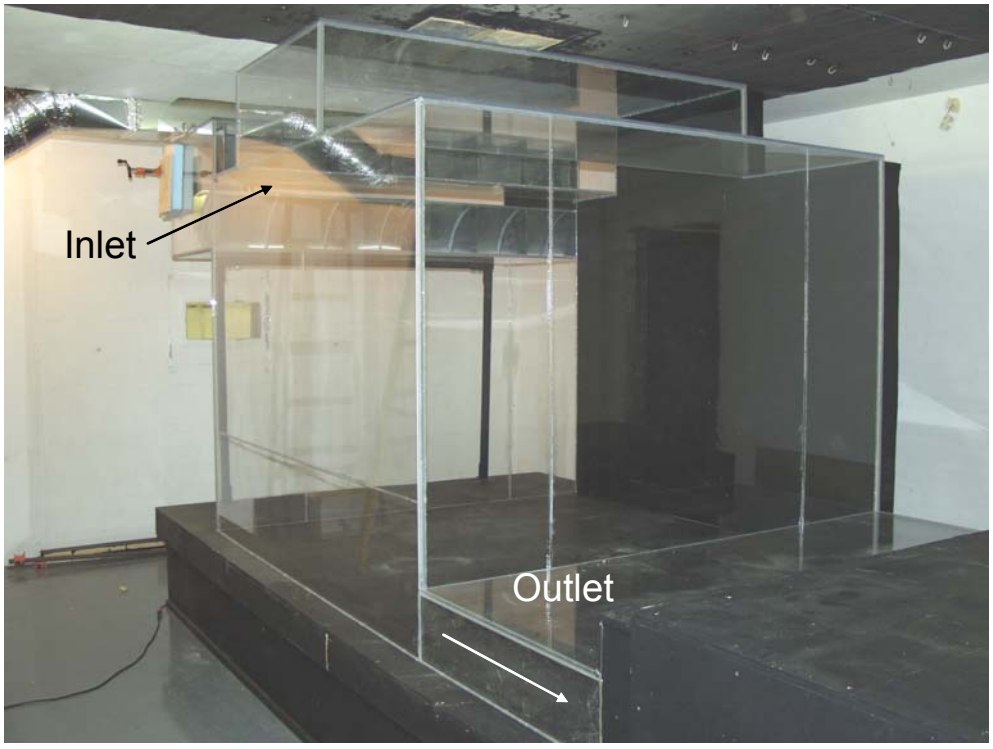

Figure 3-1: Half-cabin model of aircraft cabin section (test cabin).

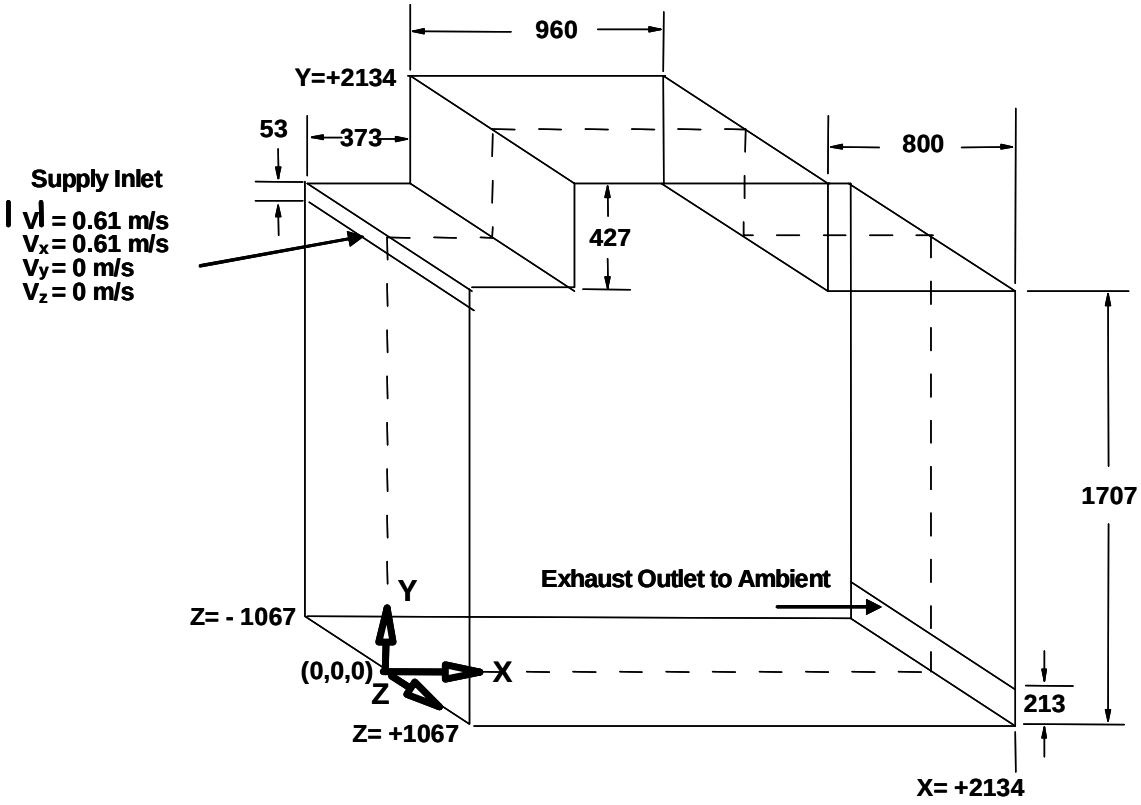

Figure 3-2: Schematic of half-cabin model (test cabin). Units are in mm.

The test cabin drew its air supply from the environmental chamber through a single inlet and exhausted the air through a single outlet. A one horsepower Madison Manufacturing (model PW11) radial pressure blower, powered by a Magnetek (model GPD205-1001, serial N9W0436-016-16) variable frequency system (VFD), was connected to the test cabin inlet by 203.2 mm (8 in) diameter, galvanized steel ducts. An identical blower, powered by a Yaskawa (model CIMR-V7AM22P2, serial 1W03X7345140083) VFD, was connected to the test cabin outlet. Both blowers were connected to Hewlett Packard (HP) 34970A data acquisition and control systems. The HP systems were controlled remotely by a LABVIEW program developed by P.A. Lebbin. See (Lebbin 2006) for details on the program. A calibrated, 101.6 mm (4 in) in diameter, Davis Inotek rotating vane anemometer (model A/4) and a type-K (Nickel-Chromium/Nickel-Aluminum) thermocouple (Omega model 5TC-TT-K-20-36) were located in the inlet duct and connected to an HP system to monitor the volumetric flowrate and air supply temperature, respectively. A 300 mm (12 in) square HEPA filter was also located in the inlet duct to ensure that the air supply into the cabin did not contain particles in the size range of interest. The HEPA filter had a manufacturer reported efficiency of 99.97% for particles with a diameter of 0.3 micron. Along the inlet, just before the nozzle that had a radius of 305 mm (12 in), a perforated board was installed to ensure uniform air velocity and distribution into the test cabin.

3.3 Particle Injection System

The particle injection system consisted of a vibrating orifice aerosol generator, a compressed air delivery system and an injection line with two different injection geometries. Each of these components along with their subcomponents is described in the following sections.

3.3.1 Vibrating Orifice Aerosol Generator

A TSI Vibrating Orifice Aerosol Generator (VOAG) system (TSI Model #3450, serial #70613226) was used to generate monodispersed particles. A photograph of the VOAG system is shown in Figure 3-3. The VOAG is capable of generating both liquid and solid particles of a desired size. Solid particles can be generated from sodium chloride solution, but the generated particles are not spherical because they are formed by re-crystallization of the solute when the solvent evaporates. Furthermore, the particles tend to accumulate and obstruct the injection system leading to a lengthy cleaning process before the VOAG can be used again. Therefore, only liquid particles were generated. The VOAG uses a solution of a solvent and solute to

generate liquid particles. The ratio of solute to solvent determines the particle size. After the initial particle is generated the solvent evaporates leaving the liquid solute particle of the desired size. To generate the solutions, two mass scales – a Mettler Toledo PR8002 and a Ohaus ARC210 – were used to weigh the amount of solvent (Certified ACS 2-Propanol) and solute (Dioctyl phthalate 99+% Phthalsaeure-bis-(2-ethylhexylester) (DOP) oil).

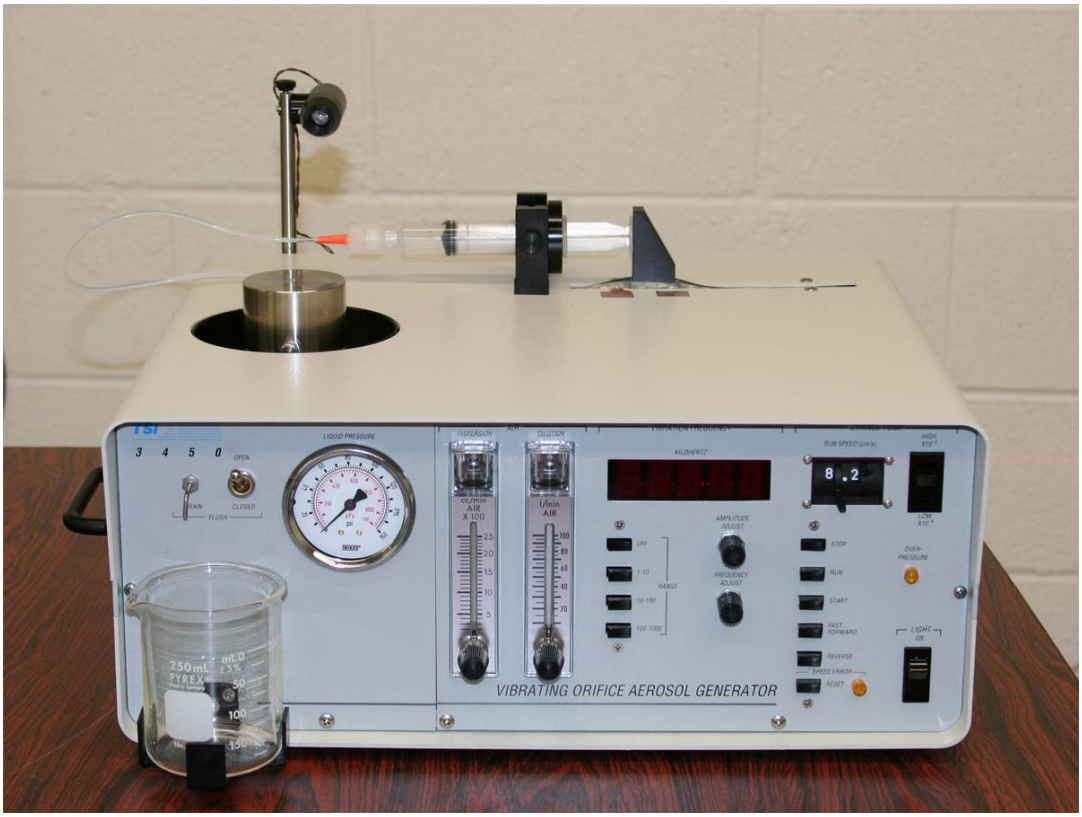

Figure 3-3: Vibrating orifice aerosol generator (TSI 3450).

A 20 mL or 60 mL syringe held the solution and a precise stepper motor injected the solution into the VOAG and through a 20 micron vibrating orifice. Due to the small diameter of the orifice and differences in its manufacturing, the optimum operating frequency had to be determined experimentally. This frequency was within the range of 49 to 69 kHz. The precise frequency was not critical, as long as the frequency was within about a third of a kilohertz and no satellite droplets were being formed. Satellite droplets are particles that are not of the desired size that can be formed in between particles of the desired size at certain frequencies. During each oscillation of the orifice a single particle was formed. The initial diameter of the particle was 40 microns for a 20 micron orifice. After the solvent (propanol) evaporated only the solute (DOP) particle of the desired particle size remained. Before being injected into the test cabin,

the particles passed through a TSI Aerosol Neutralizer (model #3054A) to neutralize any electrostatic charge. A diagram of the VOAG system is shown in Figure 3-4.

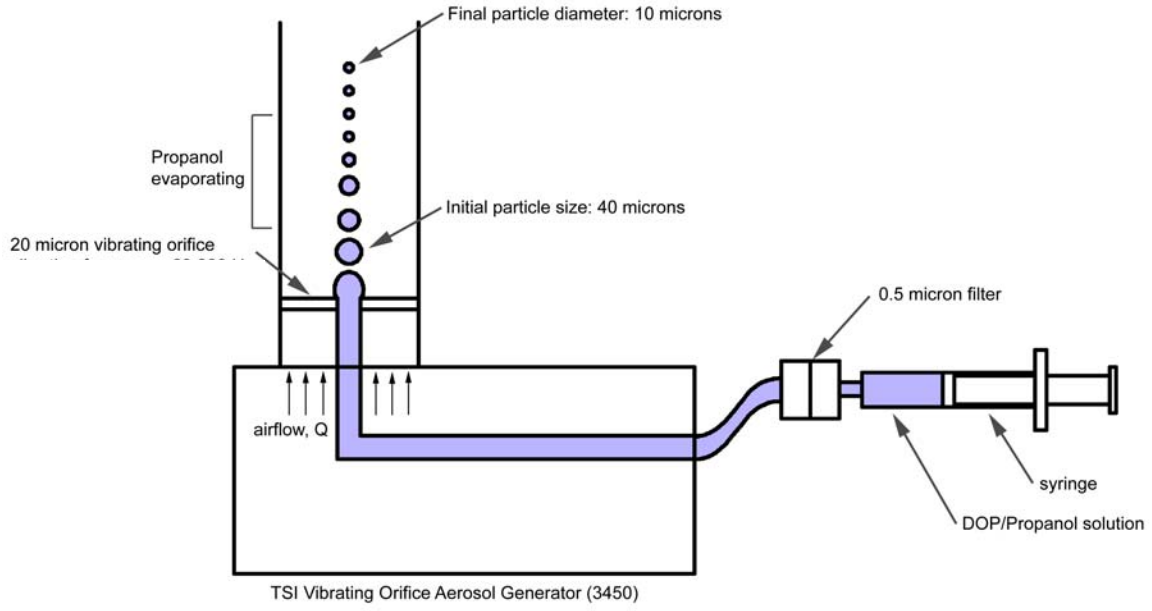

Figure 3-4: Schematic of vibrating orifice aerosol generator.

3.3.2 Compressed Air Delivery System

After the particles are formed by the VOAG they are diluted with a clean air supply and injected into the cabin. The air source was an Ingersoll Rand compressor (model SS3L3, serial 0612220236) equipped with a 60 gallon tank. After passing through 26000 mm (1032 in) of supply lines the air passed through a series of traps, filters and regulators to clean and condition the air and to decrease the pressure. Prior to entering the VOAG, the air passed through a Dayton water condensate trap and regulator (model 4ZK91) to remove the initial moisture from the air and reduce the pressure to about 50 psig. The air then passed through a Wilkerson condensate trap (model WSA-02-FM0B) to remove more moisture from the air. The pressure was then further decreased down to about 29 psig using a ControlAir Incorporated regulator (model 700). Then a Wilkerson desiccant drier (model X06-02-000) was used to remove the rest of the moisture present in the air stream. The desiccant was designed to remove moisture from 17 m^3 (600 ft^3) of high moisture air and could be replaced. A Wilkerson coalescing filter (model M08-02-BK00) was used to remove any contaminant particles larger than 0.5 μm. Then, the air pressure and flow were measured using a pressure gage and an Omega FL series

rotameter (model FL-115, serial 54217 with a glass float). Finally, the air passed through a TSI filtered air supply (model #3074B) before entering the VOAG.

3.3.3 Particle Injection Setup

After the diluted particles passed through the neutralizer, they entered 1372 mm (54 in) of PVC tubing before entering the approximately 1829 mm (72 in) long injection line. The injection line was a stainless steel tube with a 22.1 mm (1 in) inner diameter that routed the particles beneath the cabin before injecting them vertically into the cabin along the centerline of the half-cabin test section. Two different injection geometries were used in the cabin. The first was a vertical stainless steel tube that had an inner diameter of 22.1 mm (1 in) and a height of 595 mm (23.4 in). A schematic of the injection system, in relation to the test cabin and sampling locations, is shown in Figure 3-5 and a photograph of the injection tube inside the cabin is shown in Figure 3-6. The second injection geometry used was a diffuser cone made out of acrylonitrile butadiene styrene (ABS) plastic with dimensions shown in Figure 3-7.

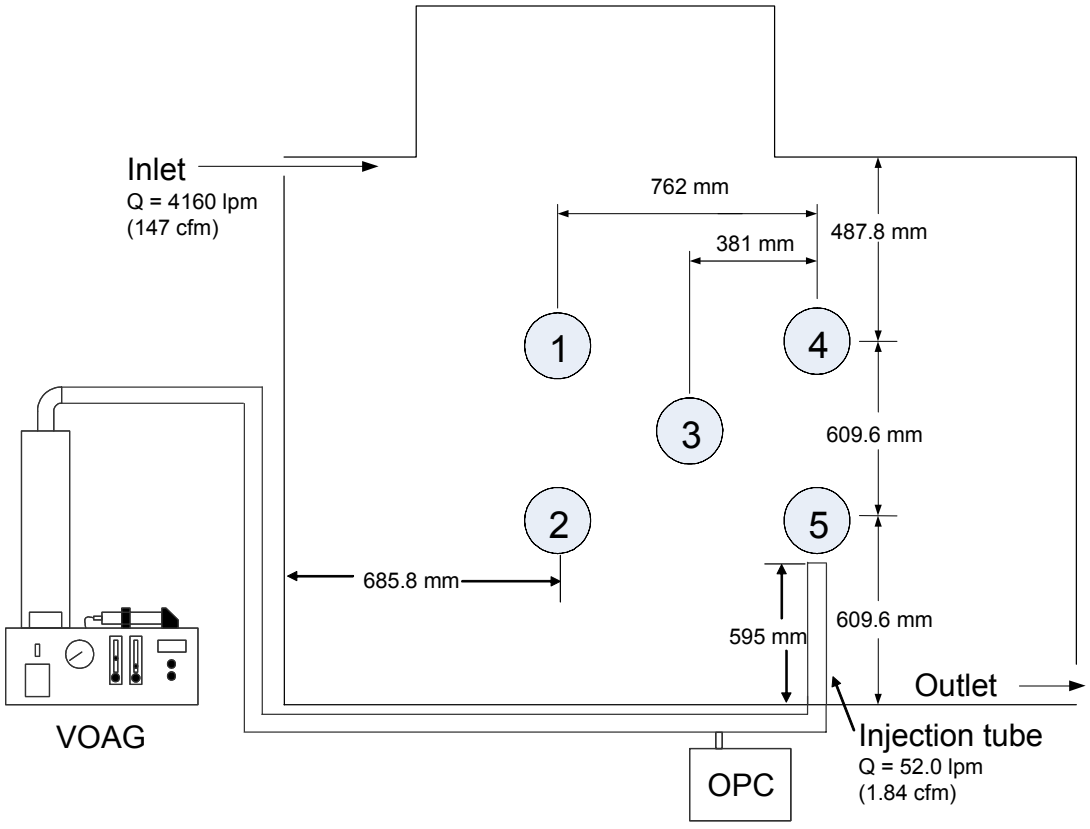

Figure 3-5: Schematic of injection setup relative to the test cabin and sampling locations.

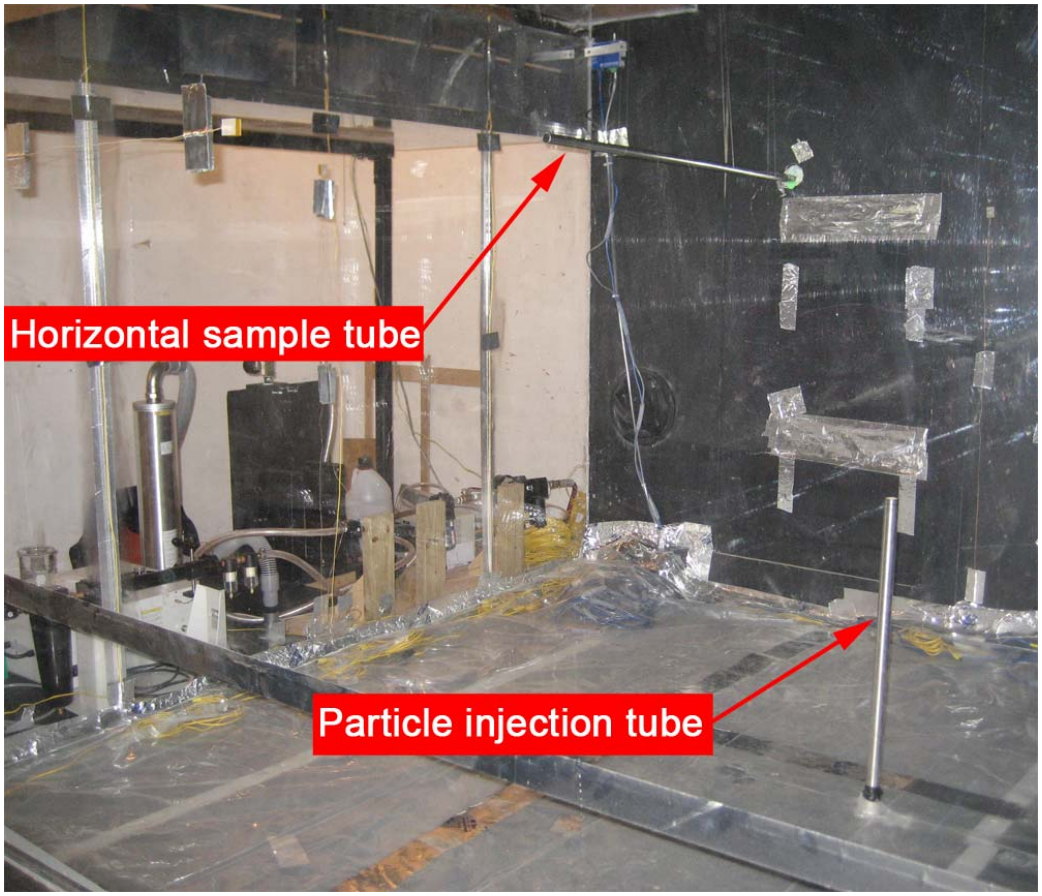

Figure 3-6: Photograph of injection tube and sampling tube (at location 1) in the test cabin.

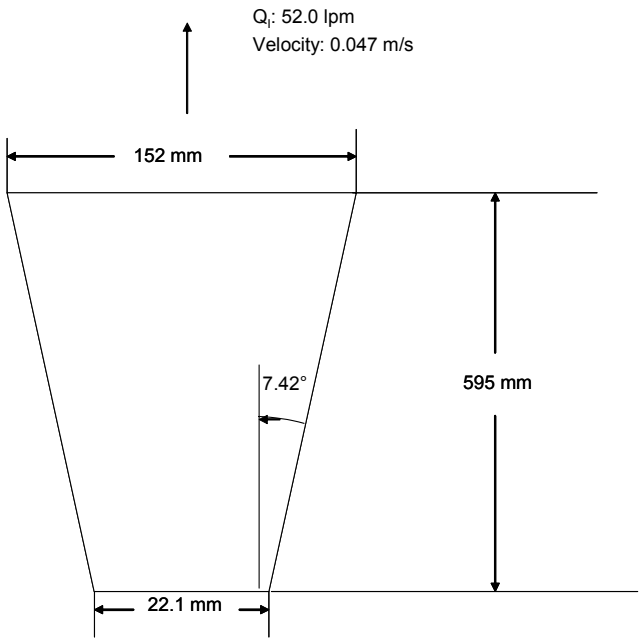

Figure 3-7: Injection cone schematic.

3.4 Particle Measurement

3.4.1 Aerodynamic Particle Sizer

The primary instrument used to measure the particle size and concentration in the test cabin was a TSI Aerodynamic Particle Sizer (APS) system (TSI Model #3321, serial #70626096). The APS specifications are shown below in Table 3-1. The APS uses the time-of-flight method described in Chapter 2 to determine particle size. A photograph of the APS device is shown in Figure 3-8. Data was collected by the APS via the Aerosol Instrument Manager (AIM) software that accompanied the device. The APS was located outside of the test cabin. Therefore, a 1000 mm (39.36 in) long horizontal stainless steel tube, with an inner diameter of 18.92 mm (0.745 in), was used to take a sample. A photograph of the sample tube inside the test cabin is shown in Figure 3-6. Connecting the stainless steel tube to the APS was 1220 mm (1219 in) of flexible PVC tubing, with an inner diameter of 38.1 mm (1.5 in). This was replaced partway through the testing with 1830 mm (72 in) of clear, braided, plastic PVC tubing with an inner diameter of 19.05 mm (0.75 in). This was done to reduce the number of connections and to reduce the possibility of particles getting caught in the small grooves of the tubing since the new tubing had a smoother interior wall. The particle loss in both of the sample tube assemblies was found experimentally; the procedure and results are described in Chapter 5.

Table 3-1: TSI Aerodynamic Particle Sizer specifications.

Range	0.5 to 20 μm
Channels	52 (logarithmic scale)
Size Resolution	0.02 μm at 1.0 μm diameter 0.03 μm at 10 μm diameter
Flow Rate	Total flow: 5.0 lpm ±1% Sheath flow: 4.0 lpm ±1% Aerosol Sample: 1.0 lpm ±10%
Atmospheric Pressure Correction	Automatic correction 400-1,030 mbar Full automatic correction 700-1,030 mbar
Concentration Limits	1,000 pt/cm^3 at 0.5 μm (2% coincidence loss) 1,000 pt/cm^3 at 10.0 μm (6% coincidence loss)
Communications	RS232
Operating Conditions	10 to 40°C (50 to 104°F) 10 to 90% RH

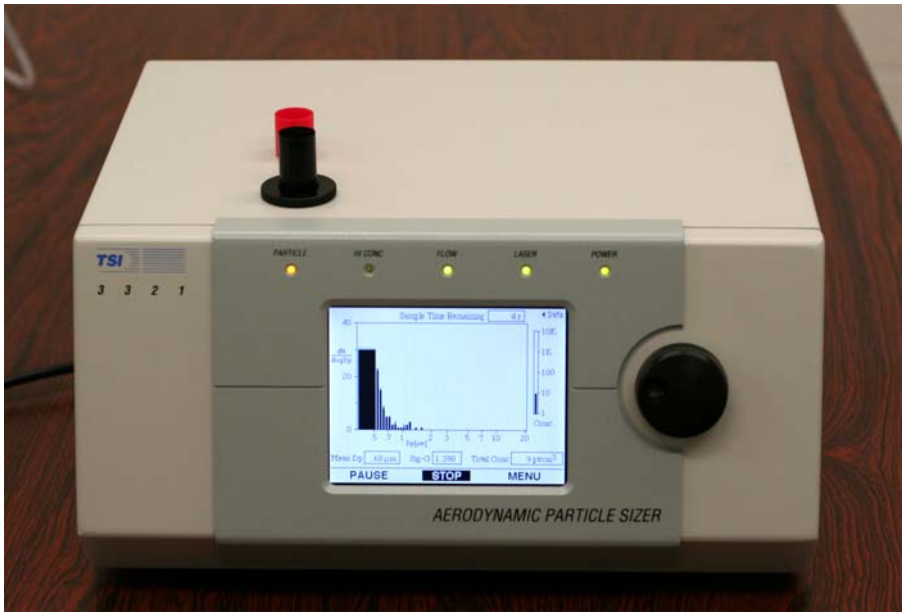

Figure 3-8: TSI Aerodynamic Particle Sizer (APS).

3.4.2 Optical Particle Counter

Four Lighthouse Remote 5014 optical particle counters (OPC) were used to measure the particle concentration in the inlet, outlet, particle injection line, and various locations inside the test cabin. The only OPC that was not located inside the test cabin was in the injection line. Figure 3-9 is a photograph of the injection line assembly with the OPC connections beneath the test cabin. For all of the other OPCs, the wiring went through a NEMA 4 enclosure on the plywood wall in order to maintain the test cabin's seal. One OPC was located inside the test cabin in the inlet to ensure only clean air entered the cabin. In later tests, another OPC was used to measure the concentration in the outlet. A photograph of the fourth OPC assembly, which was used to sample at various locations inside the cabin, is shown in Figure 3-10. That OPC was fitted with a sampling tube 300 mm (12 in) long and with an inner diameter of 15.2 mm (0.6 in). The flow rate through the sampling tube was 2.83 lpm (0.1 cfm) and the sampling velocity was 0.259 m/s (0.85 ft/s). The data for all four OPCs was taken using the same LABVIEW program that controlled the pressure and flow rate in the test cabin.

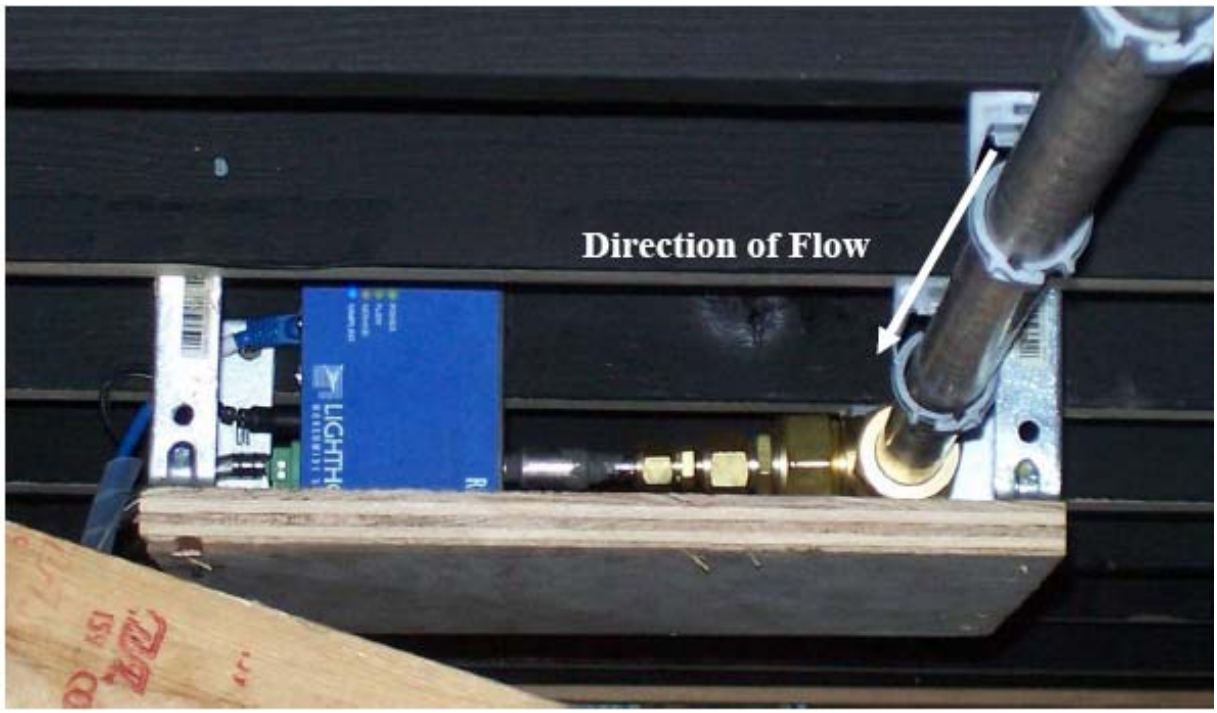

Figure 3-9: OPC in the injection line beneath the cabin.

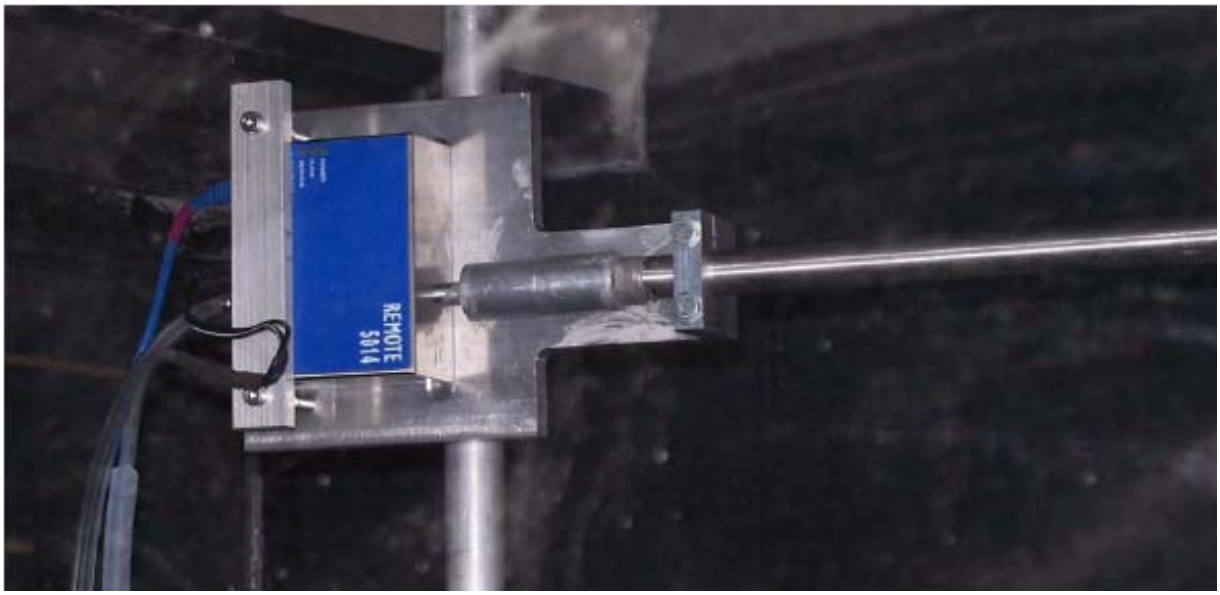

Figure 3-10: OPC assembly for sampling in the cabin.

The specifications for the Lighthouse optical particle counters are given in Table 3-2. As indicated in Table 3-2, the OPCs required a vacuum line connection capable of greater than 18 in Hg of vacuum to operate properly. This was achieved by connecting all four OPCs to an oilless rotary vane vacuum pump (model 0523-V350Q-G588DX, serial 0607600156) that had a ¼ hp

motor, and a maximum vacuum capacity of 26 in Hg. A pressure gage was used inline with the vacuum pump to monitor the pressure.

Table 3-2: Lighthouse remote 5014 optical particle counter (OPC) specifications.

Range	0.5 to 25 μm
Channel Sizes	0.5 and 5.0 μm
Flow Rate	0.1 cfm
Vacuum Requirements	Greater than 18 in Hg.
Counting Efficiency	50% @ 0.5 μm 100% @ 0.75 μm and larger
Concentration Limits	2,000,000 particles/ft^3 (5% coincidence loss)
Communications	RS-232
Operating Conditions	10°C to 40°C 20% to 95% RH

3.5 Temperature and Humidity

Temperature and later relative humidity and barometric pressure measurements were taken along with the concentration measurements. To measure temperature, type-K thermocouples were connected to the Hewlett Packard systems, which were in turn connected to the same LABVIEW program discussed above. These thermocouples were installed in various locations including the interior and exterior of each of the test cabin's walls. There were also three thermocouples installed along the inlet and three along the outlet of the test cabin. Finally, a thermocouple was also installed in the inlet air line and in the injection air line. Towards the end of the experiments, the relative humidity and the barometric pressure were measured using an Oregon Scientific, 433 MHz, cordless weather station located in the outlet of the test cabin.

CHAPTER 4 - **Procedures**

This section describes the procedures used to inject particles into the cabin and to measure them both before and after injection. It also describes how other measurements were taken. Moreover, it briefly describes the software used to take all of the measurements.

4.1 Measurement and Injection Locations

Particles were injected into the cabin through an injection tube or diffuser cone located at x=1447 mm (57 in), y= 595 mm (23.4 in) and z=0 mm. For the straight tube injection setup, particle concentration measurements were taken at each of the five locations shown in Figure 4-1, but only in the C-plane. Table 4-1 provides the (x, y) coordinates of each measurement location (1-5) and the five z-position planes (A-E) where concentration measurements were taken. After taking measurements with the straight injection tube, it was removed to avoid introducing a high speed air jet within the cabin and it was replaced by a cone of the same height. For the diffuser cone injection setup, particle concentration measurements were taken at each location, in each of the five planes. Later testing performed using the diffuser cone focused on taking measurements in the B, C and D planes only. Figure 4-2 shows a front view of the relative location of the injection setup with the diffuser cone installed, and Figure 4-3 shows an end view of the relative locations of the APS and sample tube.

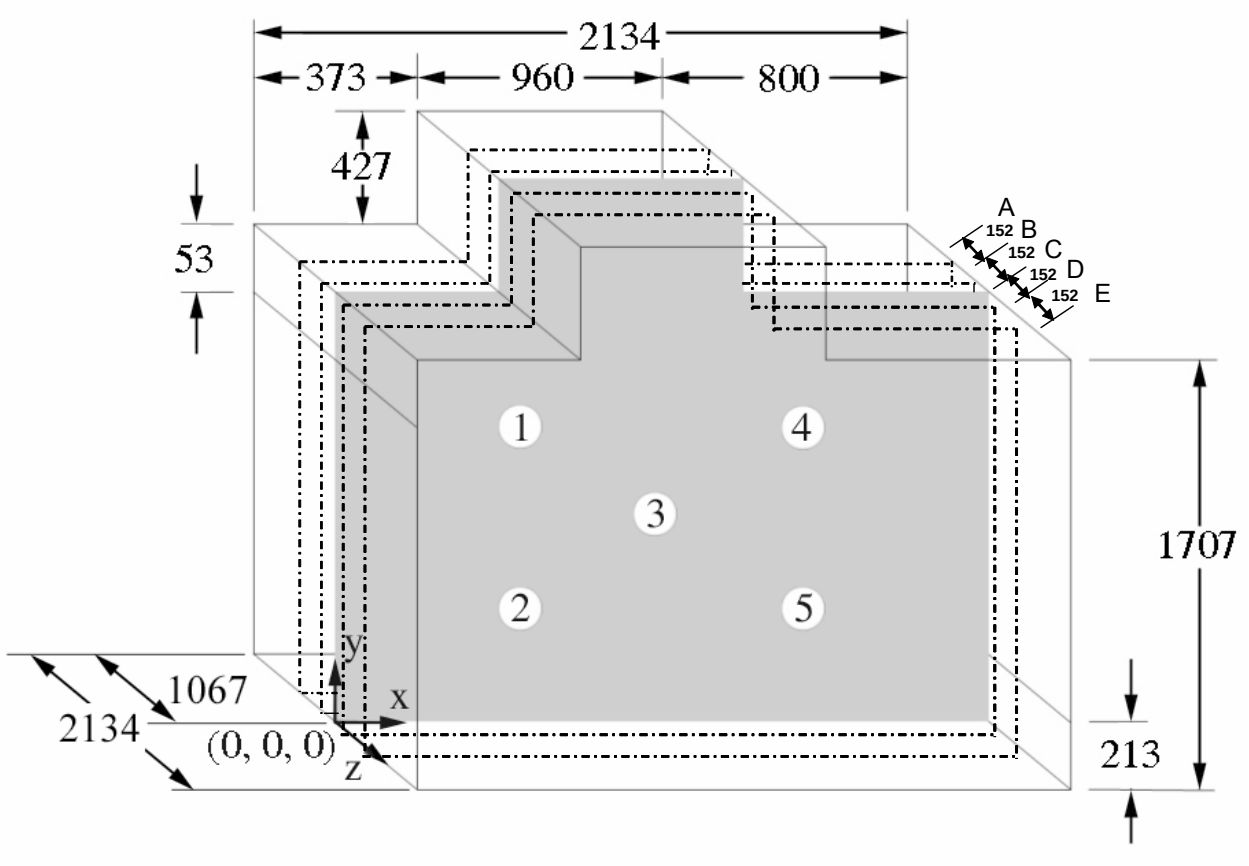

Figure 4-1: Particle measurement locations in the test cabin (units are in mm).

Table 4-1: Particle measurement locations.

Location	x (mm)	y (mm)	Plane	z (mm)
1	685.8	1219.2	A	-304.8
2	685.8	609.6	B	-152.4
3	1066.8	914.4	C	0
4	1447.8	1219.2	D	152.4
5	1447.8	609.6	E	304.8

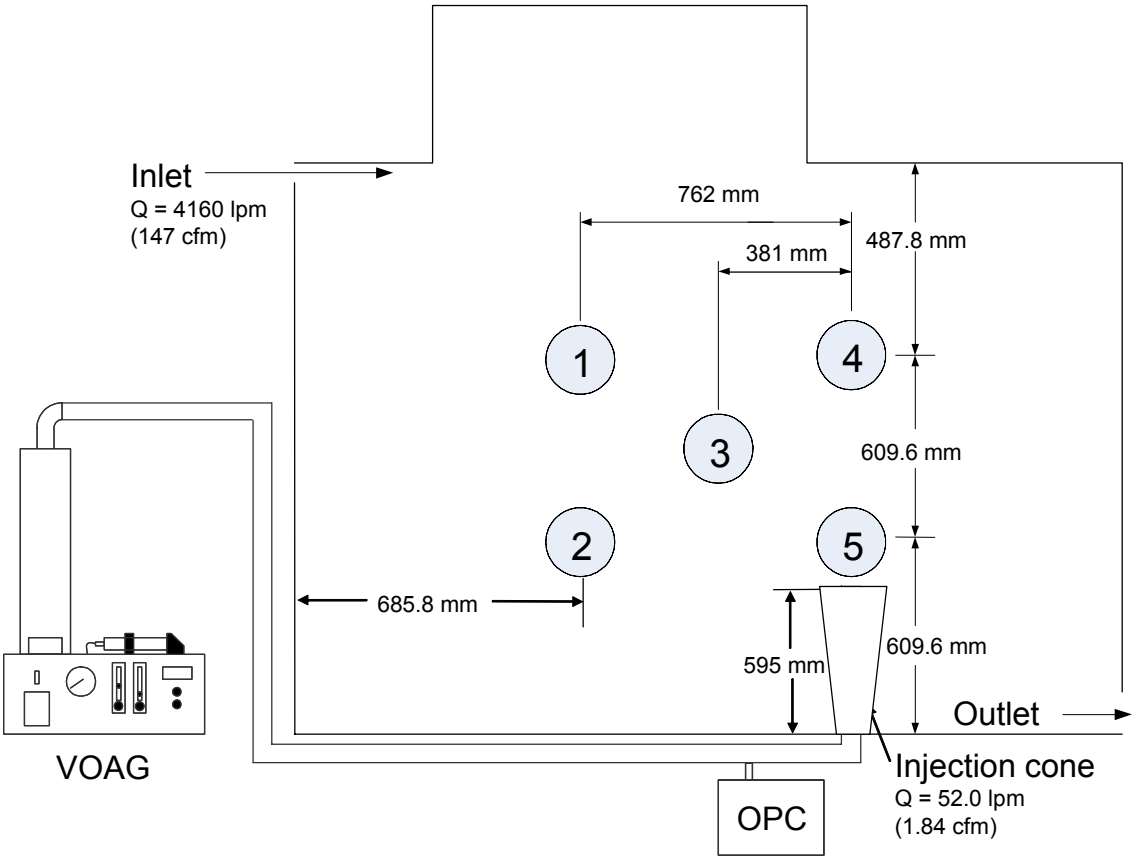

Figure 4-2: Test cabin measurement locations (z=0) with injection cone (front view).

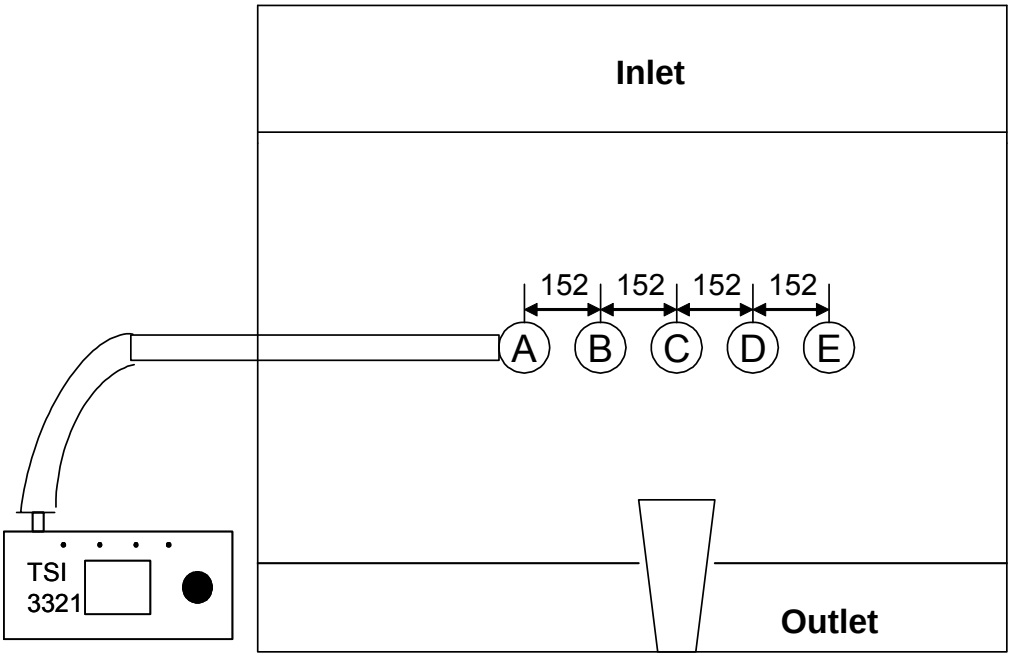

Figure 4-3: Test cabin measurement locations (units in mm) in the z direction (end view).

4.2 Injection and Sampling Procedure

Prior to measuring the concentration at each sample location, the test cabin was run for an hour to an hour and fifteen minutes. This was done by first turning on the blower connected to the outlet to establish the flow rate and then turning on the blower connected to the inlet to establish the cabin pressure. Thirty minutes of the start up time was allotted to ensure that the desired cabin pressure and the inlet flow rate had been reached and any residual particles in the cabin were flushed out. The flow parameters into and out of the cabin are shown in Table 4-2. Initially, the cabin pressure was set to 0 gage pressure. Later during the cone injection phase, the interior cabin gage pressure was changed from 0 in of H_2O to 0.025 in of H_2O, so that the interior of the cabin was at a slightly higher pressure than the ambient pressure outside of the cabin. To verify that the background concentration was zero for the size range that was being tested, a fifteen minute background sample was taken. The background concentration results and analysis can be found in Appendix B.

Table 4-2: Flow parameters into and out of the test cabin.

Location/Device	Cross Section	Length	Q (lpm)	Q (cfm)	V_{avg} (m/s)	Reynolds Number
Cabin Inlet	53 x 2134 mm (rectangular)	-	4160	147	0.640	4200
Injection						
Straight tube	22.1 mm diameter	595 mm	52.0	1.84	2.27	3300
Diffuser cone	22.1 mm inlet, 152 mm outlet diameter	595 mm	52.0	1.84	0.047	484
APS Sample Tube	18.9 mm diameter	1000 mm	5.00	0.177	0.296	370
Outlet OPC	2 mm diameter	25.4 mm	2.83	0.1	15.0	2000

After the background sample was taken, the VOAG was started and particles were injected into the test cabin. The VOAG was set to a vibration frequency of around 49 kHz, which yields a theoretical concentration of 54 particles/cm^3. Fifteen minutes were allotted to letting the VOAG warm up and to allow the particles to become well mixed in the cabin. The VOAG warm up time was later increased to thirty minutes near the end of the testing, because it was found that fifteen minutes was not sufficient to ensure that the concentrations at locations off the centerline had reached steady state.

Then particle count measurements were collected continuously at each sample location shown in Figure 4-1 over period of sixty minutes. For the straight tube injection, measurements were only taken on the C plane. For the cone injection, measurements were taken continuously on all five planes. Therefore, first measurements were taken on the E plane for sixty minutes. Then 200 seconds were allotted to move the sampling tube to the D plane, where measurements

were taken for another sixty minutes. The sampling tube was moved to each of the next planes (C, B and A) in this manner until measurements had been taken on all five planes. A single sample tube was used for taking measurements at all of the locations, so moving the sample tube from location to location could have an affect on the particle dropout in the tube.

Both the LABVIEW program and the AIM software were run continuously during both the warm up and sampling time. The LABVIEW program controlled the cabin air flow rate and the cabin pressure. It also collected temperature measurements from the thermocouples and concentration measurements from the OPCs. These measurements were taken every three seconds. A screen capture of the user interface window of the LABVIEW program used to collect data is shown in Figure 4-4. Full details of the program can be found in (Lebbin 2006) 2006). The AIM software that collected data from the APS took thirty second measurements continuously over the warm up and sampling time. A screen capture of the user interface window of the AIM software can be found in Figure 4-5. For the last set of testing the humidity and barometric pressure were also monitored using an Oregon Scientific weather station. These measurements were taken periodically (about once an hour) over the warm up and sampling time.

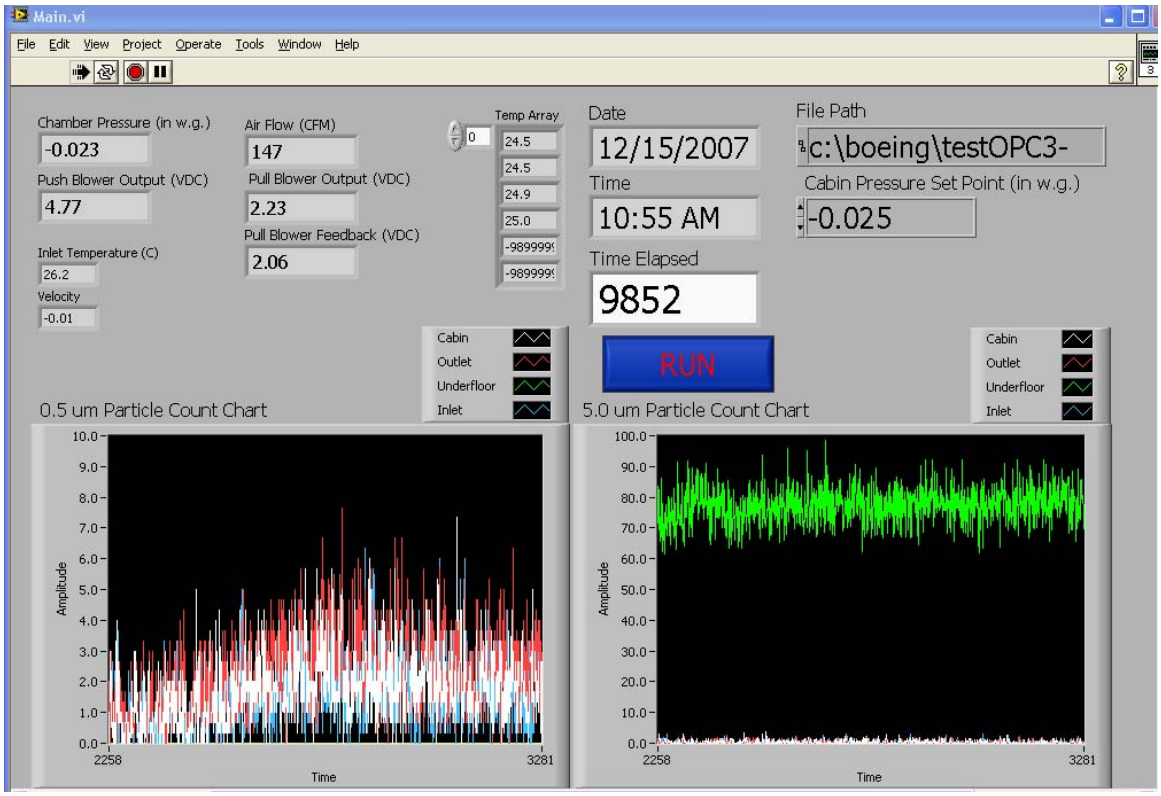

Figure 4-4: Screen capture of LABVIEW program used to monitor and collect data.

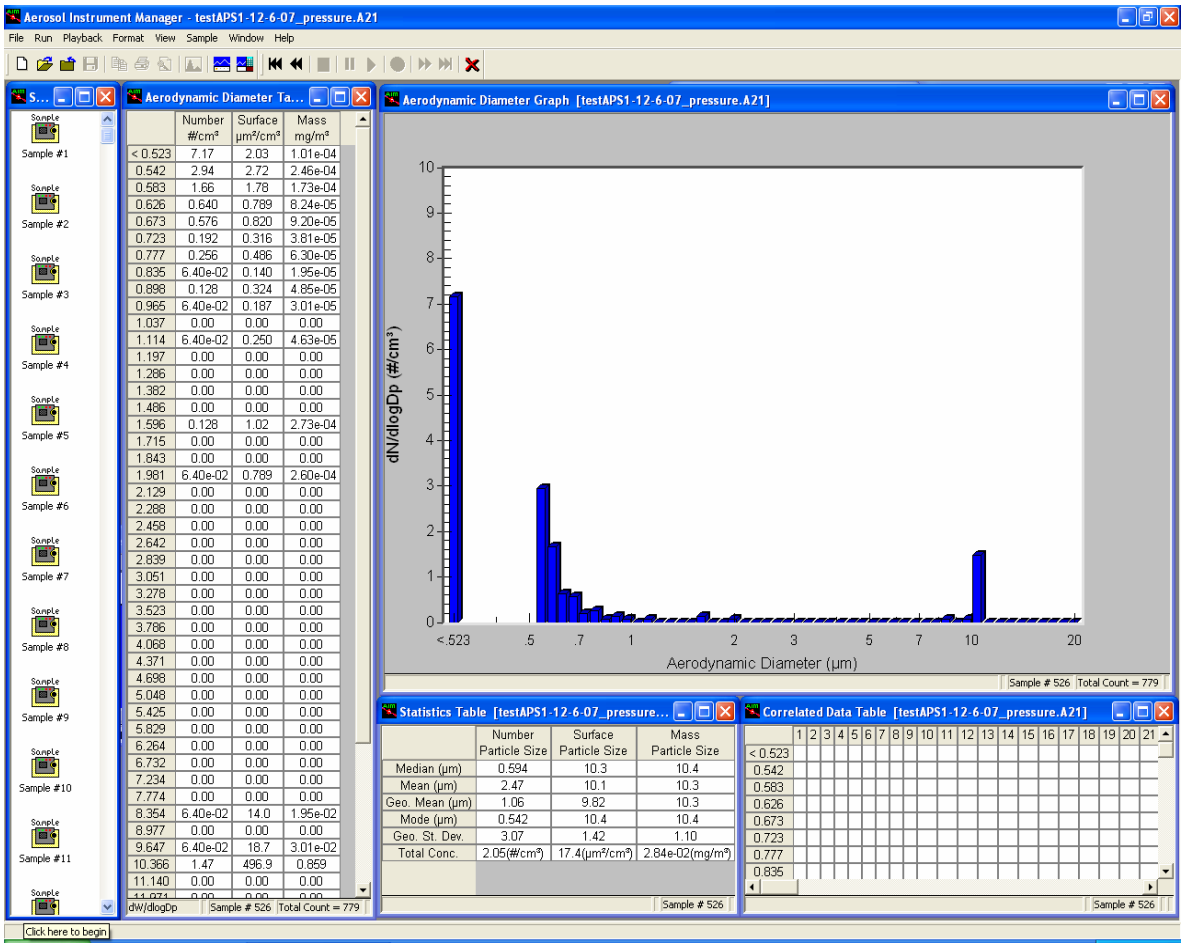

Figure 4-5: Screen capture of AIM software user interface window.

4.3 Outlet Sampling Procedure

Concentration data was also taken in the outlet for the ten micron particle testing. For the straight tube injection, the outlet concentration was measured, using an OPC, in a separately conducted experiment in order to determine the particle concentration profile in the outlet. The concentration was first measured at five locations approximately 356 mm (14 in) apart and 51 mm (2 in) above the cabin floor. Then to give increased resolution, the concentration was measured at six more locations around the centerline. Each new location was approximately 102 mm (4 in) apart and 51 mm (2 in) above the cabin floor. Figure 4-6 below shows a diagram of the outlet locations measured. Three second samples were taken for ten minutes at each location.

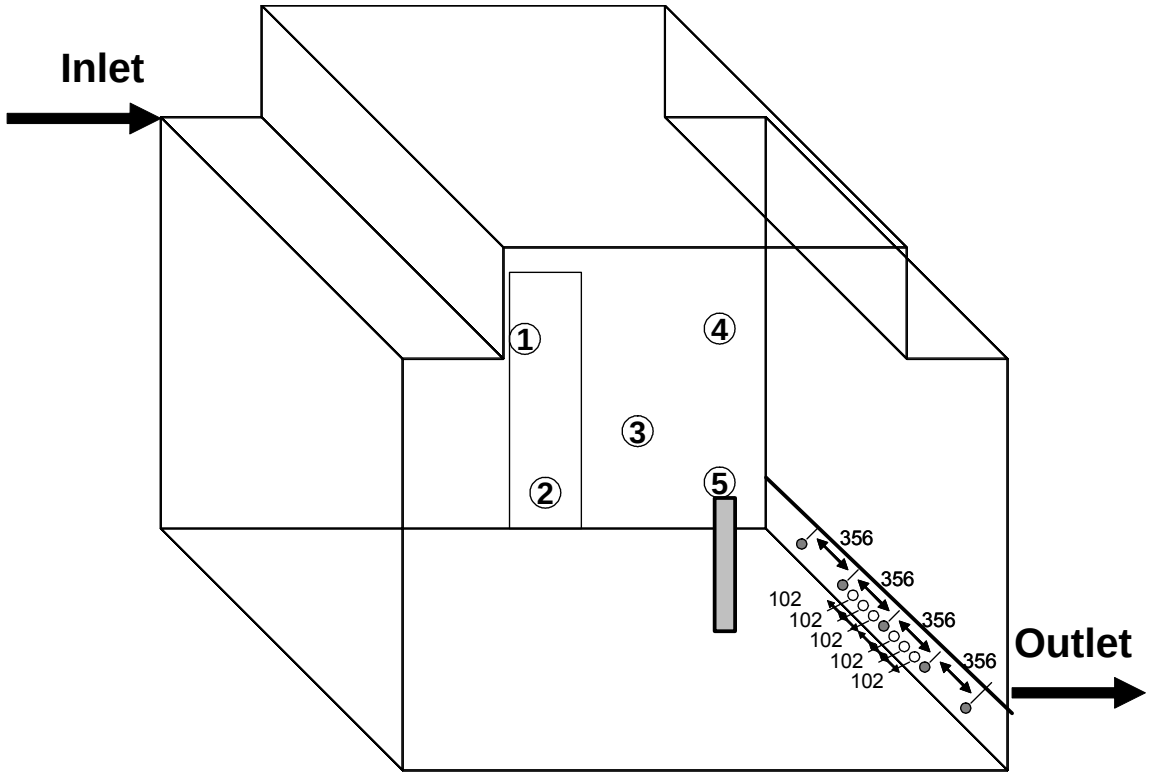

Figure 4-6: Outlet measurement locations in the test cabin. Units in mm.

For the cone injection, the outlet concentration measurements were taken simultaneously with the sample concentration measurements. Initially, a profile was measured in the outlet using and OPC. This was done by measuring the concentration in the planes (A-E) for an hour each. Refer to Figure 4-1 and Table 4-1 for the plane locations. It was found that the profile was nearly flat over this range. Then the OPC measuring the outlet concentration was placed in the C plane for the remainder of the testing. Later a third set of tests were taken using the APS to measure the concentrations in the test cabin outlet. The measurements were taken in the planes (A-E) for twenty minutes each. This was done for the cone injection with a positive interior cabin pressure only.

CHAPTER 5 - **Results**

This section first describes the adjustments and normalizations applied to the data. Then the data is presented with the adjustments applied. Further details on how the concentrations were calculated can be found in Appendix A. Supplemental test results, including background concentration data, can be found in Appendix B.

5.1 Data Normalizations and Adjustments

5.1.1 Particle Loss Adjustment

All of the concentration data had to be adjusted to account for the loss of particles in the tubing that went from the sample location to the aerodynamic particle sizer (APS). Initially, a rough estimate of the particle loss was calculated using the following procedure. Later the actual particle loss in the sampling tube was found experimentally. For the following calculation, only the particle loss in the horizontal, stainless steel tube is calculated, and the particle loss within the PVC tubing that connects the stainless steel tube to the APS is neglected. Furthermore, the round tube is modeled as a square duct. To calculate the percentage of particles lost in the sample tube it was assumed that a uniform particle concentration distribution entered the tube. Then the terminal settling velocity, V_{TS}, of a single particle was calculated from the following (Hinds 1999):

$$V_{TS} = \frac{\rho d^2 g}{18\mu} \tag{5.1}$$

where ρ is the density of the particle

d is the diameter of the particle

g is the acceleration due to gravity

μ is the dynamic viscosity of air at 20 deg C

Next, the time, t, the particle was in the sampling tube was calculated using:

$$t = \frac{L}{V_x} \tag{5.2}$$

where L is the length of the stainless steel sampling tube

V_x is the velocity in the axial direction of the sampling tube

Using the terminal settling velocity and the time the particle was in the tube, the vertical distance traveled in the tube (i.e., the vertical distance the particle fell due to gravity), y, was calculated using:

$$y = V_{TS} * t \tag{5.3}$$

The distance the particle fell was compared to the diameter of the sampling tube. If the distance the particle fell while in the tube was greater than the diameter of the tube then it was assumed that the particle drops out. If the particle density is uniform, then the fraction of particles that drop out, F_d, is the same as the fraction of area occupied by the dropped out particles entering the tube. The fraction of area and subsequently the fraction of the particles that dropped out was calculated as follows:

$$F_d = \frac{\Delta A}{A} = \frac{y}{D} \tag{5.4}$$

where D is the diameter of the sampling tube

A is the cross sectional area of the sampling tube

ΔA is the area occupied by the dropped out particles

The resulting fraction of particles that dropped out in the sampling tubing for the three micron particles was 0.047. For the ten micron particles, the resulting fraction was 0.526. Therefore, using this procedure, about five percent of the three micron particles were expected to dropout and just over half of the ten micron particles were expected to dropout in the horizontal, stainless steel tube sampling tube alone. However, these are only estimates because this method assumes a square geometry and a uniform velocity profile inside of the tube when in actuality the sampling tube is round and the velocity profile is presumably parabolic. Furthermore, not all of the particles that hit the tube wall may stick.

To find the actual particle loss in the sampling tube and to take into consideration the particle loss in the PVC tubing along with the particle loss in the horizontal stainless steel tube, the particle loss was measured experimentally. This was done by first measuring the concentration of particles produced by the particle generator. Then the particle generator was connected directly to one end of the sampling tube and the APS was connected to the other end via the PVC tubing. By comparing the two concentration measurements, a particle loss of 10% was found for the three micron particles. All of the three micron data collected using the APS

was corrected using the 10% adjustment instead of 4.7%. This same procedure was done for the ten micron particles and the experimental particle loss was found to be 61%. Later this procedure was repeated for the ten micron particles when the flexible PVC tubing was replaced with the clear braided PVC tubing. (The braiding was within the tube walls to reinforce the tube walls; therefore, the walls were smooth.) The particle loss percentage found after the PVC tubing was changed was 68%. As with the three micron data, the experimental particle loss in the sample tube was used to correct the data.

Some of the ten micron data were collected using an optical particle counter (OPC), and the theoretical particle loss for the sample tube connected to the OPC was 28%. The theoretical particle loss for the OPC was calculated in the same manner described above for the particle dropout for the APS. An experimental test was not performed to determine experimentally the particle loss in the OPC sample tube, so the theoretical particle loss was used to correct the ten micron data taken using the OPC.

5.1.2 Concentration Normalizations

Along with accounting for the particles lost in the sampling process, the particle concentrations were also normalized. Both the three micron and the ten micron particle concentration data were normalized. This normalization took into consideration the airflow into the cabin through the inlet and the injection as well as the number of particles injected. A HEPA filter was installed on the inlet to the test cabin so the number of particles that entered the cabin through the inlet airflow was negligible. This was verified experimentally. The normalized concentrations, C, were calculated as follows:

$$C = \frac{C_m \times Q_{\text{sup}}}{C_I \times Q_I} \tag{5.5}$$

where C_m is the measured sample concentration corrected for particle loss
in the sampling tube
C_I is the calibrated injected concentration
Q_{sup} is the supply flow (inlet and injected)
Q_I is the injected flow

Details of how each parameter in equation (5.5) was calculated can be found in Appendix A.

5.2 Three Micron Particles Straight Tube Injection Results

The following results are for the three micron particles. The cabin was at 0 inches of water gage pressure and the particles were injected into the cabin through a straight, vertical tube. Each location was sampled twice and all the measurements were taken on the C plane (centerline). The results, given in Figure 5-1 below, show that the injection normalized concentration ratio is about one for all of the locations except for location 4 and location 5. Locations 4 and 5 were above and at the injection site, respectively. The estimated uncertainty of 20% is also shown on the figure. The sample locations were described in Chapter 4 and the estimate of the uncertainty is calculated in Chapter 6.

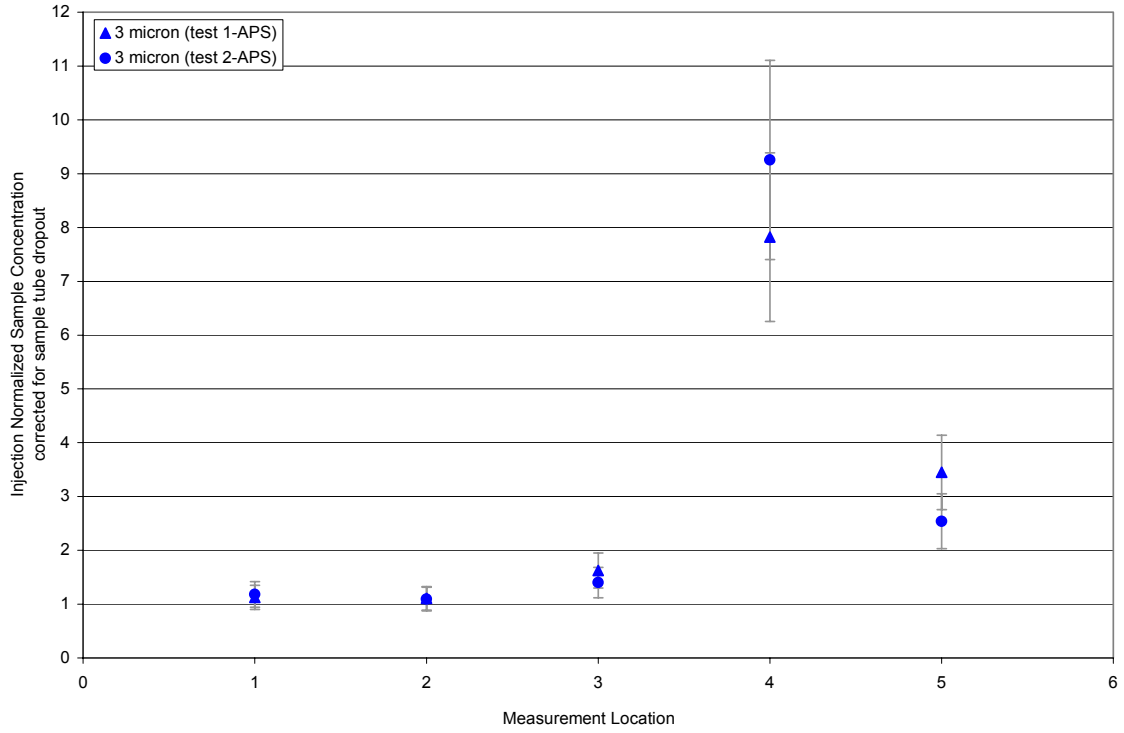

Figure 5-1: Injection normalized concentration at each location for three micron particles.

5.3 Results for Ten Micron Particles

5.3.1 Straight Tube Injection

The following results are for the ten micron particles that were injected through a straight vertical tube. The cabin was at 0 inches of water gage pressure. The results with an uncertainty estimate of 39% are shown in Figure 5-2, and a zoomed-in view is shown in Figure 5-3. In both

figures it can be seen that the injection normalized concentration ratio is well below unity for all of the locations except for location 4, which is directly above the injection site.

The results for the outlet concentration for ten micron particles through the straight injection tube are shown in Figure 5-4. The outlet profile is asymmetrical, with the peak occurring 152 mm (6 in) off the centerline.

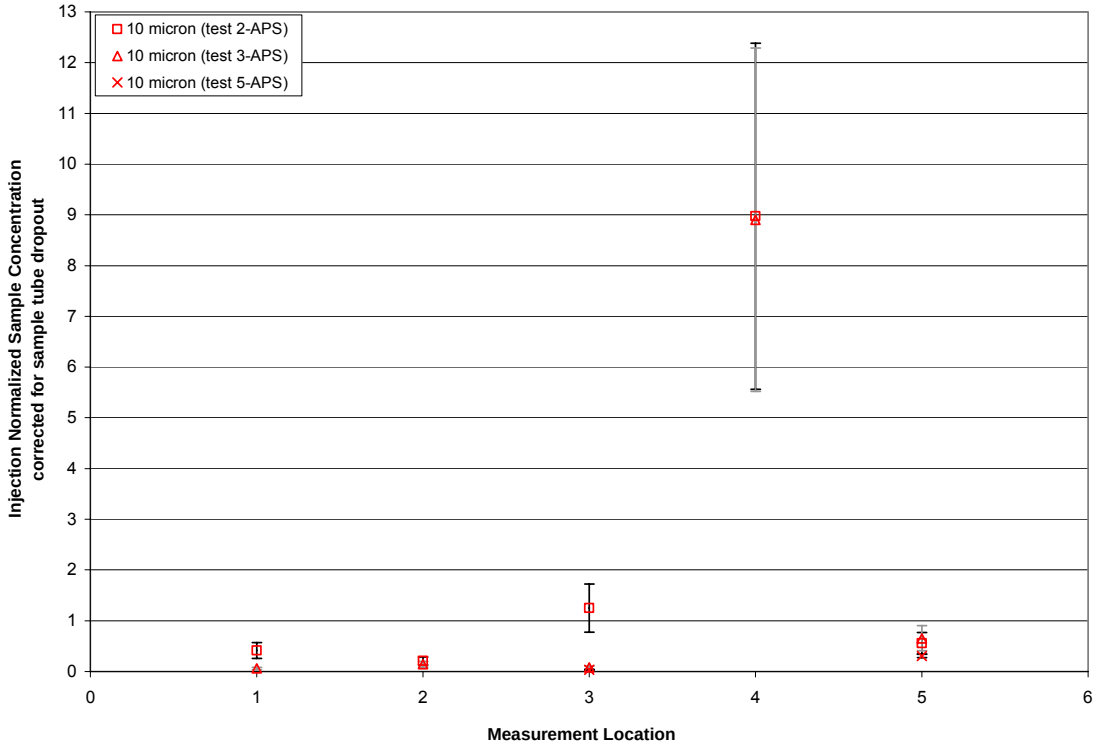

Figure 5-2: Injection normalized concentration for ten micron particles.

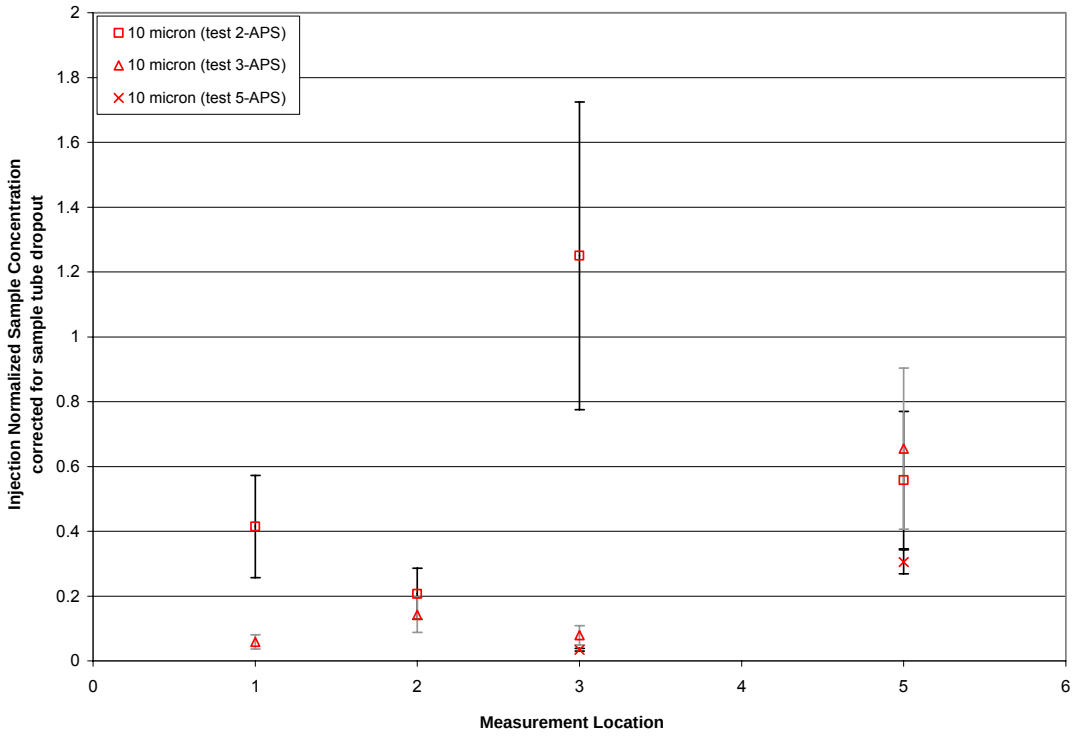

Figure 5-3: Zoomed-in view of injection normalized concentration for ten micron particles.

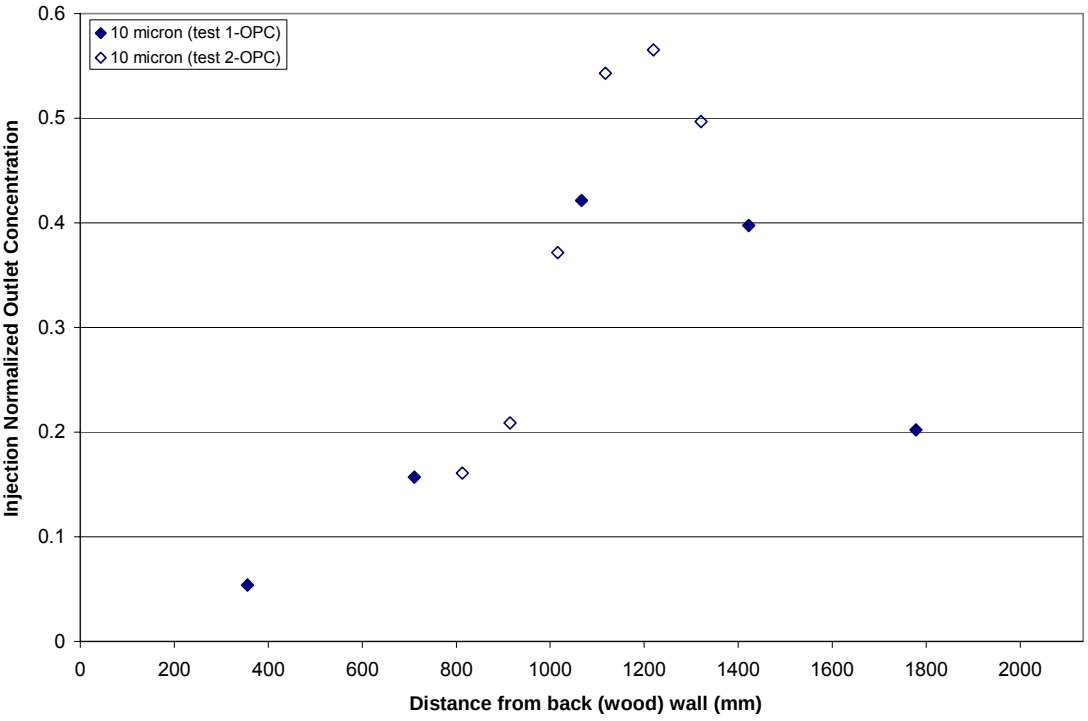

Figure 5-4: Injection normalized concentration at each outlet location in the test cabin.

5.3.2 Diffuser Cone Injection

In order to reduce the velocity of the particles into the cabin, the straight injection tube was replaced with a diffuser cone. The injection of particles was kept unchanged at location 5. The following tests were taken with a diffuser cone at the injection and with an interior cabin gage pressure of 0 inches of water. Figure 5-5 through Figure 5-9 show the ten micron injection normalized, sample concentration at each measurement location in the test cabin. Each test was performed twice at each location. The figures show that not only is there a substantial difference in concentration from one test to the next, but there is also a difference in the trend of the curve going from one location (A-E) to the next.

As in the case of the straight tube injection, the concentration in the outlet was measured at various positions along its length. Figure 5-10 shows the results for the outlet concentration with the cone injection. Unlike the straight tube injection the outlet profile is relatively flat.

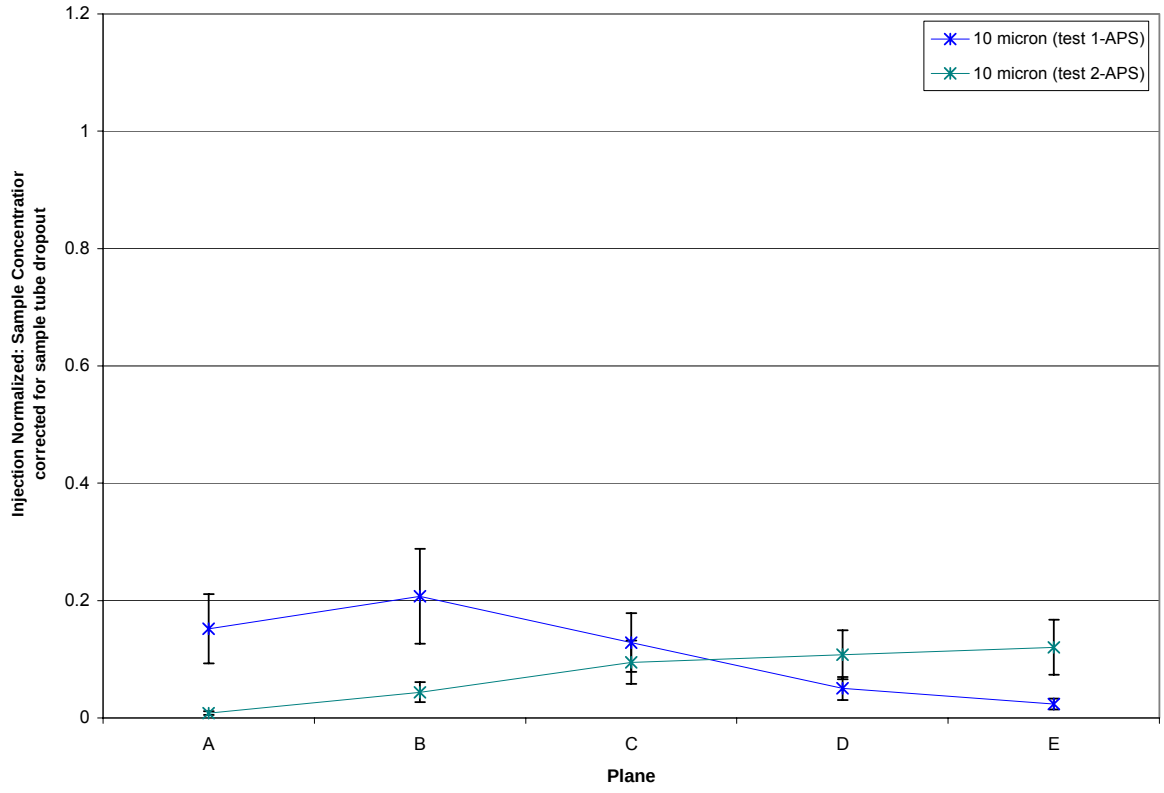

Figure 5-5: Injection normalized sample concentrations at location 1.

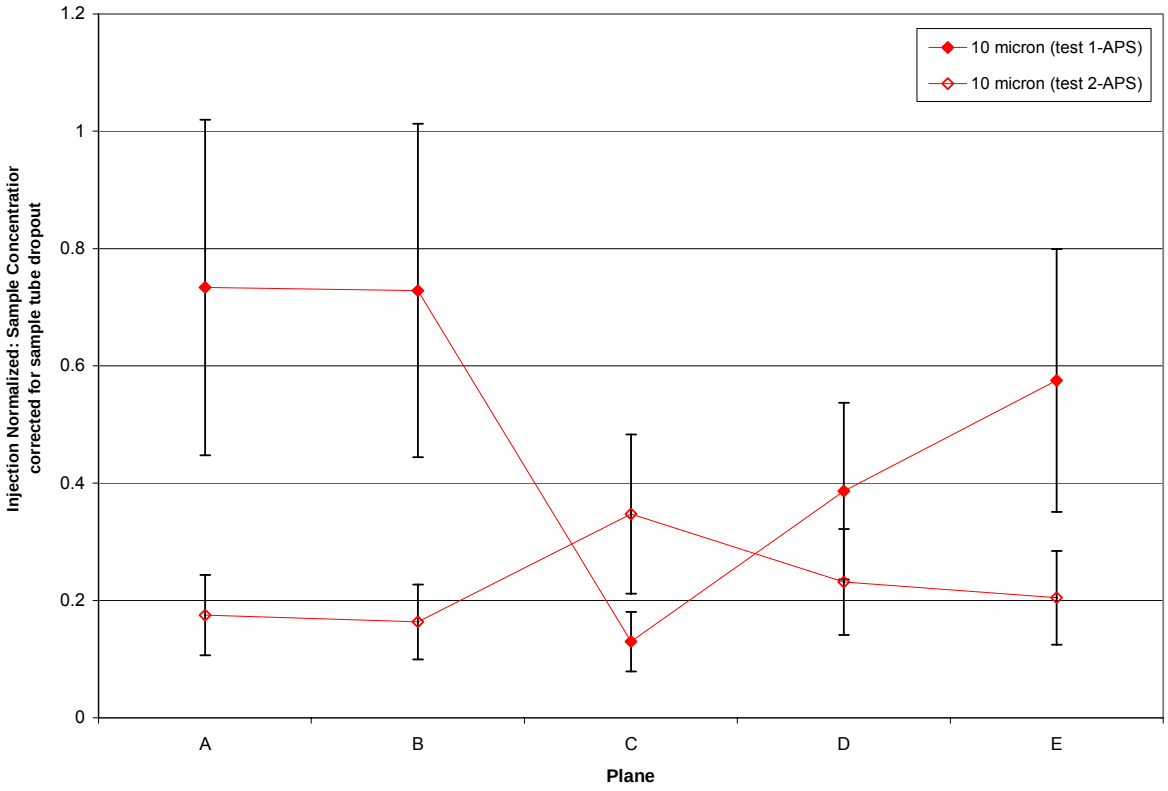

Figure 5-6: Injection normalized sample concentrations at location 2.

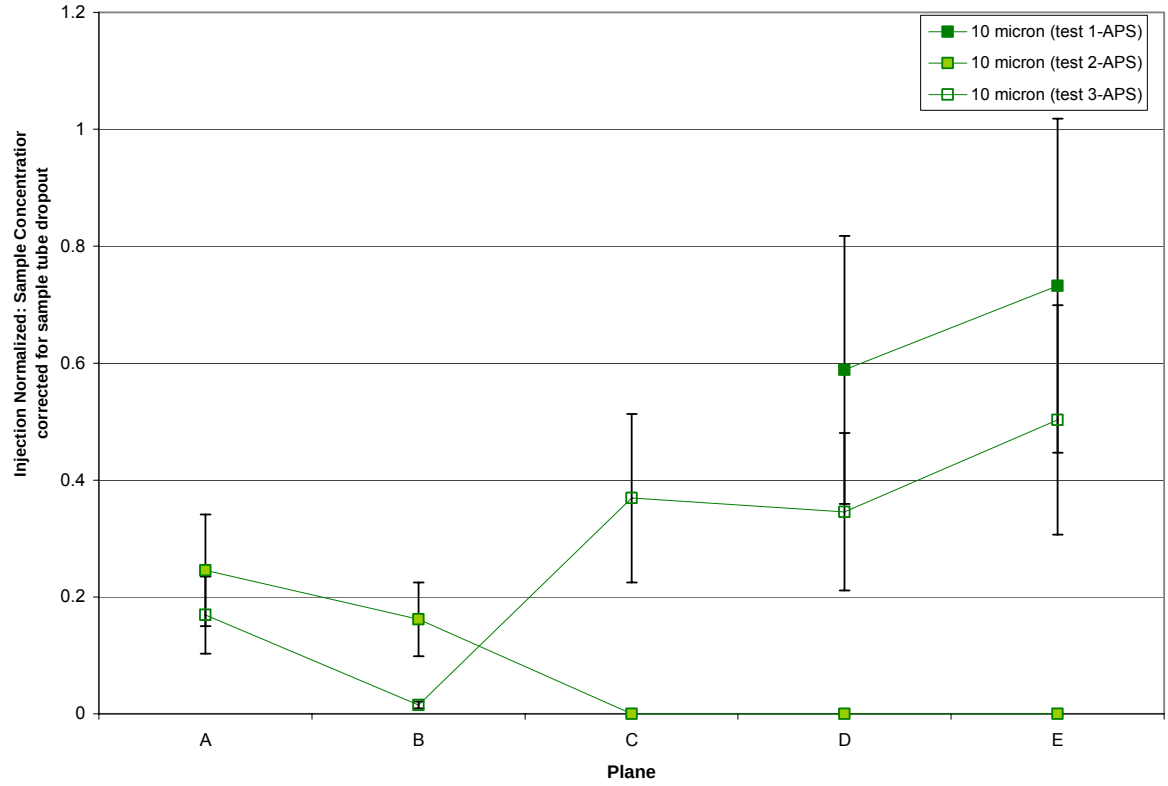

Figure 5-7: Injection normalized sample concentrations at location 3.

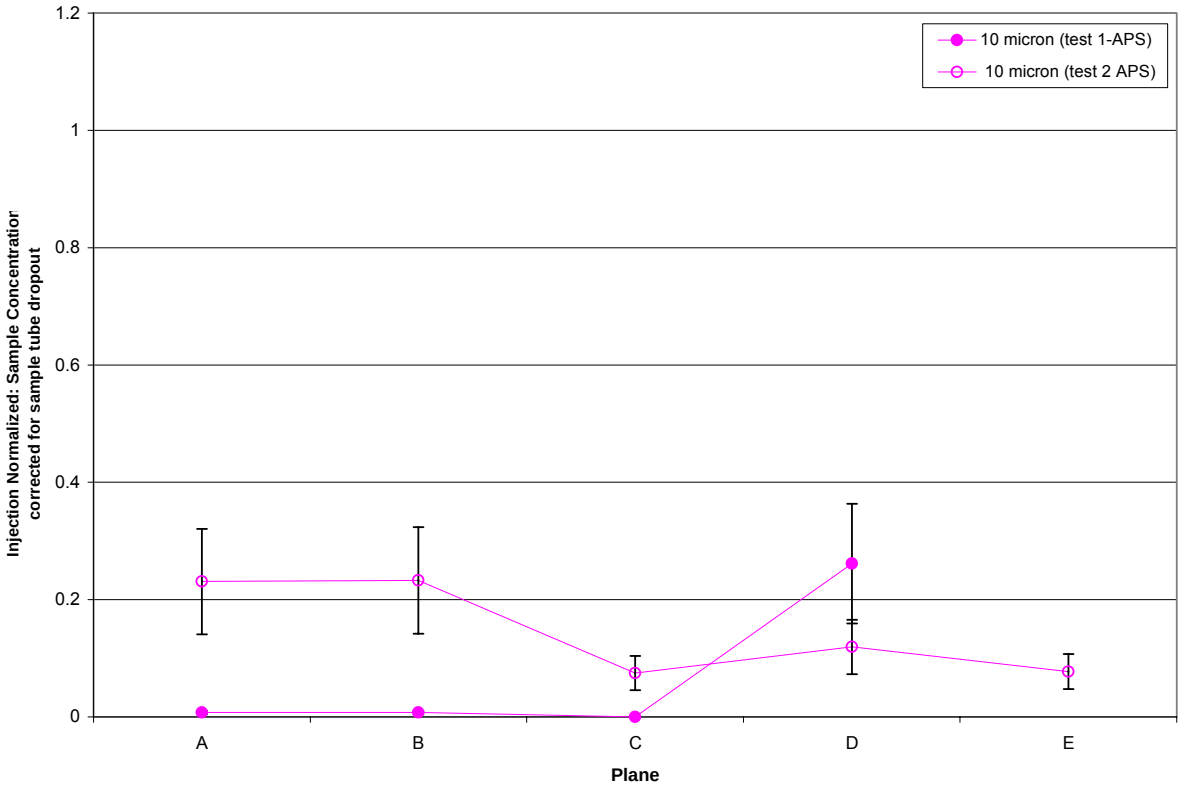

Figure 5-8: Injection normalized sample concentrations at location 4.

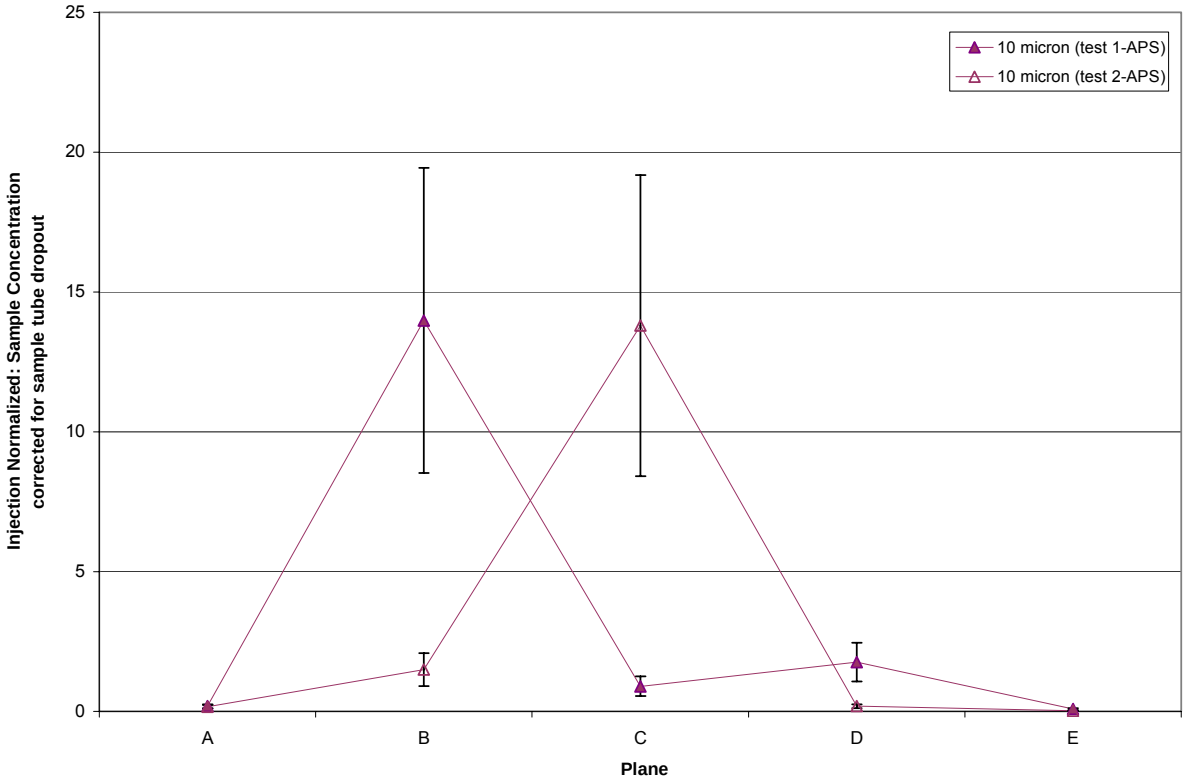

Figure 5-9: Injection normalized sample concentrations at location 5.

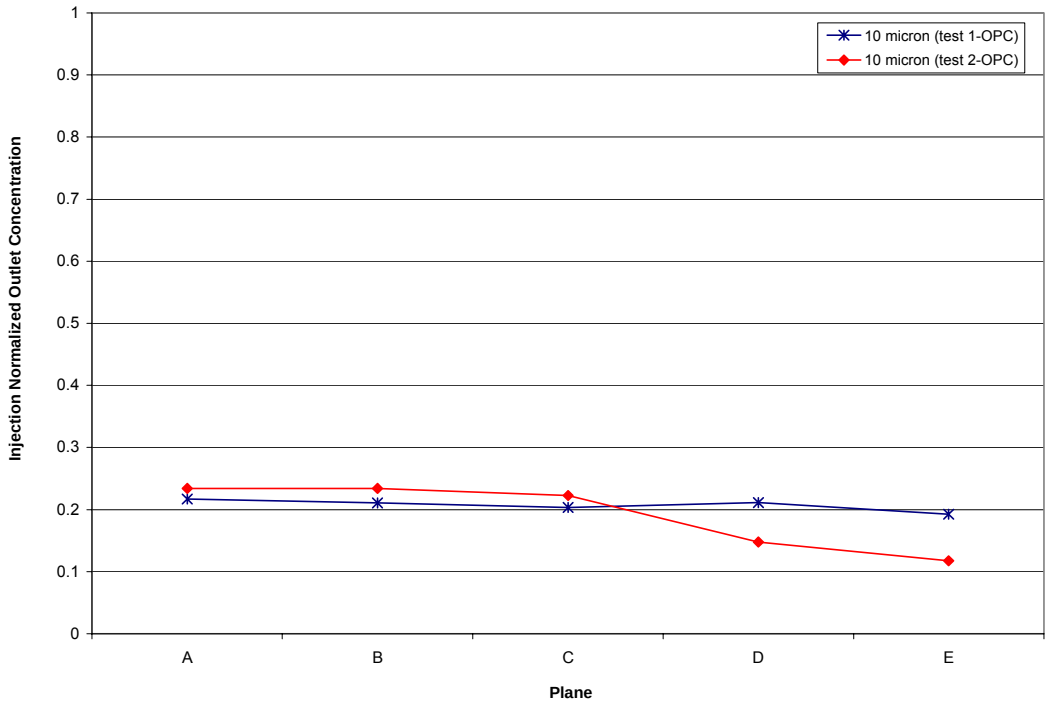

Figure 5-10: Injection normalized outlet concentration with cone injection.

Due to the inconsistency of the concentration profiles presented in the figures above, the cabin pressure was increased above ambient pressure. The idea to investigate the effect of cabin pressure came from a previous study performed by Lebbin 2006. In the study, cabin pressure had an effect on carbon dioxide measurements in the test cabin. It was found that the flow in the test cabin was bi-stable so sometimes the flow would tend to flow towards the front of the cabin and sometimes it would tend to flow towards the back of the cabin (the front of the cabin being the positive z direction as shown in Figure 4-1 in Chapter 4). Due to leakage through the wall with the access door, pressurizing the cabin can induce the flow to repeatedly go in one direction. Further explanation on the investigation of the effect of pressure on particle concentration measurements can be found in Chapter 6.

All of the following tests were conducted with the interior of the cabin pressurized to 0.025 inches of water. The sample line tubing was also replaced and installed with tighter connections. Figure 5-11 through Figure 5-14 show the normalized concentration at each of the locations in the test cabin. They also show the average for each location with the nominal estimated uncertainty calculated in Chapter 6 applied to it. Figure 5-15 shows the injection normalized outlet concentration profile taken using the APS. The outlet profiles are roughly parabolic and the average normalized concentration is approximately 0.56 for all three tests.

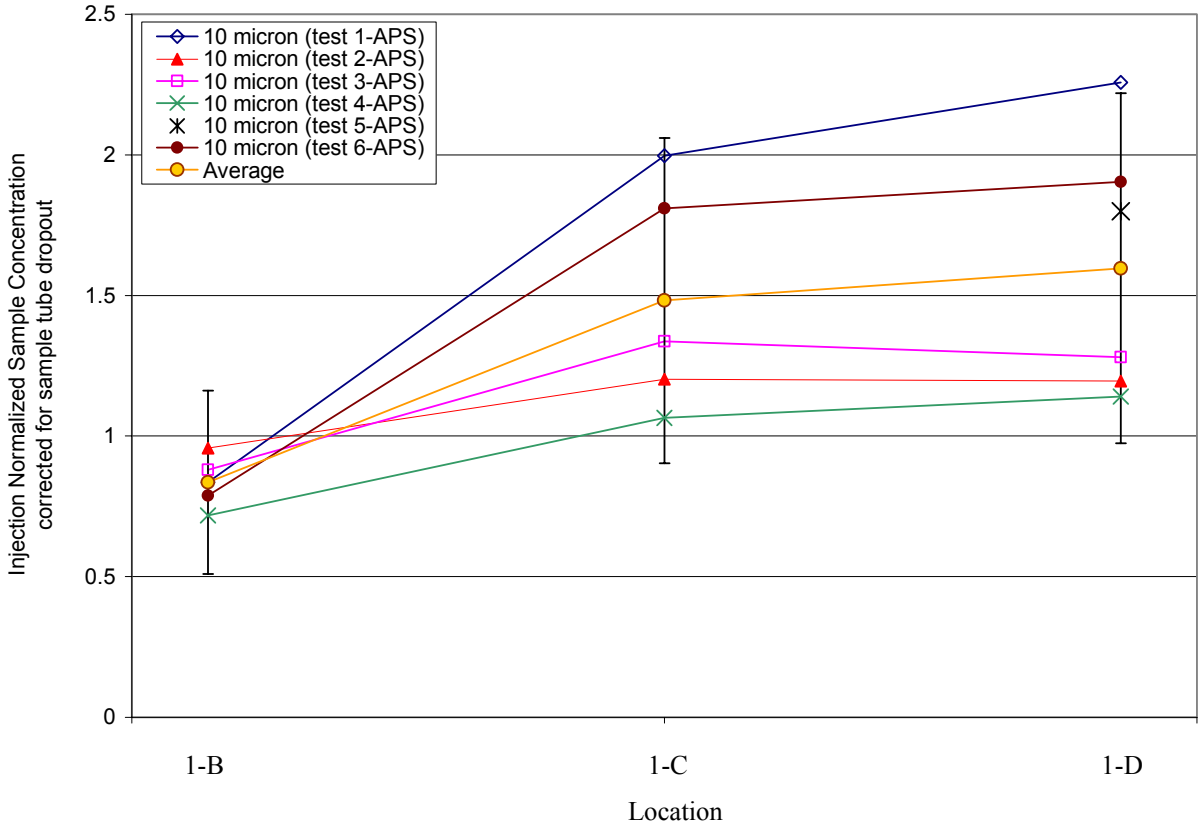

Figure 5-11: Injection normalized sample concentrations at location 1.

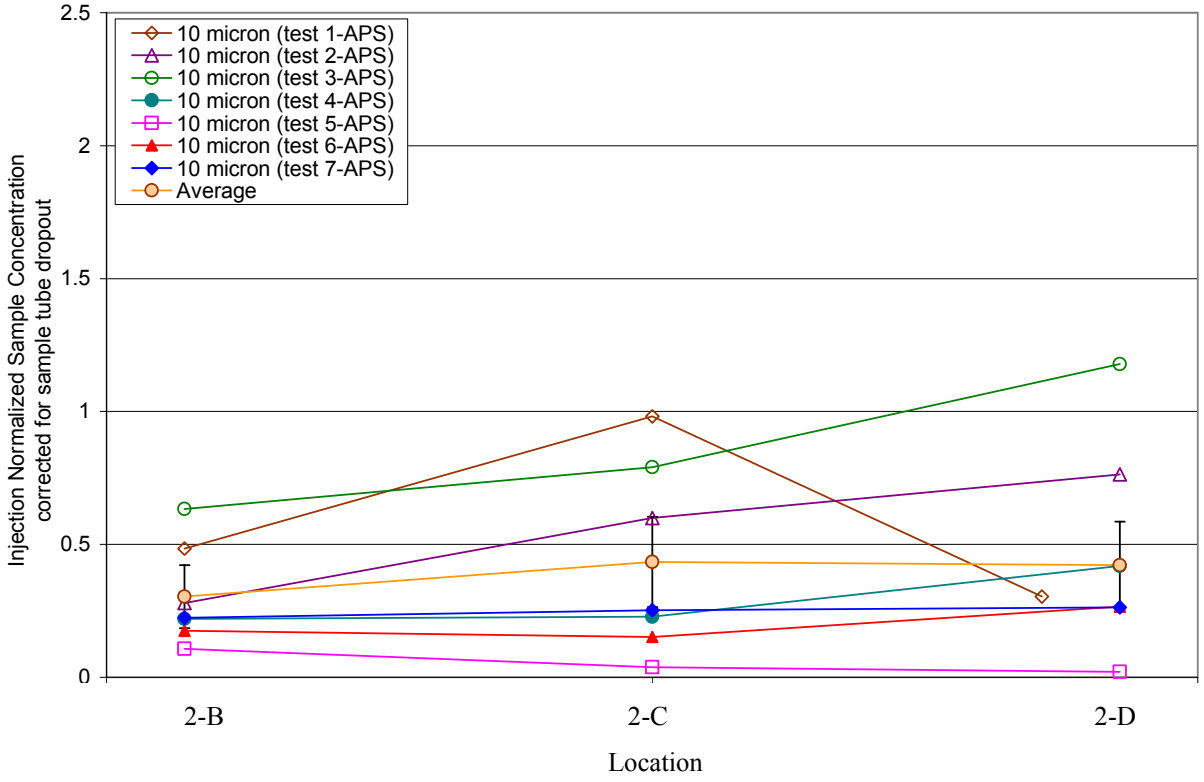

Figure 5-12: Injection normalized sample concentrations at location 2.

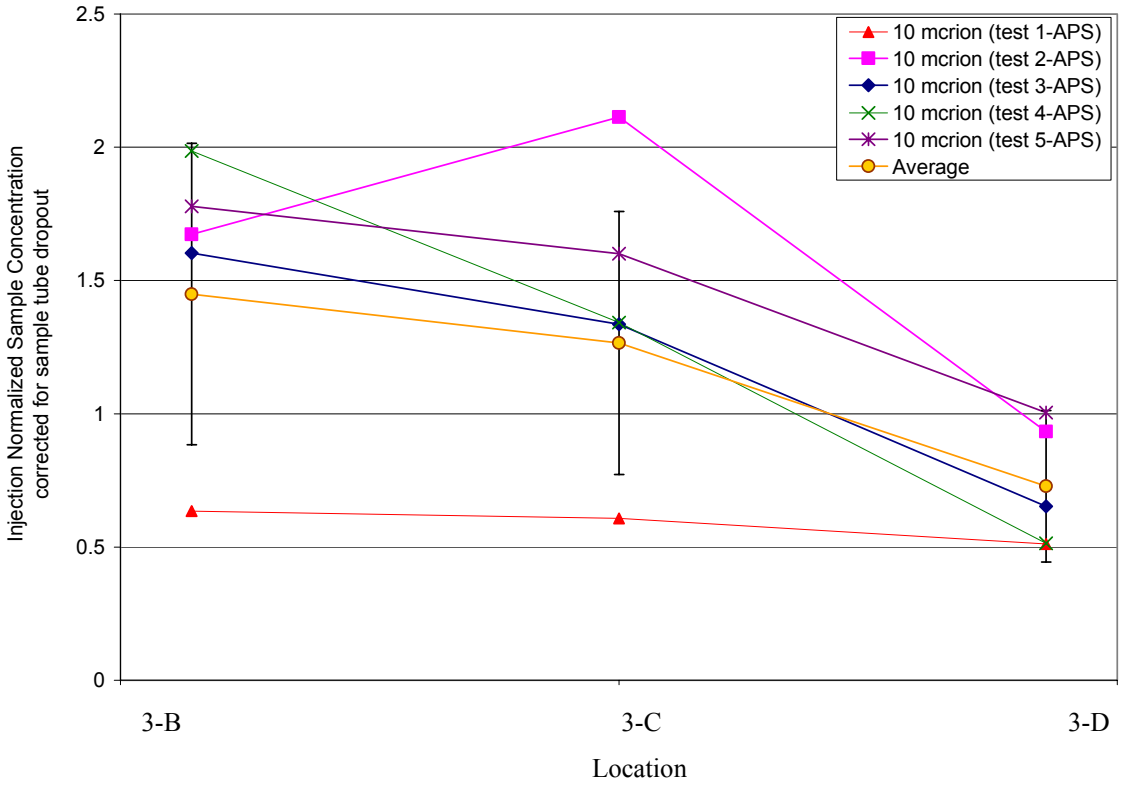

Figure 5-13: Injection normalized sample concentrations at location 3.

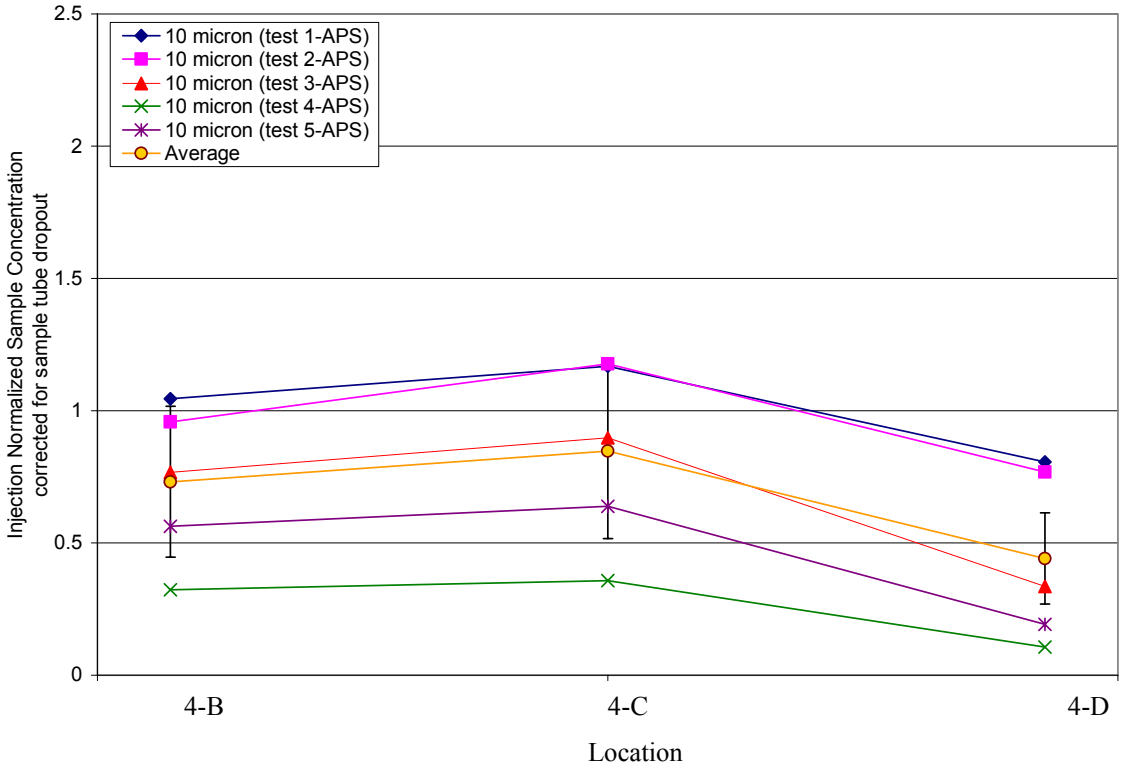

Figure 5-14: Injection normalized sample concentrations at location 4.

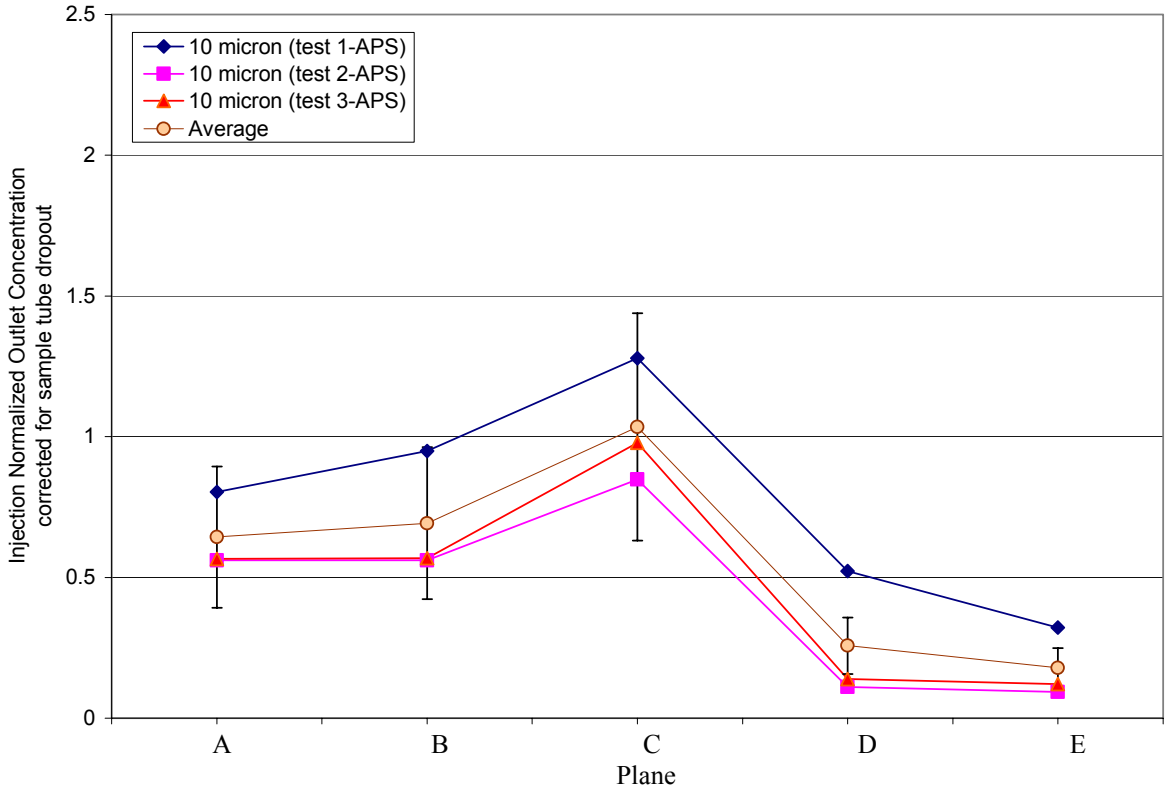

Figure 5-15: Injection normalized outlet concentration taken with APS.

5.4 Results for Temperature and Humidity

The temperature and humidity in the cabin were also monitored and investigated. Over the course of the testing, the temperatures in the test cabin ranged from 25 °C to 31 °C (77 °F to 90 °F). However, during a single test for a specific location the temperature did not vary more than 1°C (2°F). Furthermore, the temperature of the air entering through the test cabin inlet and the air that carried the particles and entered the test cabin through the injection line did not vary more than 1°C (2°F). Over several tests the relative humidity was also measured. At temperatures ranging from 25 °C to 31 °C, the relative humidity varied from 10% to 20% but during a single, one hour test, the relative humidity did not change more than one percent.

CHAPTER 6 - **Data Analysis**

6.1 Three Micron Particle Analysis

Only a single configuration was used to measure the three micron particle concentrations. The concentration results measured using the straight tube injection agreed with expected results and were repeatable within the uncertainty range. Therefore, further investigations using different configurations were not performed.

The theoretical particle concentration produced by the vibrating orifice aerosol generator (VOAG) is given by

$$C_{th} = \frac{f}{Q_{inj}} \tag{6.1}$$

where f is the frequency

Q_{inj} is the volumetric flowrate through the VOAG

A frequency of 49 kHz and a flowrate of 54.8 lpm (1.94 cfm) were inserted into the equation, which yielded a theoretical concentration of 54 particles/cm^3.

The aerosol particle sizer (APS) was used to measure the particle concentration generated by the VOAG after the particles had passed through the neutralizer. It was found that only 40% of the theoretical particle concentration exited the neutralizer. This results in a concentration of 22 particles/cm^3 entering the injection line. Using the same theoretical method for the injection line loss, as described in Chapter 5, a particle loss of 1% was calculated for the injection line. Therefore, the predicted three micron particle concentration was 22 particles/cm^3. The calibrated particle concentrations measured in the injection line by the optical particle counter (OPC) ranged from 15 to 22 particles/cm^3. Consequently, the measured three micron concentrations were in agreement with the predicted concentration.

Furthermore, the normalized three micron particle concentrations in the test cabin were about one for the locations not directly above the injection site; see Chapter 5 for concentration results. This means that the measured concentrations were approximately the same as the well-mixed concentration. The well mixed concentration is defined as the concentration in the test cabin if the test cabin is uniformly mixed. The measured well-mixed concentration for the three

micron particles was 0.2-0.3 particles/cm^3. Consequently, either the particles dispersed rapidly throughout the test cabin or the majority of the particles were quickly exhausted from the test cabin after injection. Since the normalized concentrations at each of the three locations that were not above the injection site were all about one, it is probable that the particles were well mixed in the test cabin. However, this cannot be verified without further testing; particularly, taking concentrations away from the centerline and in the outlet, similar to what was done for the ten micron particles. Off centerline measurements would determine if the particles were well mixed at other positions in the cabin and the outlet measurements could be used to determine how many particles were exiting the test cabin.

6.2 Ten Micron Particle Analysis

Multiple configurations were attempted in order to produce consistent results for the ten micron particles. The main factors identified that caused variations in the results were injection concentration, injection flow rate and velocity, cabin pressure, cabin inlet flow rate, and the relative sampling velocity. Turbulence in the cabin also caused variations, but that could not be controlled. The verifications of the flow rates are shown in Chapter 7, while the other factors are discussed here.

The first factor investigated was the injection concentration. Since the theoretical particle concentration produced by the VOAG does not depend upon the final particle diameter, the same theoretical concentration was generated for the ten micron particles as was for the three micron particles. However, the percentage of particles measured at the exit of the neutralizer was smaller for the ten micron particles as compared to the three micron particles. For the ten micron particles, 30% of the particles were measured by the APS. This results in a concentration of about 15 particles/cm^3. Using the same theoretical procedure for the calculation of losses within the injection tube, as described in Chapter 5, a particle loss of 15% was calculated for the injection tube. Thus, the predicted ten micron particle concentration at the injection is approximately 12 particles/cm^3. The calibrated OPC concentrations measured in the injection line were 7-9 particles/cm^3. These concentrations are very close. Due to the slight variation in injection concentrations, all of the concentrations measured in the test cabin were normalized by the injection concentration.

After measuring very low concentrations within the test cabin for the ten micron particles, the regular fixed diameter straight injection tube was replaced with a diffuser cone. As a result, the air velocity at which the particles were injected into the cabin was decreased by a factor of about 50. The lower air velocity of 0.047 m/s, at which the particles were injected into the cabin, decreased the disturbance to the overall cabin flow. This led to higher particle concentrations within the cabin. However, the overall shape of the concentration profiles measured at each location were still not very repeatable.

Due to the inconsistency of the concentration profiles, the effect of the interior cabin pressure was investigated. In the Lebbin 2006 study, neutral pressure was defined as less than ±0.0401 inches of water. Taking that information into consideration, tests were conducted at location 2 with interior cabin pressure of +0.1 inches of water and –0.1 inches of water. It was discovered that when the interior of the cabin was at a pressure less than the outside of the cabin, there were no ten micron diameter particles sampled at location 2-B. Then when the interior of the cabin was at a higher pressure than the outside of the cabin, ten micron diameter particles were sampled at location 2-B. Consequently, at neutral pressure the air flow in the cabin does not have a preferred direction. Sometimes the airflow would have a slight drift in the positive z direction and sometimes it would have a slight drift in the negative z direction. (Refer to Figure 3-2 for test cabin coordinates.) To ensure that the airflow in the cabin had a preferred direction, the cabin was pressurized to 0.025 inches of water. With the cabin pressure slightly above ambient, the shape of the concentration profiles became repeatable for all locations except location 2. Taking into account the dominant circular flow structure in the cabin, described in Lebbin 2006, clockwise from the inlet to the outlet, location 2 would be directly downstream of the particle injection into the cabin. Since location 2 was closest to the injection site, it appears that it was the most sensitive to how the flow exited the cone. Any inconsistencies in how the flow exited the cone could have changed the concentration at location 2, thus explaining the inconsistent concentration profiles measured at that location.

Furthermore, the pressurized cabin tests with the diffuser cone injection had concentrations in the cabin around the well mixed value of 0.09 particles/cm^3, especially taking into consideration the uncertainty of the measurements. As in the three micron case this can either mean that the concentration in the cabin is well mixed or most of the particles are exiting the cabin. However, unlike the three micron case concentration measurements were taken in the

outlet. The concentration measurements in the outlet of the cabin taken using the APS had a roughly parabolic shape with the maximum concentration occurring at the centerline of the test cabin. Furthermore, the concentrations in the outlet were similar to the well mixed concentration. These measurements indicate that higher concentrations exited the cabin near where the particles were injected into the cabin. They also indicate that the concentrations in the test cabin are similar to the concentrations in the outlet and that all of the particles were not immediately exhausted from the cabin. Consequently, for the steady state configuration used in these experiments, the particles were in the cabin long enough to become mixed along the test cabin centerline before exiting the cabin.

Care was taken to make sure that the sampling tube connected to the APS sampled the particle concentrations in the test cabin at a velocity on the same order as the velocities found in the cabin. Furthermore, the velocity in the outlet of the test cabin was similar to the APS sampling velocity. Although the velocity in the cabin was similar to the sampling velocity, the direction of the flow was not taken into consideration. Moreover, less care was taken to ensure that the measurements taken in the outlet by the OPC were sampled at the same velocity as the velocity found in the outlet of the cabin. This could have led to erroneous measurements for the outlet concentrations for the testing configurations that had a neutral cabin pressure. Consequently, the mass balances done using the OPC outlet measurements might not be very accurate due to these sampling issues.

6.3 Uncertainty Analysis

An uncertainty analysis of the normalized concentrations was performed for both the three and ten micron data. The injection normalized concentration at each location was calculated using equation (5.5) in Chapter 5, reproduced here:

$$C = \frac{C_m \times Q_{\text{sup}}}{C_I \times Q_I} \tag{6.2}$$

where C_m is the measured sample concentration corrected for particle loss
in the sampling tube
C_I is the calibrated injected concentration
Q_{sup} is the supply flow (inlet and injected)
Q_I is the injected flow

Details of this calculation can be found in Appendix A. In order to estimate the uncertainty in this ratio, each parameter used to calculate the sample concentration, supply flow rate, injection concentration and injection flow rate was assessed as to the amount of uncertainty it contributed to the normalized injection concentration. Then equation (6.26) was used to find the overall uncertainty in the ratio.

6.3.1 Uncertainty for Three Micron Data

As shown in equation (6.2), there are four components to the normalized concentration ratio. Some typical values for the injection normalized concentrations for three micron particles are shown in column three of Table 6-1.

Table 6-1: Typical values for 3 micron particle concentration normalizations.

Test #	Location	Injection Normalized Sample Concentration corrected for sample tube dropout
1	1	1.12
1	2	1.11
1	3	1.62
1	4	7.82
1	5	3.45
2	1	1.18
2	2	1.10
2	3	1.40
2	4	9.25
2	5	2.54

The concentration measured using the APS, C_m, at a particular location in the test cabin has two primary sources of uncertainty: the indicated concentration, C'_m, and the particle dropout correction factor, F_d. The uncertainty corresponding to the indicated concentration can be subdivided into the instrument bias uncertainty and the random measurement uncertainty. Therefore, equation (6.3) was used to find the uncertainty in the concentration measured using the APS.

$$u_{C'_m} = \sqrt{(u_{C'_m,random})^2 + (u_{C'_m,bias})^2} \tag{6.3}$$

The instrument bias uncertainty reported by TSI for the APS was ±10%. To calculate the absolute uncertainty in the random measurement of the concentration, some typical values for

three micron particles, shown in Table 6-2, were used along with equation (6.4), where $N_{C'm}$ was 40, the effective number of samples.

$$U_{C'_m} = \pm t_{95\%} \frac{\sigma_{C'_m}}{\sqrt{N_{C'_m}}} = \pm 2 \frac{0.0512}{\sqrt{40}} = \pm 0.017 \tag{6.4}$$

where $\sigma_{C'm}$ is the standard deviation of a single sample for the sample concentration

$N_{C'm}$ is the effective number of samples for a single test

This took into consideration that there appears to be some correlation between the concentration samples, thus reducing the number of independent samples. From the rough period of the oscillating time history data, it was estimated that the effective number samples is closer to about a third of the number of samples actually taken, yielding an effective number of samples of 40 instead of 120. Then to calculate the relative uncertainty, the total uncertainty calculated in equation (6.4) and a typical value for the indicated APS measured concentration, shown in Table 6-2, were inserted into equation (6.5) to yield a value of ±6.4%.

$$u_{C'_m} = \frac{U_{C'_m}}{C'_m} = \pm \frac{0.017}{0.264} = \pm 6.4\% \tag{6.5}$$

Finally, equation (6.3) was used to find an uncertainty of ±12% in the indicated concentration measurement.

Table 6-2: Average values for 3 micron particle concentrations.

Location	APS Sample Average Conc. (particles/cm^3)	APS Sample Conc. Std. Dev. (particles/cm^3)	OPC Injection Average Particle Count (particles/s)	OPC Injection Average Conc. (particles/cm^3)	Calibrated Injection Conc. (particles/cm^3)
1	0.297	0.030	175	3.71	23.63
2	0.248	0.040	153	3.24	20.62
3	0.368	0.062	160	3.40	21.63
4	1.747	0.272	139	2.94	18.73
5	0.737	0.132	164	3.47	22.12

To calculate the uncertainty in the particle dropout correction factor, equations (5.2) through (5.4) were combined to yield

$$F_d = \frac{L}{D} \frac{V_{TS}}{V_x} \tag{6.6}$$

where L is the length of the stainless steel tube

D is the diameter of the stainless steel sampling tube

V_{TS} is the terminal settling velocity of the particle

V_x is the velocity in the axial direction sampling tube

It was assumed that the length of the sampling tube and the diameter of the sampling tube were well-known. It was also assumed that the volumetric flow rate through the sampling tube was well-known and consequently the velocity in the axial direction of the sampling tube was well-known. Looking at equation (5.1), it was assumed that the only parameter in the terminal velocity that would yield significant uncertainty was the diameter of the particle. Therefore, the relative uncertainty was found using an average diameter of 3.5 microns and an average standard deviation of ±0.27 micron for the three micron particles, as follows:

$$u_{V_{TS}} = \pm t_{95\%} \frac{\sigma_d}{d} = \pm 2 \frac{0.27}{3.5} = \pm 16\% \tag{6.7}$$

where σ_d is the average standard deviation of the diameter of the three micron particles

d is the average diameter of the three micron particles

Looking at the values in Table 6-3, these values seem reasonable. The experimentally measured particle dropout for the three micron particles, used to correct the measured concentration, was 10%. Therefore as shown in equation (6.8), to find the absolute uncertainty in the correction factor 16% was multiplied by 10%.

$$U_{F_d} = u_{V_{TS}} \times F_d = (0.16)(0.10) = 0.016 \tag{6.8}$$

where F_d is the average particle loss in the sample tube

This result was inserted into equation (6.9), yielding a relative uncertainty of ±1.7% for the particle loss correction factor.

$$u_{F_d} = \pm \frac{U_{F_d}}{1 - F_d} = \pm \frac{0.016}{1 - 0.1} = \pm 1.7\% \tag{6.9}$$

Taking the root mean square (RMS) of the uncertainty in the indicated concentration measurement and the correction factor due to dropout in the sampling line using equation (6.10) yields a relative uncertainty of ±12% for the APS measured concentration.

$$u_{C_m} = \sqrt{(u_{C_m'})^2 + (u_{F_d})^2} = \sqrt{(12)^2 + (1.7)^2} = \pm 12\% \tag{6.10}$$

Table 6-3: Typical values for 3 micron particle parameters.

Location	Inlet Flow Rate (cfm)	Inlet Temp. (deg. C)	Injection Temp. (deg. C)	Orifice Freq. (kHz)	Injection Flow Rate (liters/min)	APS Mean Dia. (μm)	APS Dia. Std. Dev. (μm)
1	149	27.51	27.19	49.41	52.00	3.47	0.273
2	149	27.51	27.15	49.44	52.00	3.32	0.253
3	145	27.93	27.30	49.22	52.00	3.40	0.266
4	152	27.30	26.96	49.41	52.00	3.77	0.312
5	146	28.22	27.74	49.32	52.00	3.47	0.231

The main source of uncertainty in the supply volumetric airflow rate comes from the uncertainty in the calibration for the vane anemometer due to calibration drift over time. Using the calibration data in Figure 7-10, the calibration drift was estimated to be 5 cfm; this was assumed to be the absolute uncertainty in the calibration. Then to find the relative uncertainty, the absolute uncertainty and a flow rate of 150 were inserted into equation (6.11), yielding a relative uncertainty of 3.3% in the supply volumetric flow rate.

$$u_{Q_{sup}} = \pm\frac{U_{VA}}{VA} = \pm\frac{5}{150} = \pm 3.3\% \qquad (6.11)$$

where VA is the average volumetric flow rate measured by the vane anemometer

The injection concentration measured by the OPC was calculated by multiplying the indicated particle count by the calibration factor, as shown below.

$$C_I = C_I' \times R \qquad (6.12)$$

where C'_I is the indicated injection concentration

R is the calibration factor

Consequently, there are two primary sources of uncertainty for the injection concentration measured by the OPC: the uncertainty in the indicated particle count and the uncertainty in the calibration against the APS. The uncertainty in the indicated particle count was subdivided into the instrument bias uncertainty and the random measurement uncertainty. The instrument bias uncertainty was assumed to be no better than the APS (at least for the injection measurements), since the OPC was calibrated against the APS. Therefore, the instrument bias uncertainty was assumed to be 10%. This assumed that the injection concentration is stable over time and relatively repeatable. Therefore, this assumption is only valid for OPC measurements taken in

the injection line. The OPC instrument bias may be larger for measurements taken inside of the test cabin.

The absolute uncertainty was calculated using

$$U_{C_I'} = \pm t_{95\%} \frac{\sigma_{C_I'}}{\sqrt{N_{C_I'}}} = \pm 2 \frac{9.43}{\sqrt{250}} = \pm 1.2 \tag{6.13}$$

where $\sigma_{C'_I}$ is the standard deviation of a single sample for the injection particle count

$N_{C'_I}$ is the effective number of samples for the injection

Similar to the random uncertainty calculations for the APS measured concentration, this took into consideration that there appears to be some correlation between the concentration samples. It was estimated that the effective number samples is closer to about four to five times smaller than the number of samples actually taken, yielding an effective number of samples of about 250 instead of 1200. It appeared that there may be some lower frequency measurement dependence as well, which would reduce the effective number of samples even further, but they were neglected for these calculations. Then the relative uncertainty of the injected concentration was calculated using some typical particle counts for the random measurement uncertainty, shown in column four of Table 6-2 and equation (6.14), yielding a relative uncertainty of ±0.72% for the random part of the indicated injected particle count.

$$u_{C_I'} = \pm \frac{U_{C_I'}}{C_I'} = \pm \frac{1.2}{167} = \pm 0.72\% \tag{6.14}$$

To find the total uncertainty of 10% in the indicated injected particle count the following was used:

$$u_{C_I'} = \sqrt{(u_{C_I',random})^2 + (u_{C_I',bias})^2} = \sqrt{(0.72)^2 + (10)^2} = \pm 10\% \tag{6.15}$$

The calibration ratio, R, was defined as follows:

$$R = \frac{C_{APS}}{c_{OPC}} \tag{6.16}$$

where C_{APS} is the concentration measured by the APS in particles/cm^3

c_{OPC} is the particle count measured by the OPC in particles/sec

It was used to calibrate the OPC's to the APS and it also adds to the uncertainty. However, since the APS was used in the ratio and in the concentration measurements the bias uncertainty would probably partially cancel in equation (6.2). Nevertheless, as a worst case scenario, the possible

cancellation will be ignored in these calculations. Furthermore, for these calculations it will be assumed that injection concentrations and sample concentrations are independent. The calibration ratio is defined in equation (6.16), where the numerator has units of particles/cm^3 and the denominator has units of particles/sec. This ratio was used instead of a dimensionless ratio to make reducing the data easier.

A sample of seven tests (used to partially generate Figure 7-13) was used to calculate the random uncertainty of the calibration ratio. These tests resulted in an average calibration ratio of 0.134 (particles/cm^3)/ (particles/sec) with a standard deviation of 0.0038 (particles/cm^3)/ (particles/sec). Using equation (6.17) to calculate the absolute uncertainty and equation (6.18) to calculate the relative uncertainty, a relative uncertainty of ±5.7% resulted.

$$U_R = \pm 2\sigma_R = \pm 2(0.0038) = 0.0076 \tag{6.17}$$

$$u_R = \pm \frac{U_R}{C_R} = \pm \frac{0.0076}{0.134} = \pm 5.7\% \tag{6.18}$$

This value was combined with the ±10% bias uncertainty for the instruments using

$$u_R = \sqrt{(u_{R,random})^2 + (u_{R,bias})^2} = \sqrt{(5.7)^2 + (10)^2} = \pm 12\% \tag{6.19}$$

This yielded a relative uncertainty of ±12% for the calibration ratio. Taking the RMS, using equation (6.20), of the uncertainty in the indicated injection concentration measurement and the calibration ratio yields a relative uncertainty of ±15% for injection concentration.

$$u_{C_I} = \sqrt{(u_{C'_I})^2 + (u_R)^2} = \sqrt{(10)^2 + (12)^2} = 15\% \tag{6.20}$$

The final parameter to be assessed in equation (6.2) is the injected volumetric flow rate, which was calculated by multiplying the indicated flow rate by a pressure correction ratio, as shown below.

$$Q_I = Q'_I \times P_c \tag{6.21}$$

where Q'_I is the indicated volumetric flow rate

P_c is the pressure correction factor

The uncertainty in the indicated volumetric flow rate comes from the uncertainty in the reading. The average uncertainty in the reading according to OMEGA is ±2% of full scale. Therefore after using equation (6.22), a relative uncertainty of ±4.9% was calculated.

$$u_{Q_I'} = \pm\frac{0.02(FS)}{QR} = \pm\frac{0.02(100)}{41} = \pm 4.9\% \tag{6.22}$$

where FS is the full scale value

QR is the indicated reading on the rotameter

Within the ability to read the meter, there was no noticeable difference in the flow measurement both during a particular test and from test to test. Consequently, any uncertainty corresponding to the randomness in the measurements was neglected.

The pressure correction calculation – equation (A.3) in Appendix A – was documented in several sources; however, the corresponding uncertainty of the calculation was not listed. Therefore, it was assumed that the only contribution to uncertainty for the pressure correction factor came from the uncertainty in the accuracy of the pressure gage reading. The absolute uncertainty in the pressure reading was calculated as follows:

$$U_P = \sqrt{\left(\frac{\Delta P}{2}\right)^2 + \left(0.02 \times FS\right)^2} = \sqrt{\left(\frac{1}{2}\right)^2 + \left(0.02 \times 30\right)^2} = 0.78 \tag{6.23}$$

where ΔP is the division size on the pressure gage in psi

It was assumed that the uncertainty in the reading was ±2% of full scale. Then, since the pressure correction factor is calculated by taking the square root of the pressure ratio, equation (6.24) below was used to calculate a relative uncertainty of ±1.3%.

$$u_{P_c} = \pm\frac{1}{2}\frac{U_P}{P} = \pm\frac{1}{2}\frac{0.78}{29} = \pm 1.3\% \tag{6.24}$$

where P is the average gage pressure reading in psi

Taking the RMS, using equation (6.25), of the uncertainty in the indicated flow rate and the pressure correction factor gives a relative uncertainty of ±5.1% for the injection volumetric flow rate.

$$u_{Q_I} = \sqrt{(u_{Q_I'})^2 + (u_{P_c})^2} = \sqrt{(4.9)^2 + (1.3)^2} = \pm 5.1\% \tag{6.25}$$

All of the calculated relative uncertainties of ±12% for the APS measured concentration (C_m), ±3.3% for the supply flow rate (Q_{sup}), ±15% for injection concentration (C_I) and ±5.1% for the injection flow rate (Q_I) were inserted into equation (6.26) to calculate the total relative uncertainty for the injection normalization ratio.

$$u_{total} = \sqrt{(u_{C_m})^2 + (u_{Q_{sup}})^2 + (u_{C_I})^2 + (u_{Q_I})^2} \tag{6.26}$$

This yielded a total relative uncertainty of ±20% for the three micron particles.

6.3.2 Uncertainty for Ten Micron Data

The same procedure to calculate the uncertainty for the three micron particles was used to calculate the uncertainty for the ten micron particles. Furthermore, the uncertainty in the supply volumetric airflow and the injected volumetric flow rate remain the same at ±3.3% and ±5.1%, respectively. Some typical values for the injection normalized concentrations are shown in column three of Table 6-4.

Table 6-4: Typical values for 10 micron particle concentration normalizations.

Test	Position	Injection Normalized Sample Concentrations Corrected for Sample Tube Dropout	Outlet Normalized Sample Concentrations Corrected for Sample Tube Dropout	Injection Normalized Outlet Concentrations
1	B	0.494	3.089	0.160
1	C	0.473	4.278	0.111
1	D	0.398	3.922	0.101
2	B	1.303	6.862	0.190
2	C	1.645	6.671	0.247
2	D	0.727	1.870	0.389
3	B	1.248	5.556	0.225
3	C	1.040	2.868	0.363
3	D	0.508	1.023	0.497
4	B	1.546	4.968	0.311
4	C	1.045	2.368	0.441
4	D	0.401	0.741	0.541
5	B	1.386	5.800	0.239
5	C	1.247	4.484	0.278
5	D	0.782	2.216	0.353

As in the three micron case, the sample concentration measured by the APS, C_m, was calculated by multiplying the indicated concentration by the particle dropout correction factor. The bias uncertainty does not change for the ten micron particles, but the uncertainty in the random measurement does because smaller concentrations were measured for the ten micron particles than for the three micron particles. To calculate the absolute uncertainty in the random measurement of the concentration, some typical values for 10 micron particles, shown in Table 6-5, were used along with equation (6.4) in which the effective sample size, N, was 60, after correlation between the concentration samples was taken into account. It was estimated that the effective number samples is closer to about half of the number of samples actually taken, yielding an effective number of samples of 60 instead of 120. Then equation (6.5) was used to

calculate a relative uncertainty of ±15%. Finally, equation (6.3) was used to find an uncertainty of ±18% in the indicated concentration measurement.

Table 6-5: Typical values for 10 micron particle concentrations.

Test	Position	Sample APS Ave Particle Count (particles/s)	Sample APS Average Conc. (particles/cm³)	Sample APS Conc. Std. Dev. (particles/cm³)	OPC Injection Average Particle Count (particles/s)	OPC Injection Average Conc. (particles/cm³)	Calibrated Injection Conc. (particles/cm³)	OPC (Centerline or 2B) Outlet Average Particle Count (particles/s)	OPC (Centerline or 2B) Outlet Average Conc. (particles/cm³)	Calibrated Outlet Conc. (particles/cm³)
1	B	7.59	0.0155	0.0113	64.9	1.38	6.17	0.135	0.00286	0.0128
1	C	7.38	0.0142	0.0104	62.4	1.32	5.93	0.090	0.00190	0.0085
1	D	5.78	0.0118	0.0079	61.5	1.30	5.84	0.081	0.00172	0.0077
2	B	25.86	0.0525	0.0272	83.6	1.77	7.94	0.206	0.00437	0.0196
2	C	31.33	0.0636	0.0306	80.3	1.70	7.62	0.257	0.00545	0.0244
2	D	12.89	0.0261	0.0150	74.5	1.58	7.08	0.377	0.00798	0.0358
3	B	24.72	0.0504	0.0269	83.9	1.78	7.97	0.245	0.00519	0.0233
3	C	23.46	0.0409	0.0241	81.6	1.73	7.75	0.385	0.00815	0.0365
3	D	9.21	0.0187	0.0101	76.4	1.62	7.26	0.494	0.01046	0.0469
4	B	31.80	0.0643	0.0275	86.3	1.83	8.20	0.349	0.00740	0.0332
4	C	20.36	0.0412	0.0237	81.9	1.74	7.78	0.470	0.00996	0.0446
4	D	7.50	0.0152	0.0084	78.8	1.67	7.49	0.554	0.01174	0.0526
5	B	29.31	0.0595	0.0350	89.1	1.89	8.47	0.277	0.00586	0.0263
5	C	28.69	0.0520	0.0274	86.7	1.84	8.23	0.313	0.00663	0.0297
5	D	15.37	0.0312	0.0163	82.8	1.76	7.87	0.380	0.00805	0.0361

As in the three micron case, it was assumed that the dominant contribution to uncertainty in the particle dropout correction factor was the particle diameter. A standard deviation in the particle diameter of ±1 micron was assumed for the ten micron particles. Looking at the particle diameters and in Table 6-6, this appears reasonable. Then, equation (6.27) was used to calculate the relative uncertainty in the terminal velocity.

$$u_{V_{TS}} = \pm 2\frac{\sigma_d}{d} = \pm 2\frac{1}{10} = \pm 20\% \tag{6.27}$$

The experimentally measured particle dropout percent for 10 micron particles was 61%. Therefore, multiplying 20% by 61%, as shown in equation (6.28), yielded an absolute uncertainty of ±0.12.

$$U_{F_d} = u_{V_{TS}} \times F_d = (0.20)(0.61) = 0.12 \tag{6.28}$$

To get the relative uncertainty of ±20%, the absolute uncertainty, calculated in equation (6.28), was inserted into equation (6.9) resulting in a relative uncertainty of ±31%. Taking the RMS of the uncertainty in the indicated concentration measurement and the correction factor due to dropout in the sampling line yields a relative uncertainty of ±36% for the APS measured concentration.

Table 6-6: Typical values for 10 micron particle parameters.

Test	Cabin Pressure (inches water)	Inlet Flow Rate (cfm)	Injection Flow Rate (liters/min)	APS Mean Dia. (μm)	APS Dia. Std. Dev. (μm)	Inlet Temperature (deg. C)
1	0.000	147	52.0	10.90	0.62	27.4
2	-0.025	147	52.0	10.97	0.68	26.7
3	-0.025	147	52.0	10.28	0.72	26.4
4	-0.025	147	52.0	10.38	0.72	26.2
5	-0.025	147	52.0	10.52	0.66	26.8
6	-0.025	147	52.0	10.25	0.58	28.2

The injection concentration measured by the OPC, C_I, was calculated by multiplying the indicated particle count by a calibration ratio. Once again the instrument bias uncertainty was assumed to be 10%, since the device was calibrated against the APS. Then using some typical particle counts, shown in Table 6-5, a value of ±1.0% was calculated for the random measurement uncertainty for the 10 micron particles. This took into consideration that the effective number samples was about 250 instead of 1200. Using equation (6.15) to combine the bias and the random uncertainty a relative uncertainty of 10% was calculated for the indicated particle count.

As a worst case scenario, the both the bias and the random uncertainty in the calibration ratio, R, were taken into consideration. A sample of seven tests was used to calculate the random uncertainty in the calibration ratio of 0.095 (particles/cm^3)/(particles/sec). The calibration for the ten micron particles had a standard deviation of 0.0026 (particles/cm^3)/(particles/sec). Using equation (6.17) to calculate the absolute uncertainty and equation (6.18) to calculate the relative uncertainty, a relative uncertainty of ±5.5% was calculated for the random uncertainty in the calibration ratio. This value was combined with the ±10% bias uncertainty for the instruments using equation (6.19) and yielded a relative uncertainty of ±11% for the calibration ratio. Taking the RMS of the uncertainty in the indicated injection concentration measurement and the calibration ratio yields a relative uncertainty of ±15% for injection concentration.

All of the calculated relative uncertainties of ±36% for the APS measured concentration, ±3% for the supply flow rate, ±15% for injection concentration and ±5% for the injection flow rate were inserted into equation (6.26) to calculate the total relative uncertainty for the injection normalization ratio. This yielded a total relative uncertainty of ±39% for the 10 micron particles. Due to some of the assumptions made in the RMS method and the large estimated uncertainties,

it may not be the best method to use to calculate the relative uncertainty of the concentrations measured in this project.

6.4 Mass Balance

A mass balance was performed for the ten micron data for each of the three configurations: straight tube injection, cone injection with a cabin gage pressure of 0 inches of water, and cone injection with a cabin gage pressure of 0.025 inches of water. A mass balance was not performed for the three micron data. The number of particles lost in the cabin in each of the three cases was calculated from

$$\%loss = 1 - \frac{C_{out} \times Q_{\sup}}{C_I \times Q_I} \tag{6.29}$$

The details of how each component in equation (6.29) was calculated can be found in Appendix A, where the outlet concentration, C_{out}, was calculated in the same manner as the measured concentration, C_m, for the APS sampled concentrations. For the cases when the OPC was used to measure the outlet concentration no adjustments were made to the measured concentration because a sample tube was not used.

For the straight tube injection case, the values used to calculate the particle loss in the chamber are shown under configuration 1 in Table 6-7. The outlet concentration, C_{out}, was calculated by taking an average concentration over the length of the outlet, using the measurements shown in Figure 5-4. A typical value was used for the injection concentration, C_I, and flow rate, Q_I. The outlet flow rate, Q_{sup}, was calculated by taking the sum of the airflow entering the cabin through the inlet and the particle injection line. Using the information in Table 6-7 and equation (6.30) yields a 67% particle loss inside the cabin.

$$\%loss = 1 - \frac{C_{out} \times Q_{\sup}}{C_I \times Q_I} = 1 - \frac{(0.0253)(4247)}{(6.27)(52)} = 67\% \tag{6.30}$$

Table 6-7: Mass balance parameters.

Flow Parameters	
Q_I	52 lpm (1.84 cfm)
Q_{sup}	4247 lpm (150 cfm)
Configuration 1	
C_I	6.27 particles/cm^3
C_{out}	0.0253 particles/cm^3
Configuration 2	
C_I	7.49 particles/cm^3
C_{out}	0.0193 particles/cm^3
Configuration 3	
C_I	8.13 particles/cm^3
C_{out}	0.0573 particles/cm^3

This process was repeated for the case when the particles were injected into the cabin through a diffuser cone and the cabin had a gage pressure of 0 inches of water, configuration 2. However, instead of using an average of the outlet particle concentration over the length of the outlet, a typical concentration taken on the C plane was used. All the other parameters were selected or calculated in the same manner as the straight tube injection case. Inserting the values, under configuration 2, in Table 6-7 into equation (6.29) in the same manner as shown in equation (6.30) yields a particle loss of 79% in the cabin.

This process was repeated a third time for the case when the particles were injected into the cabin through a diffuser cone and the cabin had a gage pressure of 0.025 inches of water, configuration 3 in Table 6-7. The outlet concentration value used was found by taking an average of the concentrations measured in the outlet using the APS, shown in Figure 5-15. Using the values for configuration 3 in Table 6-7 yields a particle loss of 42% in the cabin.

Comparing the three cases, the minimum particle loss occurred for configuration 3. As mentioned previously, the outlet concentrations measured using the OPC were not taken isokinetically and the OPCs were not calibrated to use at low concentrations such as those found in the outlet of the test cabin. Consequently, these reasons could in part explain why the mass balance for configurations 1 and 2 indicate larger particle losses in the cabin than configuration 3. The exact mechanism of particle loss in the cabin is unknown. However, using the same method described in Chapter 5 to find particle settling in the sample tube, an estimate of 15-20% can be calculated for the particle settling in the test cabin. Therefore, it would not be unreasonable to assume that about half of the 42% particle loss was due to particle settling in the

cabin. Furthermore, if the uncertainties calculated in the previous section are applied to the ratio in equation (6.29) – where the outlet concentration measured using the APS is assumed to have the same uncertainty the sample concentration, $C_{m,-}$ then the particle loss in the test cabin ranges from 25% to 59%. Therefore, if the particle loss in the test cabin was only 25% and 20% of the particles lost were due to settling then that only leaves 5% of the particles unaccounted for. However, that does not account for impaction on the surfaces, which could also lead to particle loss in the cabin. Consequently, within our ability to measure and the corresponding uncertainty, mass is conserved.

CHAPTER 7 - Verifications, Calibrations and Flow Visualizations

This chapter describes the various tests that were performed to ensure accurate results (including instrument calibrations) and presents the results of these tests. This chapter also presents flow visualization results for both the tube and cone injection geometries.

7.1 Instrument Verification

7.1.1 Optical Particle Counter (OPC) Verification

Several different tests were performed to assess the accuracy of the four optical particle counters (OPCs) (A-D). OPC A was located in the inlet to the test cabin, OPC C was located in the injection line and OPCs B and D were used inside of the cabin or in the cabin outlet. In these tests the OPCs were tested against one another and against the aerodynamic particle sizer (APS). Initially only OPC-A and OPC-C were tested against one other and against the APS. They were tested by injecting particles into a mixing box, as shown in Figure 7-1, and then having each device measure approximately the same location in the box. Prior to sampling, tests were performed to ensure that the box was well mixed. During the test, all of the nozzles of the OPC's and APS sampled vertically in the mixing box (roughly 230 mm wide, 300 mm tall and 500 mm long) as close to one another as possible. Meanwhile, liquid particles were injected into the side of the box.

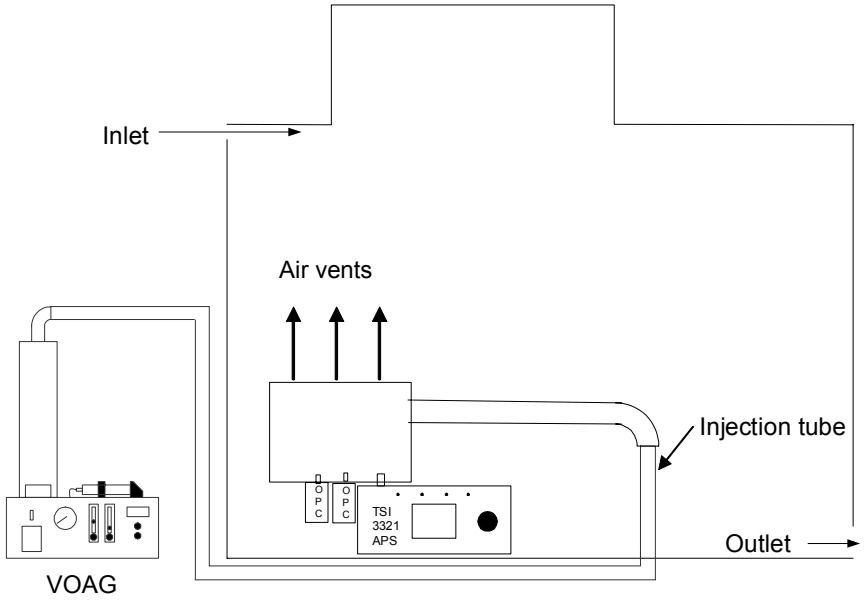

Figure 7-1: OPC and APS comparison setup in the test cabin.

This test was performed for both three micron and ten micron particles. The results for the ten micron particles are shown in Table 7-1 and the results for the three micron particles are shown in Table 7-2. These tests yield an APS/OPC ratio of 4.3 for ten micron particles and 6.8 for three micron particles.

Table 7-1: Ten micron particles OPC and APS comparison test.

Test	Device	Particle Count	Average Concentration particles/cm^3	Concentration Std. Dev.	Ratio: APS/ OPC
1	OPC-A	52.8	1.12	0.136	3.75
1	OPC-C	46.7	0.99	0.161	4.24
1	APS	2063	4.19	0.312	-
2	OPC-A	48.9	1.04	0.110	4.45
2	OPC-C	46.2	0.98	0.135	4.71
2	APS	2284	4.62	0.171	-

Table 7-2: Three micron particles OPC and APS comparison test.

Test	Device	Particle Count	Average Concentration particles/cm^3	Concentration Std. Dev.	Ratio: APS/ OPC
1	OPC-A	191	4.05	0.163	6.74
1	OPC-C	189	4.01	0.163	6.82
1	APS	13534	27.34	0.330	-

Another test was performed to compare OPC A, B and D and to assess any potential differences in the device's cabling. As shown in the diagram of the setup for these tests, Figure 7-2, OPC-C was located upstream from the other OPCs. Therefore, it was used to normalize the concentrations measured by the other OPCs. Four 10 minute long tests were performed using ten micron particles to compare the OPC devices. Between each test, the cabling (communication, electrical and vacuum) connected to each OPC was changed. The results of these tests are shown in Figure 7-3. Test 1 and test 4 had the same cabling configuration, however the flow light was flashing for OPC-B during test 1 (a flashing flow light indicates insufficient flow) so the test was repeated after the flow problem was fixed. The normalized concentrations agree within ± 0.07 or 1% for tests three and four.

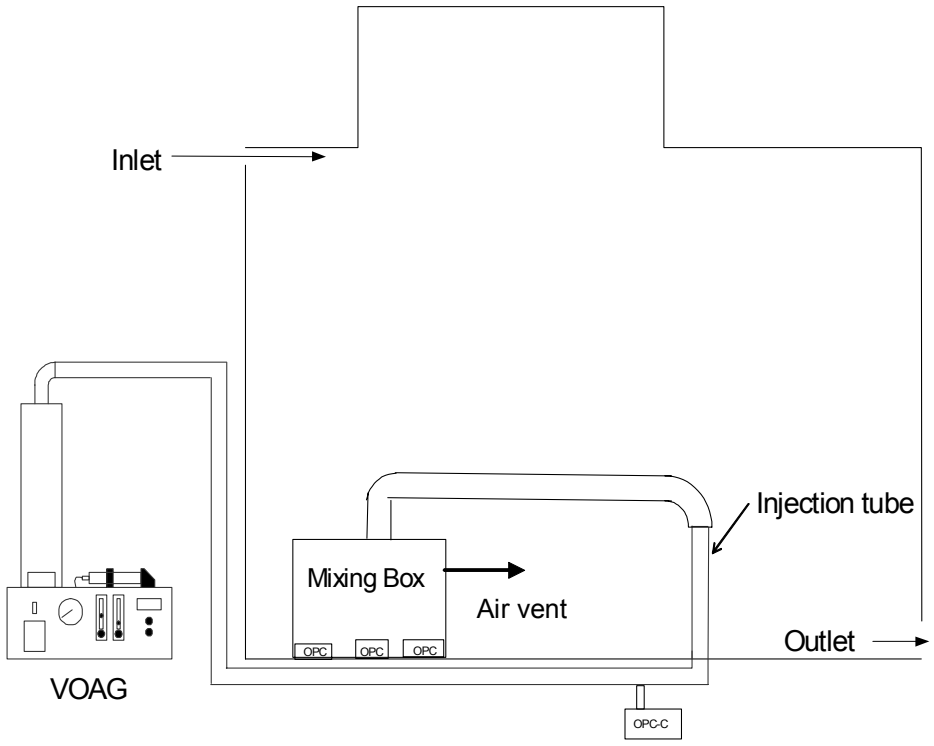

Figure 7-2: OPC comparison test setup in the test cabin.

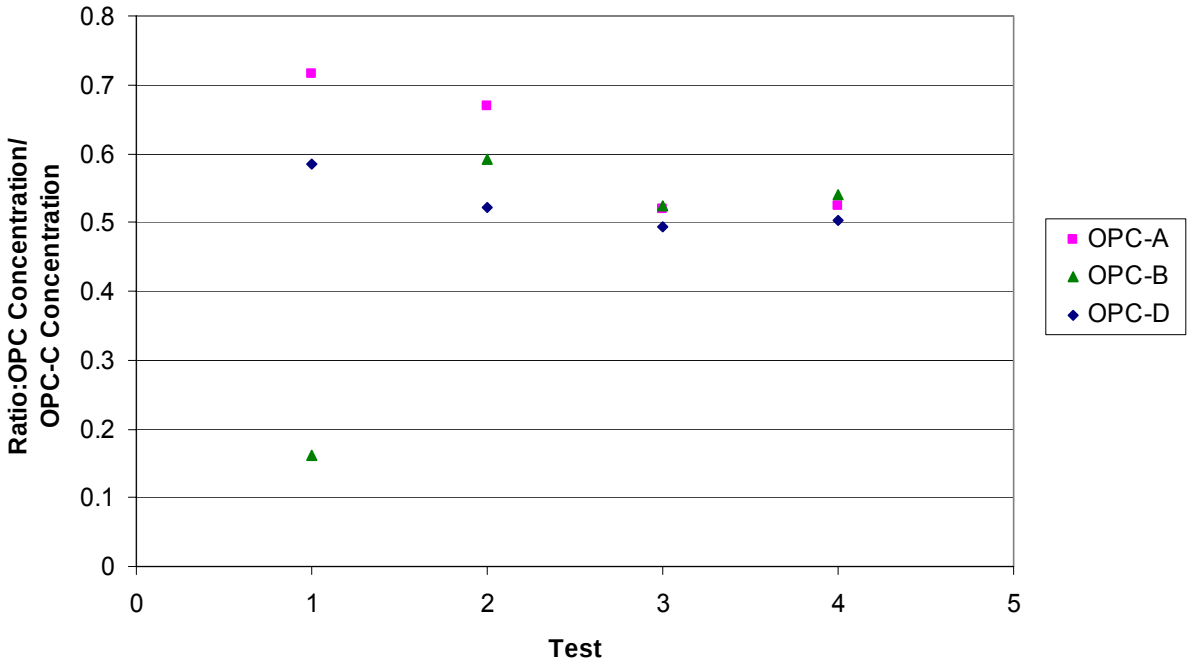

Figure 7-3: OPC comparison test results.

Another test was performed to compare the three OPC's under actual testing conditions. The results of these tests are shown in Figure 7-4. The three OPC's were placed in the outlet of the test cabin side by side during several tests. During these tests, the cabin was pressurized to a gage pressure of 0.025 inches of water; therefore the interior of the cabin was at a higher pressure than the outside of the cabin. For the results presented in Figure 7-4, all three OPC's agree within ± 0.0005 particles/cm^3 or ±10%. Furthermore, none of the adjustments described in Appendix A were made to these OPC concentrations.

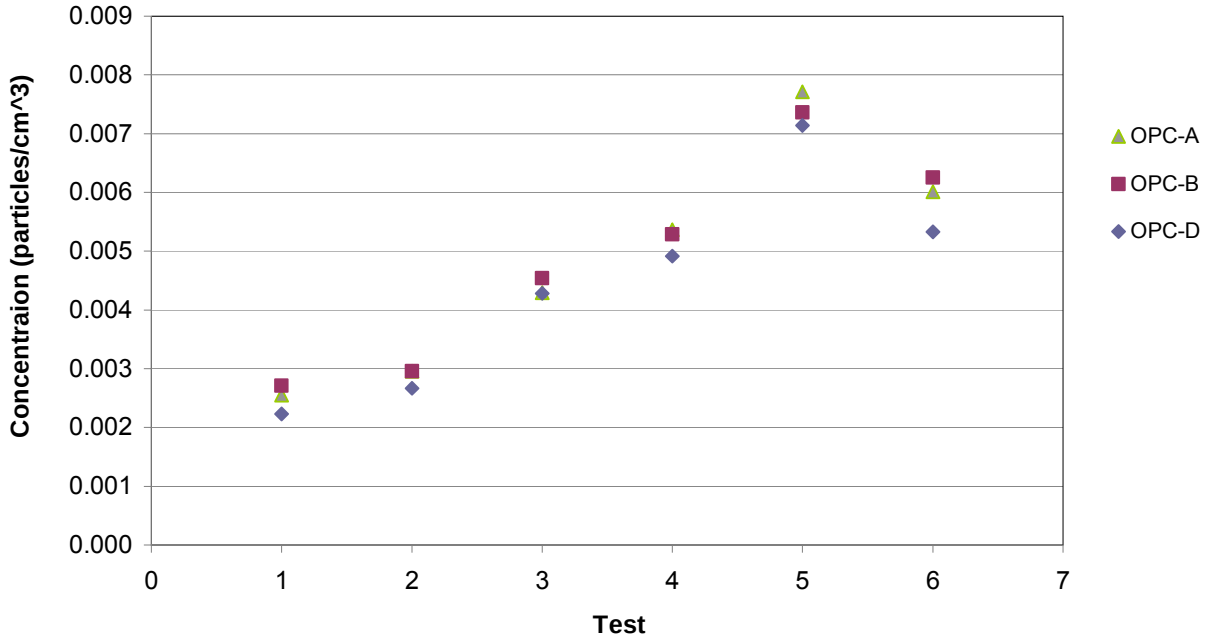

Figure 7-4: OPC comparison in outlet of test cabin.

As a result of these three series of tests, it was found that the OPCs agree well with one another. However, the OPCs do not agree well with the APS. Consequently, the OPCs had to be calibrated.

7.1.2 Aerodynamic Particle Sizer (APS) Verification

In order to assess the reliability of the measurements taken by the APS, it was compared to another APS by the same manufacturer and of same model purchased the year before by another department. Figure 7-5 shows a diagram of the testing setup of the mixing box that was used to compare the two APS devices. The comparison was done by injecting liquid particles into a mixing box and having both APS devices sample the concentration at the center of the box. The mixing box was not perfectly sealed in order to allow excess airflow to escape, since the VOAG outputs a larger airflow rate than the combined intake of both APS devices.

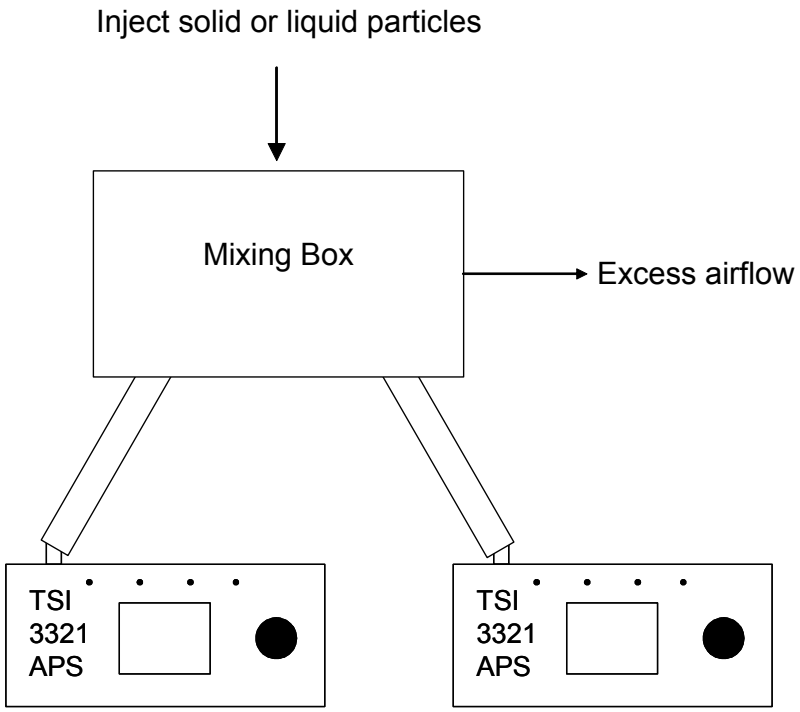

Figure 7-5: Setup for APS measurement comparison tests.

Both three micron and ten micron particles were sampled in the mixing box. The percent difference between the two devices was calculated as follows:

$$\%\_difference = \frac{C_B - C_R}{C_B} \tag{7.1}$$

where C_R is the concentration measured by the comparison APS

C_B is the concentration measured by the project APS

The results for the ten micron particles are shown in Table 7-3 and the results for the three micron data are shown in Table 7-4. The results show that for both the ten micron and the three micron data, the project APS consistently reads a concentration of about 20% higher than the comparison APS. As for the size of the particle, the project APS consistently measures a slightly smaller diameter than the comparison APS. For the ten micron particles both devices agree within 1 micron and for the three micron particles both devices agree within 0.5 microns.

Table 7-3: Ten micron particle comparison (B-project APS and R-comparison APS).

Test	Particles Counted (particles/second)	Concentration (particles/cm^3)	Mean Diameter (microns)	Mean Dia St Dev (microns)	% Difference
1-B	380	0.770	9.69	0.419	
1-R	296	0.595	10.68	0.469	22.7%
2-B	391	0.793	9.80	0.462	
2-R	303	0.616	10.70	0.494	22.3%
3-B	383	0.777	9.96	0.505	
3-R	298	0.602	10.71	0.474	22.6%
4-B	378	0.769	10.10	0.509	
4-R	302	0.609	10.70	0.488	20.8%
5-B	384	0.778	10.12	0.490	
5-R	291	0.588	10.73	0.459	24.3%

Table 7-4: Three micron particle comparison (B-project APS and R-comparison APS).

Test	Particles Counted (particles/second)	Concentration (particles/cm^3)	Mean Diameter (microns)	Mean Dia St Dev (microns)	% Difference
1-B	1972	3.98	3.55	0.137	
1-R	1599	3.20	3.56	0.160	19.5%
2-B	2351	4.77	3.55	0.122	
2-R	1930	3.91	3.55	0.149	17.9%
3-B	2771	5.59	3.55	0.135	
3-R	2207	4.47	3.55	0.157	19.9%
4-B	3498	7.06	3.58	0.213	
4-R	2776	5.61	3.59	0.237	20.5%
5-B	3841	7.73	3.67	0.369	
5-R	3266	6.64	3.72	0.467	14.1%

The project APS was also compared to one of the OPCs by having both devices sample one above the other in an actual testing situation. The tests were conducted at location 2 in the large Plexiglas test chamber; see Figure 4-1 for measurement locations. For these tests, ten micron particles were injected into the cabin through the cone. The injection normalized results for these tests are in Figure 7-6. (Refer to Appendix A for normalization calculations and Chapter 6 for the uncertainty estimate calculations). At first glance, it may appear that the results for the APS to OPC comparison tests show that there is a substantial discrepancy between the APS and OPC measurements. However, the two devices sometimes agree quite well within the estimated uncertainty as in the case of tests 2 and 4 reproduced in Figure 7-7. At other times they can differ by a factor of three as in the case of tests 1 and 3 reproduced in Figure 7-8. However, a factor of three does not necessarily mean disagreement if the large uncertainties are taken into consideration. Although the uncertainty bars do not overlap at each location in Figure 7-8, for test 3, they come very close. Consequently, it is not completely clear if the APS and OPC agree or not. These tests suggest that they might within the estimated uncertainty. Due to

the ambiguous nature of the agreement between the APS and the OPC under actual testing conditions, the estimated uncertainty for the OPC measurements, calculated in Chapter 6, should only be assumed to be valid for the OPC in the injection line.

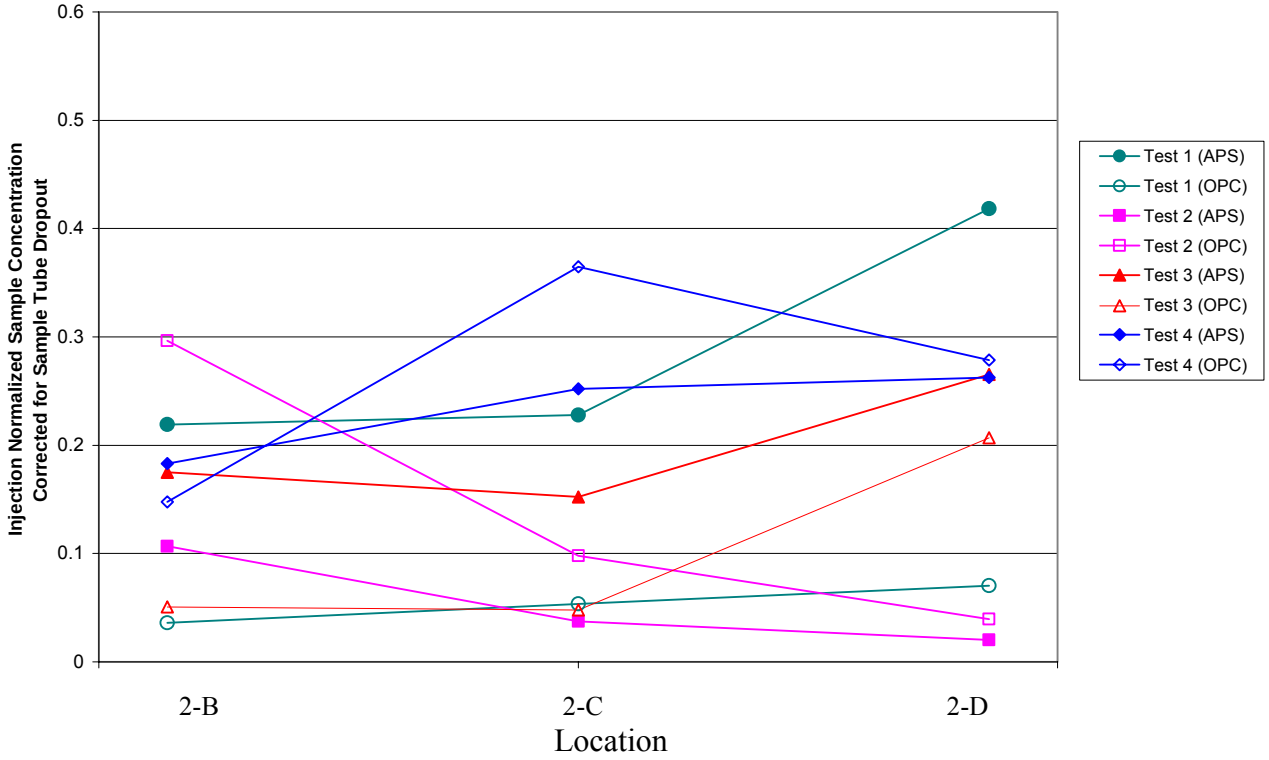

Figure 7-6: Injection normalized sample concentration for side-by-side APS to OPC comparison tests for ten micron particles.

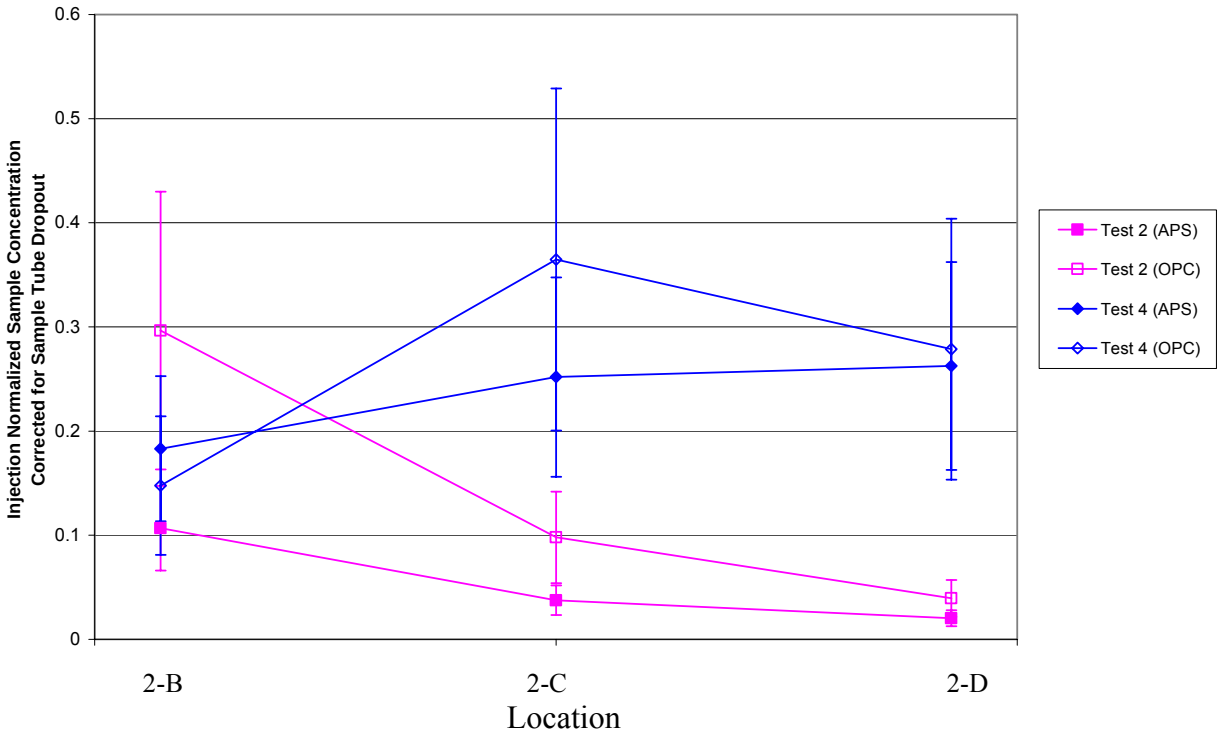

Figure 7-7: Injection normalized sample concentration for side-by-side APS to OPC comparison tests for ten micron particles (test 2 and test 4).

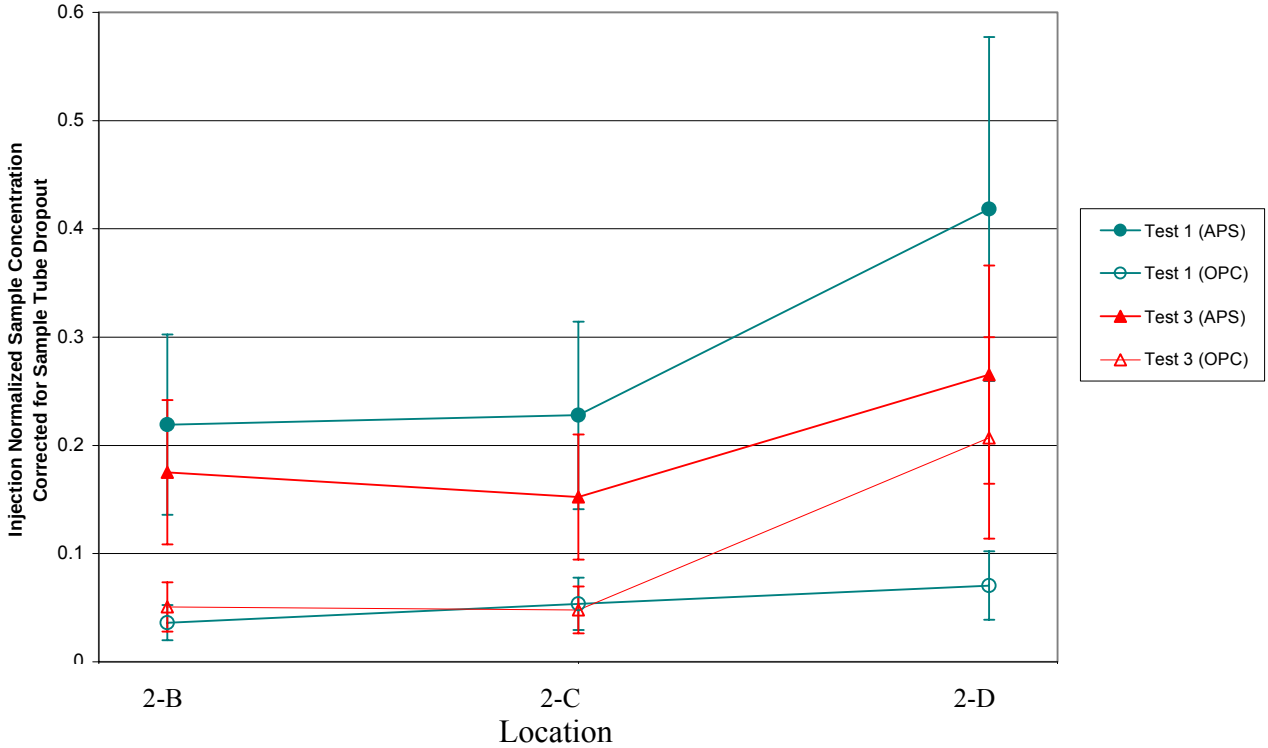

Figure 7-8: Injection normalized sample concentration for side-by-side APS to OPC comparison tests for ten micron particles (test 1 and test 3).

7.2 Calibrations

7.2.1 Vane Anemometer Calibration

The Davis Inotek rotating vane anemometer used to measure volumetric flow rate into the test cabin was recalibrated after the straight tube injection testing. The vane anemometer was 101.6 mm (4 in) in diameter and was located inside a 203.2 mm (8 in) diameter duct. Two duct sections – the one that housed the vane anemometer and the preceding section which housed flow straighteners – were removed from the test cabin and used in the calibration. A photo of the test setup is shown below in Figure 7-9.

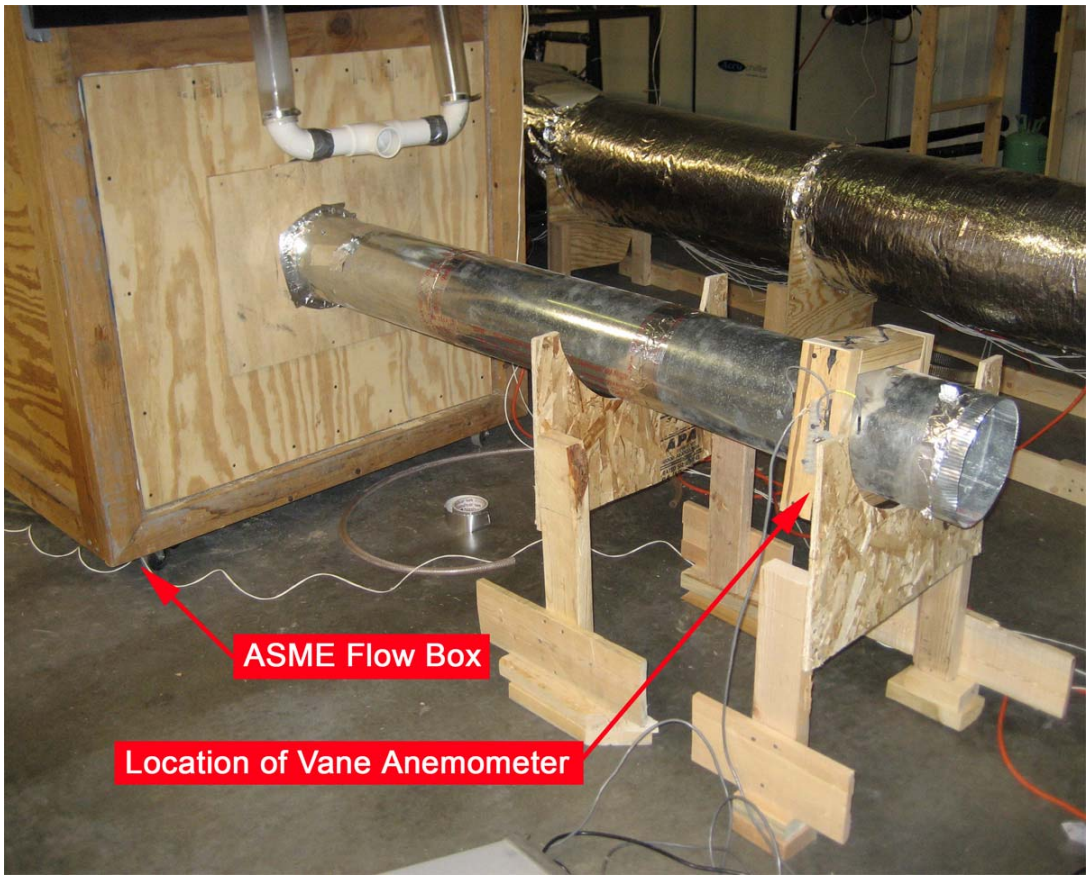

Figure 7-9: Vane anemometer calibration setup.

In order to calibrate the vane anemometer, it was placed in line with a flow box equipped with different size ASME nozzles. All the calibration testing utilized a single 63.5 mm (2.5 in) diameter ASME nozzle along with a 0-5 in H_20 pressure transducer. The actual flow rate was determined by the pressure drop across the ASME nozzle. Then the actual flow rate was

compared to the number of revolutions of the vane anemometer counted by a Hewlett Packard (HP) 34970A data acquisition and control system. The resulting calibration agreed reasonably well with previous calibrations. The most recent calibration results along with previous calibration results are shown in Figure 7-10 below. The two calibrations used in the testing done for this project – green (x) and red (*) calibrations – agree within a couple percent of each other at a flow rate of 4162 lpm (147 cfm).

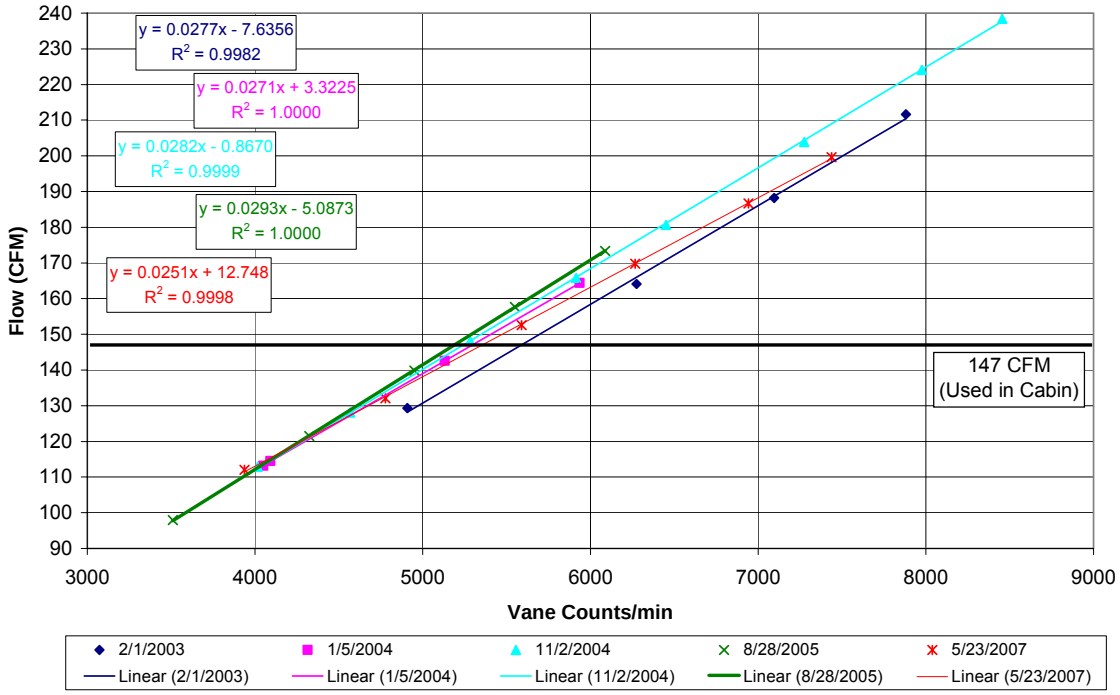

Figure 7-10: Current (red *) and past calibrations of vane anemometer used in test cabin.

7.2.2 Rotameter Calibration Curve Verification

The Omega FL-115 rotameter calibration was verified using a bell prover, shown in Figure 7-11. This verification was important because the rotameter established the flow through the injection line. The flow rate measured by the bell prover was determined by measuring the amount of time it took to displace a volume of one cubic foot. Therefore, the flow rate was determined by dividing the volume displaced by the amount of time it took. Then the flow was converted to the equivalent flow at standard pressure in liters per minute. These values are plotted on the vertical axis in Figure 7-12. The rotameter reading taken using a glass float was compared to the manufacturer provided calibration curve. These flow rates were also converted to the equivalent flows at standard pressure in liters per minute and are plotted on the horizontal

axis in Figure 7-12. The calibration was done for the range of indicated values on the rotameter, but for a lower volumetric flow rate than the actual volumetric flow rate at standard conditions that is used during testing. Nevertheless, the manufacturer calibration curve agrees well with the bell prover measurements taken. Therefore, it is likely the manufacturer calibration curve provides similar results for the higher flow rate used during testing. As mentioned in Chapter 6, the pressure correction calculation, presented in Appendix A, was found in multiple sources, but there was no estimate of the range of accuracy for the calculation. Nevertheless, it was assumed that the manufacturer's calibration curve is accurate.

Figure 7-11: Bell prover.

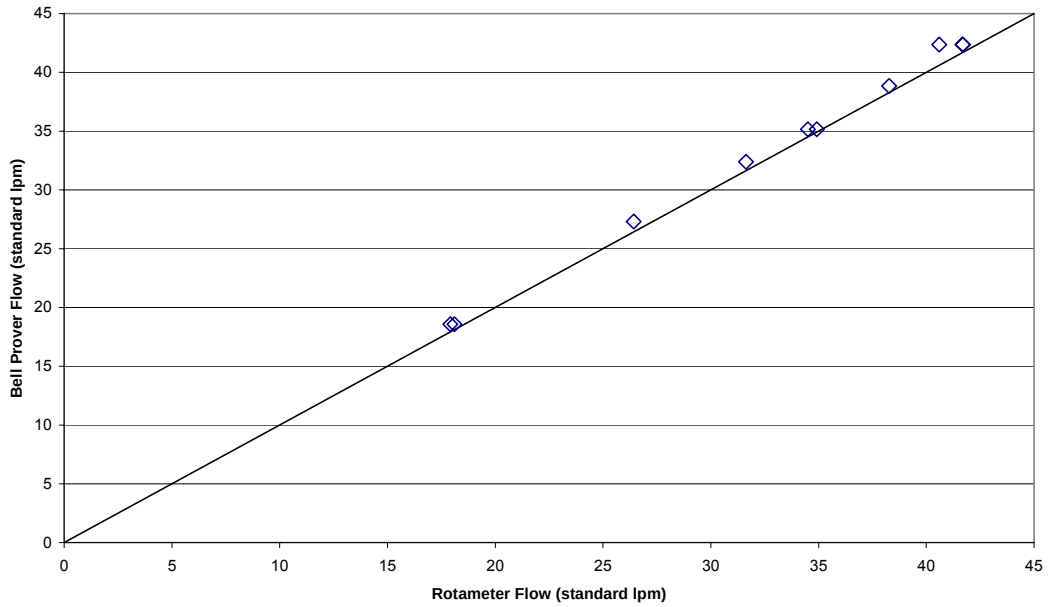

Figure 7-12: Rotameter calibration.

7.2.3 OPC Calibration

Since the OPC's gave readings lower than the APS, all data collected by the OPCs were calibrated against the APS. Therefore, both the injected concentration and the outlet concentration OPCs were calibrated using the curve from Figure 7-13 below. This curve gives the ratio of the APS concentration to OPC particle count as a function of particle diameter. This ratio becomes dimensionless if multiplied by the flow rate through the OPC, which was assumed to be constant. Looking at Figure 7-13, the correction factor for the three micron particles is 0.135 (particles/cm^3)/(particles/sec), which corresponds to a dimensionless ratio of 6.37 and the correction factor for the ten micron particles is 0.095 (particles/cm^3)/(particles/sec), which corresponds to a dimensionless ratio of 4.48. This calibration was performed for concentrations similar to those found in the injection line and may not be valid for lower concentrations such as those found in the test cabin or in the test cabin outlet.

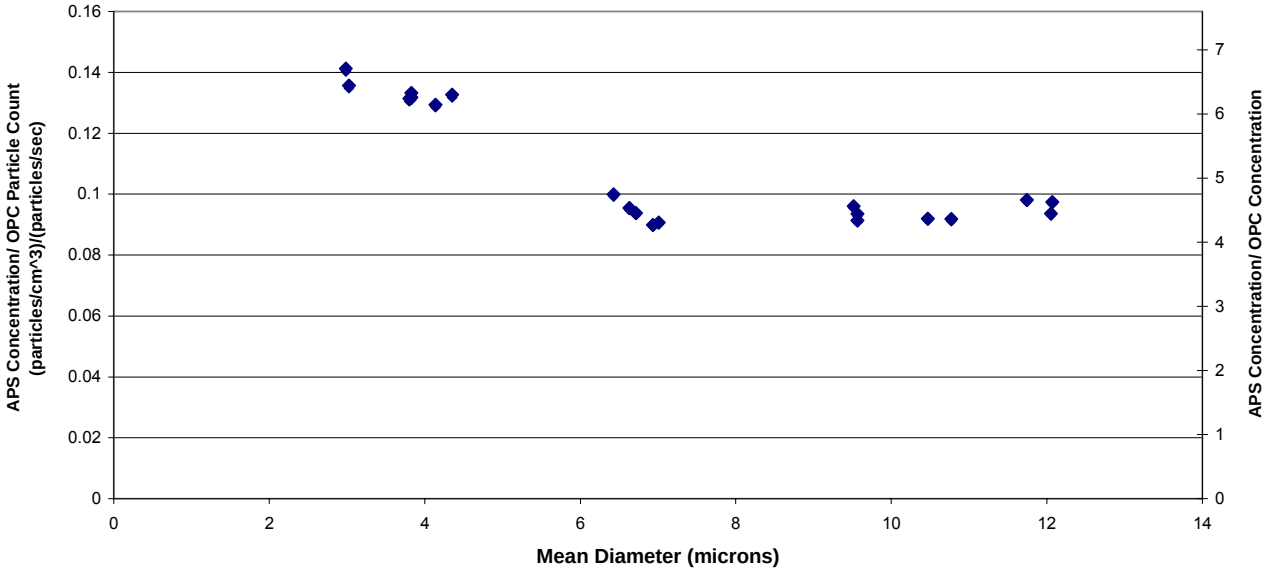

Figure 7-13: OPC calibration curve.

7.3 Flow Visualization

Flow visualization was performed both with the straight tube injection and the diffuser cone injection. A Rosco 1600 theatrical fog generator was utilized to generate the smoke that was injected into the test cabin through the injection line. To illuminate the flow, a 75 mW, 532 nm laser light source was used. The laser was equipped with a cylindrical lens in order to create a light sheet. A still camera and a video camera were used to capture images of the flow. A diagram of the test setup is shown in Figure 7-14. The same orientation of the laser and camera were used for both straight tube and diffuser cone injection.

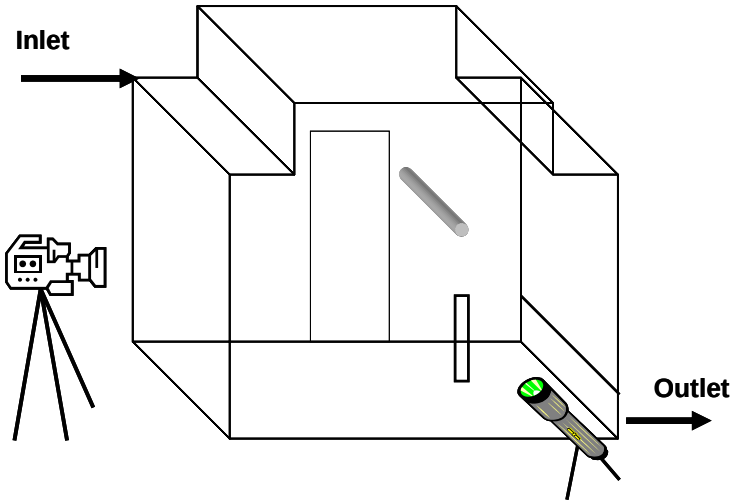

Figure 7-14: Camera and laser orientation for flow visualization photograph.

7.3.1 Straight Tube Injection

For the straight tube flow visualization, shown in Figure 7-15, the sample tube was located at position 4 and the interior cabin pressure was set to zero gage pressure. The smoke was injected into the test cabin at a rate of 54.7 lpm (1.93 cfm). After correcting for pressure at the flow meter, this was the same volumetric flow rate of air injected into the cabin as was used during testing. As can be seen in Figure 7-15, a substantial jet of air exits the injection tube. This jet extends up to sample location 4 which is about 700 mm above the exit of the injection tube; thus resulting in a higher particle concentration at location 4.

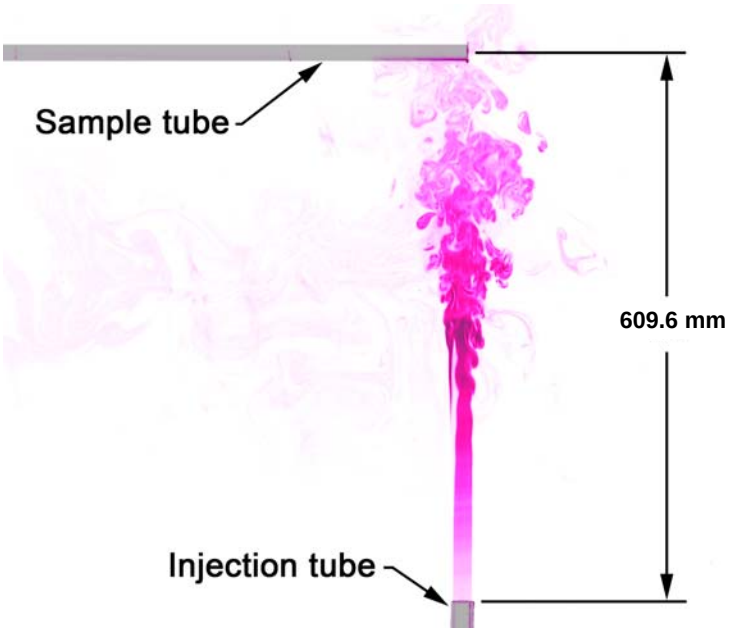

Figure 7-15: Flow visualization using straight injection tube.

7.3.2 Diffuser Cone Injection

For the diffuser cone flow visualization, shown in Figure 7-16, the interior cabin pressure was also set to zero gage pressure. The smoke was injected into the test cabin at a rate of 33.9 lpm (1.2 cfm). After correcting for pressure, this is about two-thirds of the volumetric flow rate that was used during testing. In retrospect, it would have been preferred if the flow rate used for the smoke visualization was the same as the flow rate that was used during testing. As can be seen in Figure 7-16, there is no longer a jet of air. Instead the flow appears to only reach about 75 mm high or about a tenth of the distance it used to reach using the injection tube. Also observed during the flow visualization, the smoke did not continually exit the cone. Instead

churning of the flow in the cone was observed and the smoke seemed to spill over the edge of the cone every few seconds. Moreover, once the smoke had left the cone it tended to move towards the inlet to the cabin and the positive z direction as shown in Figure 4-1.

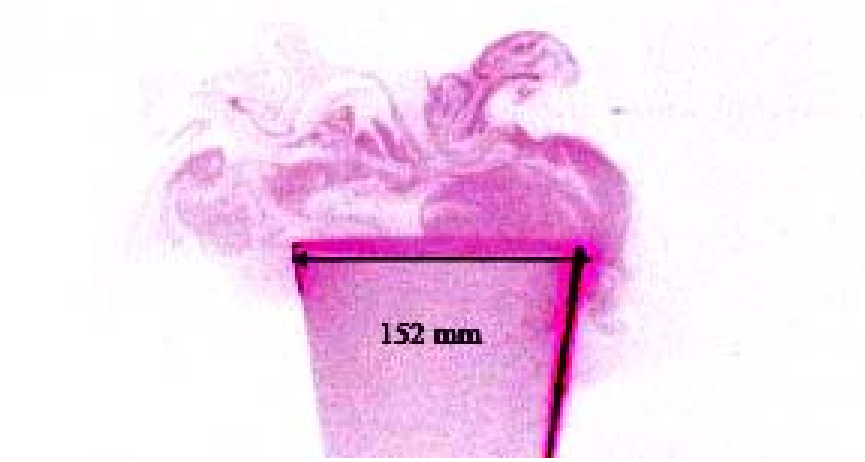

Figure 7-16: Flow visualization using diffuser cone.

CHAPTER 8 - **Summary**

The fourth phase of the experimental project funded by Boeing titled "Large Eddy Simulation Validation Lab Test – Particle Diffusion" was described in the preceding chapters. The objective of this phase of the project was to collect monodispersed particle concentration measurements inside a half cabin test section in order to help validate Boeing's computational fluid dynamics model of a Boeing 767.

Multiple steps were taken in order to meet the objective. First of all, a vibrating orifice aerosol generator was installed outside of the test cabin to generate monodispersed particles. Particles were injected pointwise into the test cabin as uniformly as possible. Four optical particle counters (OPCs) and an aerodynamic particle sizer (APS) measured the particle concentrations at various discrete locations inside the test cabin, test cabin inlet duct, test cabin outlet duct and injection line

Several tests were performed to verify that the measuring devices were providing accurate results. It was found that the OPCs gave readings about four to six times smaller than those taken by the APS, depending on the particle diameter, for concentrations in the range of the injection concentration. The reason for this is not known. However, as described in Chapter 2, it is not unusual for an optical particle counter to need to be calibrated before use in a particular application. Therefore, the optical particle counters were calibrated against the aerodynamic particle sizer and all results taken with the optical particle counters were adjusted accordingly. It was found that the aerodynamic particle sizer used for testing reads about 20% higher than another APS of the same model purchased the year before by another department. It was also found that using the vibrating orifice aerosol generator it was not possible to provide the same injection concentration from one test to the next. Thus, before comparison, all results must be normalized by the injection concentration. The data were also adjusted for the particle loss in the sample tube.

The concentration results for both the three micron and ten micron particles with the straight tube injection, and an interior cabin gage pressure of 0 inches of water, showed that the highest concentration in the cabin was at location 4 which was above the injection site. For the three micron data, the injection normalized concentration ratio was about one for all of the

locations except for location 4 and location 5. The injection normalized concentration ratio for the ten micron particles was well below one for all of the locations except for location 4. The outlet concentration profile was measured for ten micron particles and it was found that it was asymmetrical; the peak outlet concentration occurred 1200 mm (48 in) from the wooden back wall. The average outlet concentration was 0.025 particles/cm^3. After performing a mass balance it was found that 67% of the ten micron particles were apparently dropping out in the test cabin. However, this number does not take uncertainty of the measurements into consideration.

Due to the large dropout rate of the ten micron particles, the straight tube injection was replaced with a diffuser cone. Furthermore, concentration profiles were taken at each measurement location. The concentration profile results at each location were not very repeatable, but the measured concentrations were much larger than the concentration results taken using the straight tube injection. Some of the injection normalized concentrations were as high as 0.7. Furthermore, the outlet concentration profile became mostly flat instead of parabolic. Another mass balance was performed using the second configuration and the centerline outlet concentration. It was found that for the cone injection configuration with neutral cabin pressure a particle loss of 79% occurred in the test cabin. Once again, this number does not reflect the uncertainty in the measurement.

In an effort to produce repeatable results, the effect of cabin pressure, temperature and humidity were investigated along with the sampling connections. By changing the tubing on the sample line and increasing the interior cabin pressure to 0.025 inches of water, the concentration profile shapes become repeatable for most locations with the exception of location 2. Changes in temperature and humidity appeared not to affect the results. Nevertheless, there appears to remain a factor of about two difference in the concentration results. However, the uncertainty in the ten micron results was calculated and it was found that the injection normalized concentrations have a relative uncertainty of about ±38%. Therefore, the uncertainty appears to explain most of the large, observed scatter in the 10 micron results. A mass balance was performed for the third configuration, using an average outlet concentration across the length of the outlet that was measured using the aerosol particle sizer, and it was found that 42% of the particles were lost in the cabin. However if the estimated uncertainty is applied to this value then the particle loss in the test cabin ranges from 25% to 59%.

Comparing the three configurations used for the ten micron particles, the minimum particle loss occurred for configuration with the cone injection and the positive cabin pressure. The higher particle loss for the other two configurations could possibly be explained in part by the fact that the outlet concentrations measured using the OPC were not taken isokinetically and by the fact that the OPCs were not calibrated at concentrations in the range found in the cabin. The exact mechanisms leading to particle loss in the cabin is unknown, but a rough estimate of particle loss due to settling in the cabin would yield a particle loss of 15-20%. Impaction on the surfaces could also account for part of the particle loss in the cabin. Taking the uncertainty in to consideration along with the possibility that there are other unidentified mechanisms for particle loss in the cabin, a measured value of 42% is possible. The large uncertainty in the ten micron results accounts for most of the scatter for the majority of the locations. The exception is location 2, which is directly downstream of the injection site if the flow structure of the cabin is taken into consideration. Finally, the concentrations in both the cabin and the outlet measured using the aerosol particle sizer are near the well-mixed value. This indicates that the particles are mixing in the test cabin before exiting through the outlet.

CHAPTER 9 - **Recommendations**

Several modifications along with additional measurements for work to be done in the future are recommended. For the three micron particles, another series of measurements should be taken. The measurements should be taken using a test cabin pressure of 0.025 inches of water above the ambient pressure and the particles should be injected through the diffuser cone. These measurements would make it easier to compare the differences between the behavior of the three micron and ten micron particles in the test cabin.

Furthermore, concentration measurements should be taken at the outlet of the test cabin using the three micron particles. The measurements should be taken using the APS, not an OPC. Using this information, a mass balance for the three micron particles should be performed.

Ideally, all concentration measurements (injection, sample location and outlet) should be taken using an APS and all the measurements should be taken simultaneously. This was not done for these tests due to the high cost of the APS in comparison to the OPCs. Nevertheless, it is recommended to purchase at least one more APS. Also, the sample tubing used to transport the particles to the APS should be fixed in a single orientation for each location. Thus, the orientation of the tubing and consequently the particle loss through the tubing will be the same for each test performed at a specific location. The particle loss should be found experimentally for each sample tube with a single fixed orientation before it is used to take measurements in the test cabin.

An additional flow visualization using the diffuser cone injection is recommended. The primary reason is that the flow used in the flow visualization presented in chapter 7 had a lower flow rate, after correcting for pressure, than the flow used in the chamber. Also, a longer flow visualization could be performed with different views of the flow. Therefore, a second flow visualization using the diffuser cone would give a more accurate picture of the airflow behavior in the test cabin.

A final recommendation would be to inject burst particles in the cabin similar to the computational studies described in Chapter 2. A short burst of particles would more accurately represent a real-life situation. It would also give insight to the transient effects and not just the steady state effects investigated here.

References

ASHRAE. (2003). "Ch. 10-Aircraft." ASHRAE Applications Handbook, 10.1-10.10.

ASHRAE Standard 55. (2004). "Thermal Environmental Conditions for Human Occupancy." American Society of Heat, Refrigerating, and Air-Conditioning Engineers, Inc., Atlanta, GA.

Baron, and Willeke. (2001). *Aerosol Measurement*, Wiley, New York.

Bosbach, Pennecot, Wagner, Raffel, Lerche, and Repp. (2006). "Experimental and numerical simulations of turbulent ventilation in aircraft cabins." *Energy*, 694-705.

Brundrett. (2001). "Comfort and health in commercial aircraft: a literature review." *The Journal of The Royal Society for the Promotion of Health*, 121(1), 29-37.

Chen, Q. (1995). "Comparison of different k-ε models for indoor air flow computations." *Numerical Heat Transfer, Part B: Fundamentals*, 28(3), 353-369.

Chen, Y., Barber, E. M., and Zhang, Y. (1998). "Sampling Efficiency of the TSI Aerodynamic Particle Sizer." *Instrumentation Science and Technology*, 26(4), 363-373.

Cox, J. E., and Miro, C. R. (1997). "Aircraft Cabin Air Quality." *ASHRAE Journal*, 22.

EPA. (2007). "Particulate Matter."

EPA. (2008). " National Ambient Air Quality Standards (NAAQS)."

FAA. (2008a). "Electronic Code of Federal Regulations." Title 14:Aeronautics and Space.

FAA. (2008b). "FAA Aerospace Forecast Fiscal Years 2008–2025."

Gao, N. P., and Niu, J. L. (2007). "Personalized ventilation for commercial aircraft cabins." *AIAA*, 45, 6228-6239.

Gussman, R. A. (1981). "A further development of the May spinning top aerosol generator." *American Industrial Hygiene Association*, 42, 208-212.

Harding, R. (1994). "Cabin Air Quality in Aircraft." *British Medical Journal*, 308(6926), 427.

Hinds, W. C. (1999). *Aerosol Technology*, Wiley Publishing.

Horstman, R. H. "Predicting Velocity and Contamination Distribution in Ventilated Volumes Using Navier-Stokes Equations." *Proceedings of the ASHRAE Conference: IAQ 88*, Atlanta, Georgia, 209-230.

Humphreys, and Deyermond. (2005). "The effect of high altitude commercial air travel on oxygen saturation." *Anaesthesia*, 60, 458-460.

Hunt, E. H., Reid, D. H., Space, D. R., and Tilton, F. E. (1995). "Commercial Airliner Environmental Control System: Engineering Aspects of Air Quality." The Boeing Company.

Ko, K. Thompson, and Nardell, E. (2004). "Estimation of Tuberculosis Risk on a Commercial Airliner." *Risk Analysis*, 24(2), 379-388.

Lebbin. (2006). "Experimental and Numerical Analysis of Air, Tracer Gas, and Particulate Movement in a Large Eddy Simulation Chamber," Kansas State University, Manhattan.

Leder, and Newman, D. (2005). "Review: Respiratory infections during air travel." *International Medicine Journal*, 35, 50-55.

Lee, S.-C., Poon, C.-S., Li, X.-D., and Luk, F. (1999). "Indoor Air Quality Investigation on Commercial Aircraft." *Indoor Air*, 9, 180-187.

Lin, C.-H., Horstman, R. H., Dunn, Ahlers, Sedgwick, Topmiller, Bennett, and Wirogo. (2005). "Numerical Simulation of Airflow and Airborne Pathogen Transport in Aircraft Cabins-Part 1: Numerical Simulation of the Flow Field." *ASHRAE Transactions*, 111.

Lindgren, T. (2003). "Cabin Air Quality in Commercial Aircraft."

Mitchell, J. P., and Stone, R. L. (1982). "Improvements to the May spinning-top aerosol generator." *J. Physical Engineering:Science Instruments*, 15, 565-567.

Nagda, N. L., and Hodgson, M. (2001). "Low Relative Humidity and Aircraft Cabin Air Quality." *Indoor Air*, 11, 200-214.

Nagda, N. L., and Rector, H. E. (2001). "Instruments and Methods for Measuring Indoor Air Quality." Indoor Air Quality Handbook, J. D. Spengler, J. M. Samet, and J. F. McCarthy, eds., McGraw-Hill, 51.1-51.37.

Nagda, N. L., and Rector, H. E. (2003). "A Critical Review of Reported Air Concentrations of Organic Compounds in Aircraft Cabins." *Indoor Air*, 13(3), 292-301.

O'Donnell, Donnini, and Nguyen. (1991). "Air Quality, Ventilation, Temperature and Humidity in Aircraft." *ASHRAE Journal*, 42-46.

Singh, A., Hosni, M. H., and Horstman, R. H. (2002). "Numerical Simulation of Airflow in an Aircraft Cabin Section." *ASHRAE Transactions*, 108(1), 1005-1013.

Smith, A. J. (1996). "Cabin Air Quality in Aircraft: What Is the Problem? What Is Being Done or What Can Be Done About It? Who Can Do It and How?" *The Journal of Air Law and Commerce*, 61(3), 721-766.

Space, D. R., Johnson, R. A., Rankin, W. L., and Nagda, N. L. (2000). "The Airplane Cabin Environment: Past, Present, and Future Research." *ASTM Special Technical Publication*, 1393, 189-214.

Sun, Y., Zhang, Y., Wang, A., Topmiller, J., and Bennett, J. (2005). "Experimental Characterization of Airflows in Aircraft Cabins, Part I: Experimental System and Measurement Procedure." *ASHRAE Transactions*, 111, 45-52.

Thibeault, C. (2002). "Airliner Cabin Air Quality." *Occupational Medicine*, 17(2), 279-292.

TSI. (2002). "Model 3475 Condensation Monodisperse Aerosol Generator." TSI Incorporated.

Wang, A., Zhang, Y., Sun, Y., and Wang, X. (2008). "Experimental study of ventilation effectiveness and air velocity distribution in an aircraft cabin mockup." *Building and Environment*, 43.

Wang, A., Zhang, Y., Topmiller, J., Bennett, J., and Dunn, K. (2006). "Tracer Study of Airborne Disease Transmission in an Aircraft Cabin Mock-Up." *ASHRAE Transactions*, 112(2), 697-705.

Zhang, Y., Sun, Y., Wang, A., Topmiller, J., and Bennett, J. (2005). "Experimental Characterization of Airflows in Aircraft Cabins, Part II: Results and Research Recommendations." *ASHRAE Transactions*, 111(2), 53-59.

Zitter, Mazonson, Miller, Hulley, and Balmes. (2002). "Aircraft Cabin Air Recirculation and Symptoms of the Common Cold." *JAMA*, 288(4), 483-486.

Appendix A - Detailed Concentration Calculation

As described in Chapter 5, the injection normalized concentrations were calculated using equation (5.5) or equation (A.1) below.

$$C = \frac{C_m \times Q_{\sup}}{C_I \times Q_I} \tag{A.1}$$

This appendix details how each component in equation (A.1) was calculated.

Before calculating the sample concentration at a particular location in the test cabin, C_m, the indicated concentration had to be calculated from the particle count measured by the APS. The APS was programmed to measure the particle count in the test cabin in thirty second intervals. The total number of ten micron particles was summed for each thirty second interval. This value was converted to a concentration by dividing by thirty seconds and dividing by the flow rate through the APS. Then the average of all of these concentrations was corrected for the sample tube particle loss using equation (A.2) to get the concentration, C_m.

$$C_m = \frac{C'_m}{1 - F_{dropout}} \tag{A.2}$$

where C'_m is the indicated sample concentration measured by the APS

$F_{dropout}$ is the particle loss in the sample tube

See Chapter 7 for details on how the particle loss in the sample tube was measured.

The injection flow rate was measured using a rotameter at a pressure of 29 psig. Using the manufacturer provided calibration, the indicated reading of 41 on a scale from 0 to 100 – that was taken at the center of the glass float – was converted to a flow rate. Since the calibration curve was for atmospheric pressure, the flow rate had to be corrected to standard pressure using equation (A.3) (Hinds 1999).

$$Q = Q'_I \times P_c = Q'_I \times \left(\frac{P + P_{atm}}{P_{atm}} \right)^{\frac{1}{2}} \tag{A.3}$$

where Q'_I is the indicated volumetric flow rate calculated using the manufacturer's calibration

P_c is the pressure correction factor

P is the average gage pressure at which the flow reading was taken

P_{atm} is the standard pressure

Then to find the final injected flow rate that was used in equation (A.1), Q_I, the amount of particle laden airflow sampled by the OPC in the injection line was subtracted from the airflow calculated in equation (A.3).

The supply flow rate, Q_{sup}, was calculated by taking the sum of the injected flow rate and the inlet flow rate. The flow that entered the cabin through the inlet was not corrected for pressure when the cabin pressure was increased to 0.025 inches of water above atmosphere because the increase in pressure was very small compared to atmospheric pressure.

The concentration injected into the cabin, C_I, was calculated as follows:

$$C_I = C_I' \times R \tag{A.4}$$

where C'_I is the indicated concentration measured by the OPC

R is the calibration factor

Like the APS, the OPC located in the injection line measured particle counts. The OPC was programmed to take three second samples. To calculate the concentration the three-second particle count was divided by three and divided by the flow rate through the OPC. Then an average of all the concentrations measured over the one hour testing period was multiplied by the calibration factor to yield the final injected concentration value.

Appendix B - Supplemental Tests

B.1. Background Concentration

As described in Chapter 4, a fifteen minute background sample was taken before every test. Using those results, the background concentration was determined to be negligible for both the three micron and ten micron testing. The analysis below describes the determination of the background concentration.

The total number of particles sampled over an hour by the APS for a three micron injection test is shown in Figure B- 1. The total number of particles sampled is on the vertical axis, on a log scale, and the particle diameter is on the horizontal axis. In the upper, right corner of Figure B- 1 there is a list of the total number of particles sampled that were smaller than three micron, the total number of three micron particles sampled, the average number of three micron particles sampled and the total number of three micron particles sampled during the background test prior to injection. During the fifteen minute background test approximately 10, three micron diameter particles were sampled. Therefore approximately, 40 particles would be sampled in an hour. This number is much smaller than the 15,400 particles sampled during the test and therefore was neglected in all calculations. Figure B- 2 shows the total number of particles sampled during a ten micron particle injection test. No ten micron particles were sampled during the background test.

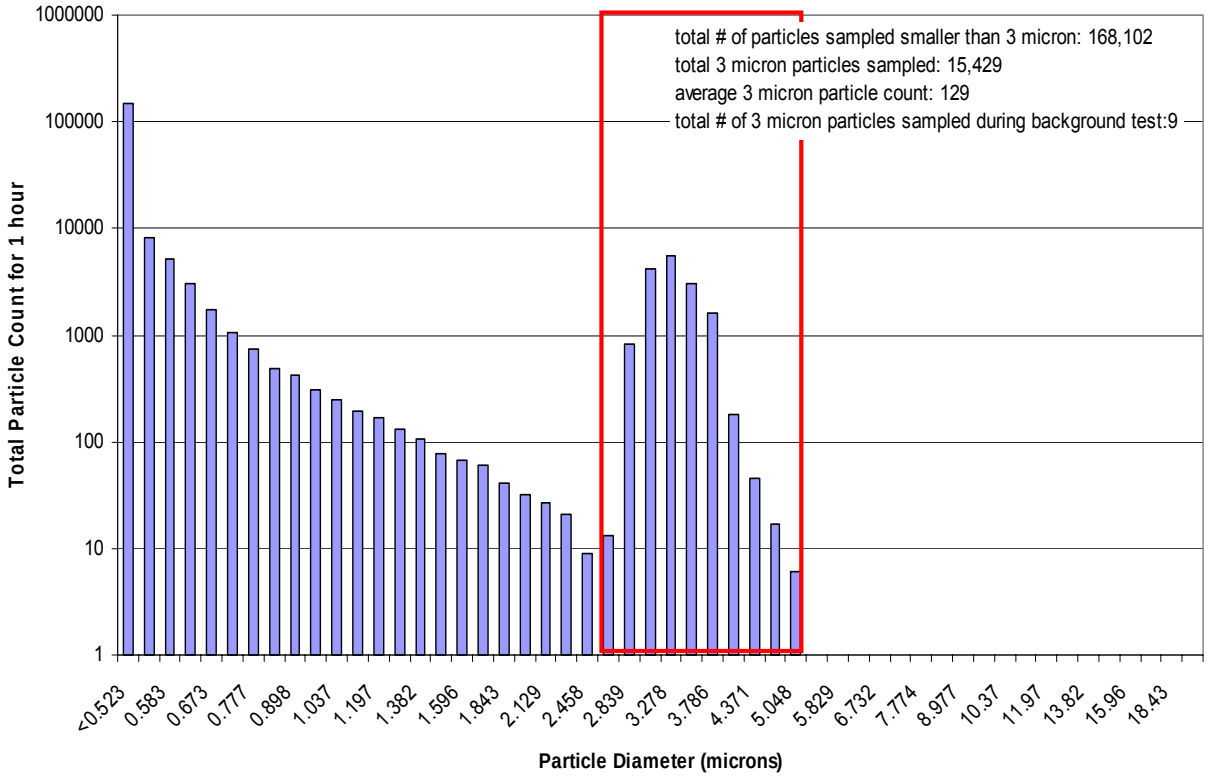

Figure B- 1: Total number of particles sampled during a three micron injection test.

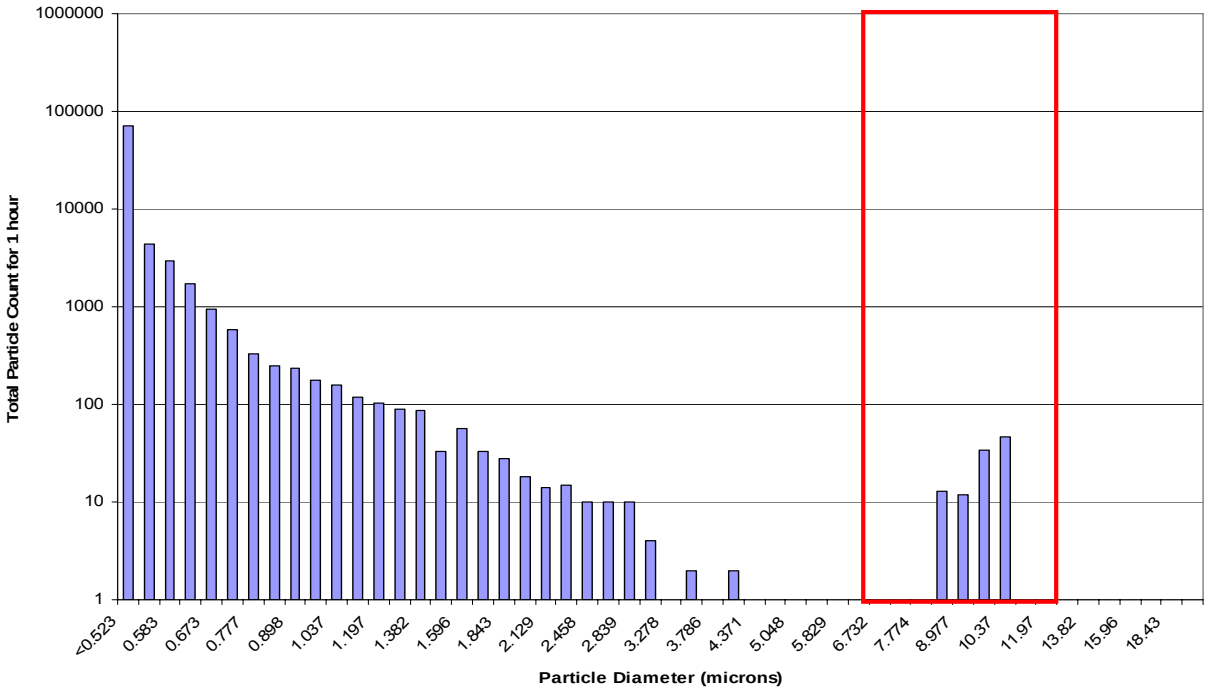

Figure B- 2: Total number of particles sampled during a ten micron injection test.

B.2. Extended Period Concentration Test

Due to the apparent inconsistency of the ten micron data, an extended period test was performed at location 1-D with an interior cabin gage pressure of 0.025 inches of water. The concentration was measured over five hours. The particles were injected into the cabin through the diffuser cone. Figure B- 3 shows the results of this test; the calibrated injection concentration is on the left axis and the sample concentration is on the right axis. Each point in the figure below is for a five minute average. Also, the typical warm-up time for the VOAG and when the sample tube would usually be moved to another location are labeled.

As can be seen, there do not seem to be any large differences in the injection concentration over time. The injection concentration increases approximately 20% over five hours. However, it does show that more than fifteen minutes should be allotted to allow the VOAG to warm-up. Looking at Figure B- 3, it appears that approximately thirty to forty minutes should be allotted instead of fifteen, since the injection concentration increases more than 30% in less than ten minutes after the original warm-up time. As a result, the warm-up time for the VOAG was increased as described in Chapter 4.

As for the sample concentration, there is substantial scatter in the data and some longer term variations. However, the overall variation, based on the trend of the data, is within ±25%. This is consistent with the estimated uncertainty, calculated in Chapter 6. This variation is a little clearer to see in Figure B- 4, where the normalized sample concentration is plotted.

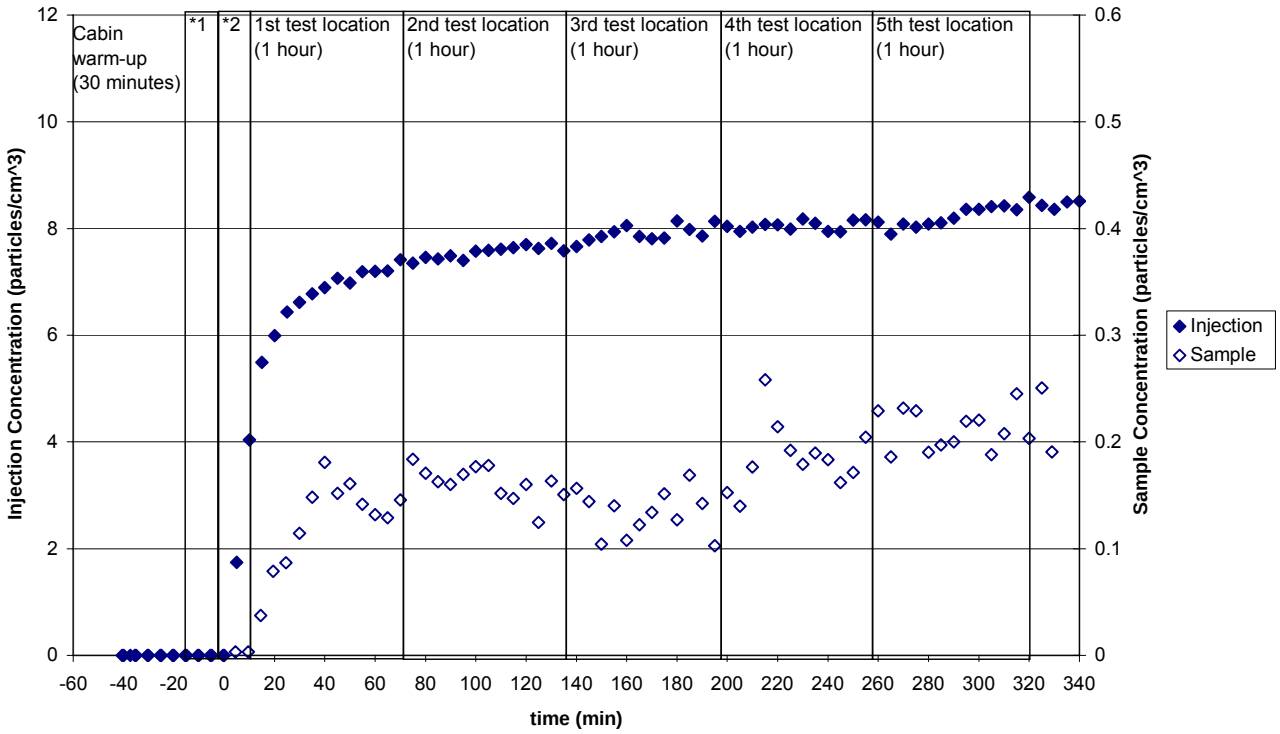

Note: *1Background Concentration Sample (15 minutes)
*2 Typical VOAG warm-up time (15 minutes)

Figure B- 3: Concentration data from long test taken at location 1-D.

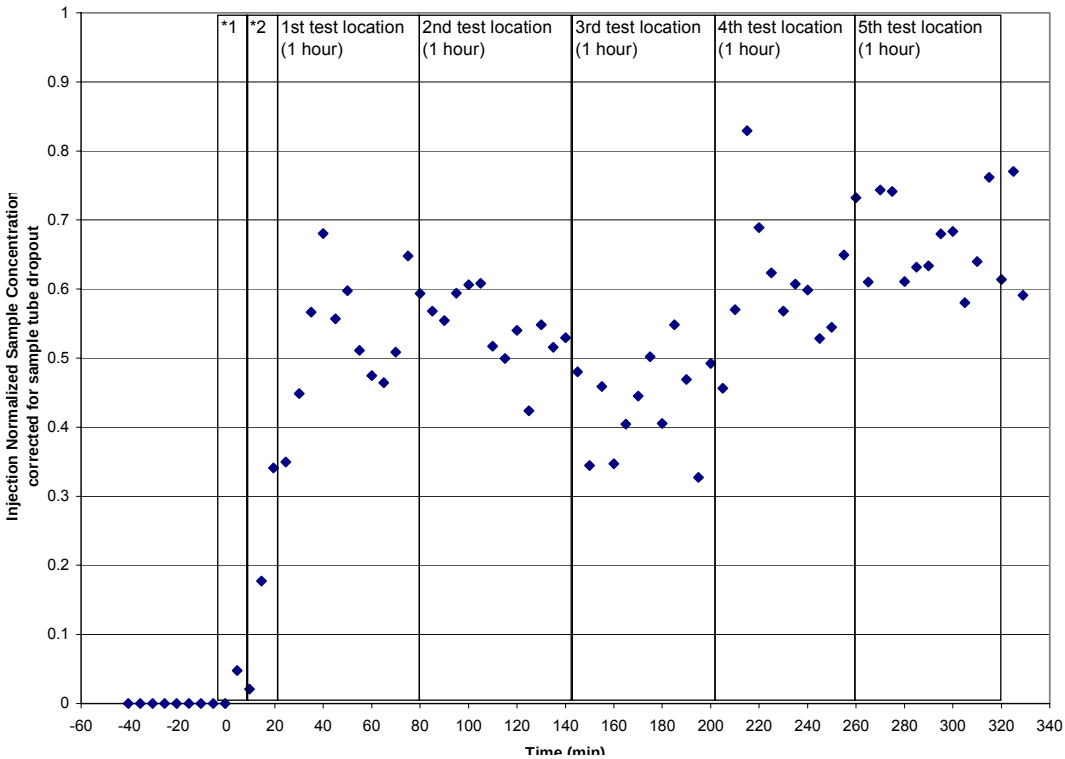

Note: *1Background Concentration Sample (15 minutes)
*2 Typical VOAG warm-up time (15 minutes)

Figure B- 4: Normalized concentration data from long test taken at location 1-D.

B.3. Injection Diffuser Cone Concentration Profile

In order to investigate the possibility of particle loss in the diffuser cone, concentration measurements were taken at several distances inside the diffuser cone shown in Figure B- 5. The average concentration measurements for each location within the diffuser cone are shown in Figure B- 6. Shown on the horizontal axis is the distance from the inlet of the diffuser cone. Shown on the vertical axis is the concentration inside of the cone divided by the injection concentration. Both concentration measurements were taken using an OPC. As can be see in Figure B- 6, there is a higher concentration in the cone near the exit. However, this increase is only 20-30%. Therefore, some of the particles may fall back into the cone instead of being injected into the cabin, but most of them would be injected into the cabin.

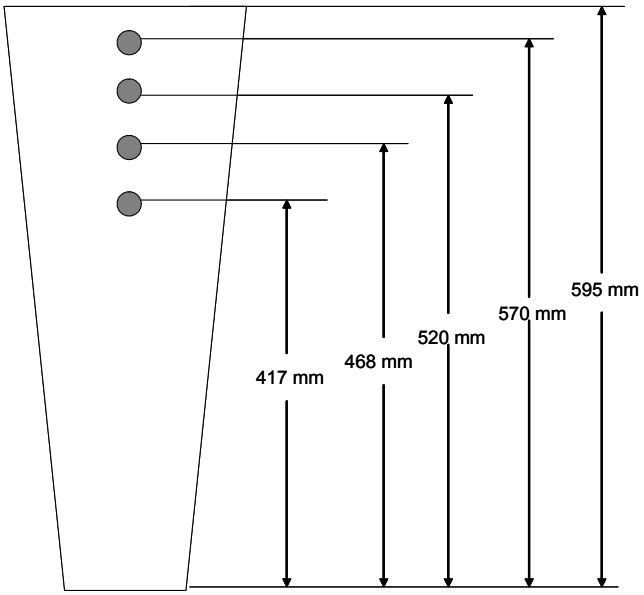

Figure B- 5: Measurement locations for diffuser cone concentrations.

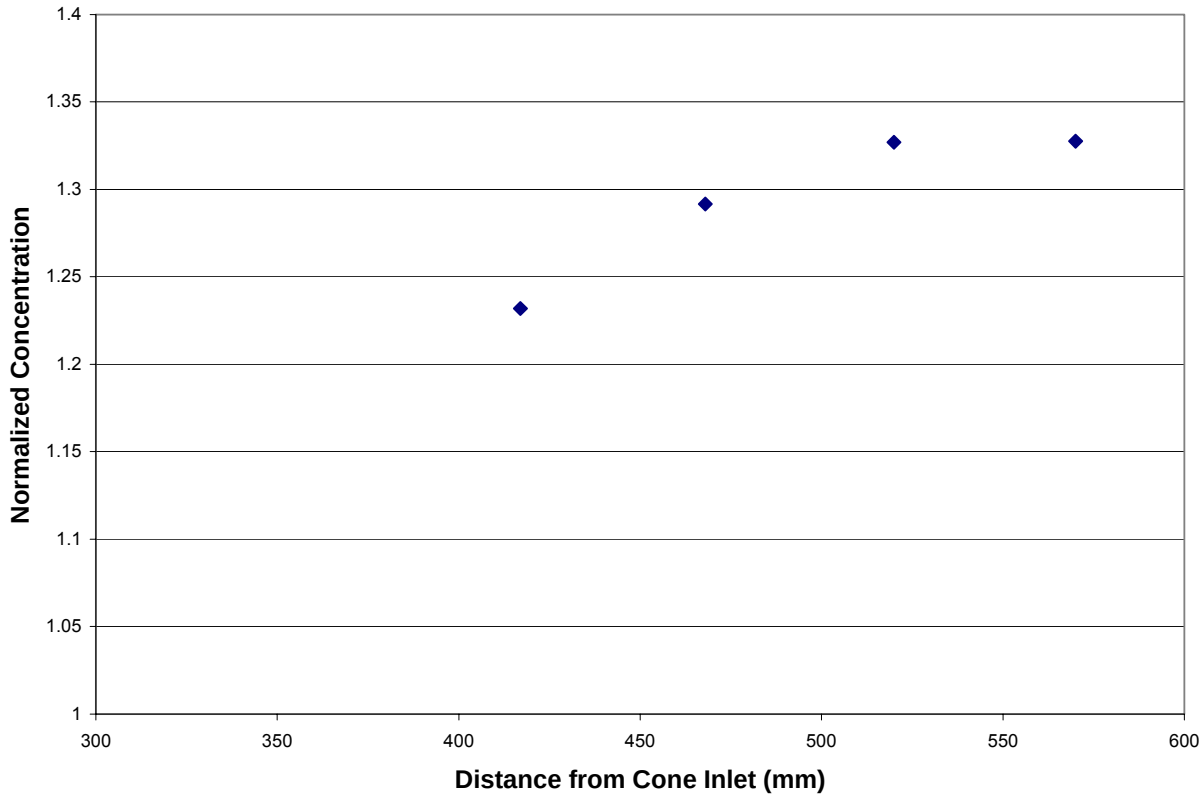

Figure B- 6: Injection diffuser cone concentration.